AD-752 762

SNARK ELECTRON BEAM DEVELOPMENT FOR MATERIALS AND STRUCTURES IRRADIATION

Steven Shope, et al

Physics International Company

Prepared for:

Defense Nuclear Agency

November 1972

DNA 2932F
NOVEMBER 1972
PIFR-301

SNARK ELECTRON BEAM DEVELOPMENT FOR MATERIALS AND STRUCTURES IRRADIATION

FINAL REPORT

S. Shope, P. Spence, and C. Stallings

Prepared for

Defense Nuclear Agency
Washington, D.C. 20305

Approved for public release;
distribution unlimited.

PHYSICS INTERNATIONAL COMPANY
2700 MERCED STREET • SAN LEANDRO, CALIFORNIA 94577 • PHONE 357-4610 (415) • TWX 891-9689 (415)

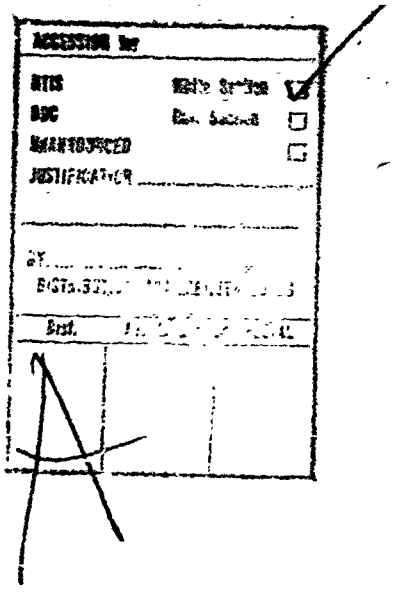

Destroy this report when it is no longer needed. Do not return to sender.

UNCLASSIFIED
Security Classification

DOCUMENT CONTROL DATA - R&D

(Security classification of title, body of abstract and indexing annotation must be entered when the overall report is classified)

1 ORIGINATING ACTIVITY (Corporate author)
Physics International Company
2700 Merced Street
San Leandro, California

2a. REPORT SECURITY CLASSIFICATION
Unclassified

2b GROUP
NA

3 REPORT TITLE
SNARK ELECTRON BEAM DEVELOPMENT FOR MATERIALS AND STRUCTURES IRRADIATION

4 DESCRIPTIVE NOTES (Type of report and inclusive dates)
FINAL REPORT

5 AUTHOR(S) (Last name, first name, initial)
Snope, Steven; Spence, Philip; and Stallings, Charles

6 REPORT DATE	7a TOTAL NO. OF PAGES	7b. NO OF REFS
November 1972	114	8

8a CONTRACT OR GRANT NO.	9a. ORIGINATOR'S REPORT NUMBER(S)
DASA 01-71-C-0045	PIFR-301
b PROJECT NO.	
c NWER Subtask Code Ac321	9b. OTHER REPORT NO(S) (Any other numbers that may be assigned this report)
d Work Unit Code 6	DNA 2932F

10 AVAILABILITY/LIMITATION NOTICES
Approved for public release; distribution unlimited.

11 SUPPLEMENTARY NOTES	12. SPONSORING MILITARY ACTIVITY
	Defense Nuclear Agency - SPAS Washington, D.C. 20305

13 ABSTRACT

This report describes development of electron beam irradiation capabilities on the Defense Nuclear Agency (DNA) SNARK facility for use in materials and structures testing. Both large (~100 cm^2) and small (~10 cm^2) irradiation areas are discussed. Electron beam generation and control for this work was accomplished by use of external pulsed magnetic guide fields. Details of the beam transport work are given along with descriptions of several pilot material and structural response experiments. The longitudinal guide field approach is shown to be an efficient ($\geq$ 75 percent) technique for energy extraction (in a useable fashion) from high-current pulsed electron accelerators. Potential applications of this approach to other generators are also discussed.

DD FORM 1473

UNCLASSIFIED
Security Classification

UNCLASSIFIED

Security Classification

14. KEY WORDS	LINK A		LINK B		LINK C	
	ROLE	WT	ROLE	WT	ROLE	WT
SNAPK Electron beams Material response Structural response Simulator						

INSTRUCTIONS

1. ORIGINATING ACTIVITY: Enter the name and address of the contractor, subcontractor, grantee, Department of Defense activity or other organization *(corporate author)* issuing the report.

2a. REPORT SECURITY CLASSIFICATION: Enter the overall security classification of the report. Indicate whether "Restricted Data" is included. Marking is to be in accordance with appropriate security regulations.

2b. GROUP: Automatic downgrading is specified in DoD Directive 5200.10 and Armed Forces Industrial Manual. Enter the group number. Also, when applicable, show that optional markings have been used for Group 3 and Group 4 as authorized.

3. REPORT TITLE: Enter the complete report title in all capital letters. Titles in all cases should be unclassified. If a meaningful title cannot be selected without classification, show title classification in all capitals in parenthesis immediately following the title.

4. DESCRIPTIVE NOTES: If appropriate, enter the type of report, e.g., interim, progress, summary, annual, or final. Give the inclusive dates when a specific reporting period is covered.

5. AUTHOR(S): Enter the name(s) of author(s) as shown on or in the report. Enter last name, first name, middle initial. If military, show rank and branch of service. The name of the principal author is an absolute minimum requirement.

6. REPORT DATE: Enter the date of the report as day, month, year, or month, year. If more than one date appears on the report, use date of publication.

7a. TOTAL NUMBER OF PAGES: The total page count should follow normal pagination procedures, i.e., enter the number of pages containing information.

7b. NUMBER OF REFERENCES: Enter the total number of references cited in the report.

8a. CONTRACT OR GRANT NUMBER: If appropriate, enter the applicable number of the contract or grant under which the report was written.

8b, 8c, & 8d. PROJECT NUMBER: Enter the appropriate military department identification, such as project number, subproject number, system numbers, task number, etc.

9a. ORIGINATOR'S REPORT NUMBER(S): Enter the official report number by which the document will be identified and controlled by the originating activity. This number must be unique to this report.

9b. OTHER REPORT NUMBER(S): If the report has been assigned any other report numbers *(either by the originator or by the sponsor)*, also enter this number(s).

10. AVAILABILITY/LIMITATION NOTICES: Enter any limitations on further dissemination of the report, other than those imposed by security classification, using standard statements such as:

(1) "Qualified requesters may obtain copies of this report from DDC."

(2) "Foreign announcement and dissemination of this report by DDC is not authorized."

(3) "U. S. Government agencies may obtain copies of this report directly from DDC. Other qualified DDC users shall request through _____."

(4) "U. S. military agencies may obtain copies of this report directly from DDC. Other qualified users shall request through _____."

(5) "All distribution of this report is controlled. Qualified DDC users shall request through _____."

If the report has been furnished to the Office of Technical Services, Department of Commerce, for sale to the public, indicate this fact and enter the price, if known.

11. SUPPLEMENTARY NOTES: Use for additional explanatory notes.

12. SPONSORING MILITARY ACTIVITY: Enter the name of the departmental project office or laboratory sponsoring *(paying for)* the research and development. Include address.

13. ABSTRACT: Enter an abstract giving a brief and factual summary of the document indicative of the report, even though it may also appear elsewhere in the body of the technical report. If additional space is required, a continuation sheet shall be attached.

It is highly desirable that the abstract of classified reports be unclassified. Each paragraph of the abstract shall end with an indication of the military security classification of the information in the paragraph, represented as *(TS), (S), (C), or (U)*.

There is no limitation on the length of the abstract. However, the suggested length is from 150 to 225 words.

14. KEY WORDS: Key words are technically meaningful terms or short phrases that characterize a report and may be used as index entries for cataloging the report. Key words must be selected so that no security classification is required. Identifiers, such as equipment model designation, trade name, military project code name, geographic location, may be used as key words but will be followed by an indication of technical context. The assignment of links, roles, and weights is optional.

DNA 2932F
NOVEMBER 1972
PIFR-301

SNARK ELECTRON BEAM DEVELOPMENT FOR MATERIALS AND STRUCTURES IRRADIATION

FINAL REPORT

S. Shope, P. Spence, and C. Stallings

Prepared for

Defense Nuclear Agency
Washington, D.C. 20305

This effort supported by DNA under:
NWER Subtask Code AC321 Work Unit Code 6

Physics International Company
2700 Merced Street
San Leandro, California 94577

SIX INCH DIAMETER RING IRRADIATED WITH SNARK ELECTRON BEAM

A1417

FOREWORD

Electron beam development work on the Defense Nuclear Agency (DNA) SNARK facility was carried out under contract DASA-01-71-C-0045 during the time period December 1970 to January 1972. Project monitors were Captain John Cockayne and Mr. Don Kohler, DNA, SPAS Division. The program at Physics International was supervised for most of its duration by Dr. Gerold Yonas. Principal investigators were Dr. Philip Spence, project manager, and Dr. Charles Stallings and Mr. Steven Shope, project physicists. Material and structural response experiments were carried out under the assistance of Drs. Tibor Stefansky and James Shea.

ABSTRACT

This report describes development of electron beam irradiation capabilities on the Defense Nuclear Agency (DNA) SNARK facility for use in materials and structures testing. Both large (~ 100 cm^2) and small (~ 10 cm^2) irradiation areas are discussed. Electron beam generation and control for this work was accomplished by use of external pulsed magnetic guide fields. Details of the beam transport work are given along with descriptions of several pilot material and structural response experiments. The longitudinal guide field approach is shown to be an efficient (≥ 75 percent) technique for energy extraction (in a useable fashion) from high-current pulsed electron accelerators. Potential applications of this approach to other generators are also discussed.

CONTENTS

ILLUSTRATIONS

ILLUSTRATIONS (cont.)

ILLUSTRATIONS (cont.)

SECTION 1
INTRODUCTION

1.1 GENERAL BACKGROUND AND SUMMARY

The goal of this program has been the development of an electron beam capability on the Defense Nuclear Agency (DNA) owned SNARK generator. The generator is a 0.55 ohm output impedance pulse-charged stripline array capable of operation at 800 kV peak output voltage. It was originally constructed in 1970 for use as a flash X-ray machine and as a test facility for electron beam generation and transport work in support of flash X-ray production. Specifically, the primary goal of this program was development of generation and control techniques required to produce uniform, large area (≈ 100 cm^2) electron beam environments for eventual use in material and structural response testing. A secondary goal was the development of techniques to provide smaller irradiation area (≈ 10 cm^2) electron beam environments for material response testing at high dose levels.

Although the majority of the work addressed the large area electron beam task, considerable success has also been achieved in the small area electron beam work. The large area electron beam environments are now an established capability. They are summarized in Section 1.2 along with the small area electron beam environments achieved both during this program and very recently during the current DNA funded "Advanced Concepts Program."

Considerable past work with high-current electron beams has involved transport and control of the beams by injecting them into neutral gas-filled drift pipes (both cylindrical and conical). The guide cone approach has been the standard beam control technique over the last 3 to 4 years and material response experiments with high-current beams have used this technique almost exclusively. Very early in the development of neutral gas transport techniques it was recognized that beam-plasma interactions (e.g., space charge neutralization, gas breakdown, current neutralization) played an important role in defining the electromagnetic field conditions in and near the beam channel (References 1 and 2). Simple variation of background gas pressure was found useful in varying the characteristics of the propagated beams. As neutral gas transport techniques were applied to higher current electron beams it became obvious that limitations on transport efficiency resulted from the generation of large transverse electron energy components in the accelerator diode. Since the diodes must be operated at relatively hard vacuum ($\lesssim 10^{-4}$ torr) to prevent insulator flashing, there was no simple way to neutralize the high self-magnetic field of the beam in the diode. Electron gyration in the self-field generated high transverse velocity components most of which could not be contained by the beam self-fields in the transport region. Those electrons that were contained in the beam channel still retained considerable transverse energy, and mean electron incidence angles at targets placed normal to the beam propagation direction have been observed to be as high as $\langle\theta\rangle \gtrsim 65$ degrees (Reference 3). Although only 25 to 35 percent of the total diode energy was available at the target location in these past experiments (300 kV, 150 kA initial beam parameters), the propagated beams were still useful for small area material irradiations.

The limitations of neutral gas transport techniques became painfully obvious when their application to higher current beams was attempted at 100 kV, 300 kA (Reference 4). In this case only 10 to 15 percent of the beam energy could be reliably delivered to a target location. Faced with the reality of even higher current electron beam generators, attention turned to development of alternative beam control techniques in which external magnetic fields were used to "overwhelm" the beam self-fields. The simplest and perhaps most versatile beam control technique for material and structural response applications is the use of an externally applied longitudinal magnetic field. In this case the field can be produced by a solenoid which surrounds the diode and transport regions and this configuration allows open access to the target area from the end of the solenoid as well as optical access (between solenoid windings) from the sides. The sample can be placed at ground since the high voltage magnet wires are located external to the transport region, thus avoiding the complications which would be inherent in other external field configurations such as a linear pinch (azimuthal magnetic field) discharge.

The longitudinal magnetic field (B_z) approach was chosen for this program for the reasons given above. Using this technique we have delivered 75 to 80 percent of the beam energy available at the diode to a target area of ≈ 100 cm^2. The beams are effectively "mapped" from the cathode surface to the target location giving control of the beam cross-sectional area shape by simply varying the cathode shape. For the large area beam experiments we concentrated on a rectangular shaped beam (7½ in. by 7 in.) to allow more efficient use of the beam energy for irradiation of rings and cantilevered beams. Work areas in the large area beam task included the following:

- Design and construction of pulsed magnetic field and diode hardware. The basic solenoid is configured in a rectangular cross-section and has 20 millisecond field period to allow field penetration into conducting targets.
- Iterations on cathode shape and surface characteristics to improve fluence uniformity.
- Measurement of fluence levels and fluence uniformity.
- Diagnosis of energy deposition and energy deposition versus depth profiles in flat and curved targets.
- Application of standard diagnostics (high speed motion pictures and strain gages) to instrument the response of rings and cantilevered beams to electron energy deposition.

The small area electron beam work has included:

- Generation, diagnosis, and application of small area (≈ 6 cm^2) electron beams to support initial materials testing experiments for McDonnell-Douglas. The neutral gas, guide cone technique was used for this work.
- High fluence, small area (≈ 10 cm^2) electron beam generation and diagnosis using a 25 cm^2 cathode and a converging (mirror) magnetic field guide. This work was supported under a different contract but is reported here for completeness.

Section 2 outlines the beam development work. Details of the hardware are given along with results of the testing. Electron beam characteristics (fluence levels, deposition profiles, uniformity) are given for both the large and small area beams.

Section 3 describes the results of "pilot" material and structural response experiments. Conclusions of this work

are discussed in Section 4. Details of electron beam diagnostics developed and/or used on this program are given in the Appendix.

1.2 THE SNARK ELECTRON BEAM FACILITY

The initial program goal to develop electron beam capabilities on SNARK has been satisfied. Because it is a user-oriented facility, it was felt desirable to summarize the available and projected electron beam environments, the diagnostics available, and support services in a manner easily accessible to potential users. This section presents that summary.

The SNARK facility is shown in Figures 1.1, 1.2, and 1.3. The machine itself is comprised of a Marx generator (which is used to pulse charge the pulse-forming lines), eight separate Blumlein circuits consisting of Mylar insulated plane-parallel striplines, and a common tube envelope (fed by the pulse-forming lines which are connected in a series-parallel configuration) containing a field emission diode load. The pulse-forming lines are contained in two flat trays which mate with a central tray containing the tube envelope. The electron beam fires vertically upward through a thin (compared to the electron range) anode window into the test chamber. Pulse synchronization is accomplished by use of eight low inductance gas rail switches (one for each Blumlein circuit) which are command triggered by a self-firing master switch. Jitter in this firing sequence is on the order of a few nanoseconds. An external trigger signal which fires the Marx generator can be used to fire the machine. Overall jitter of the electron beam pulse with respect to this user controlled trigger signal is on the order of 200 nanoseconds. The generator output impedance is approximately 0.55 ohm.

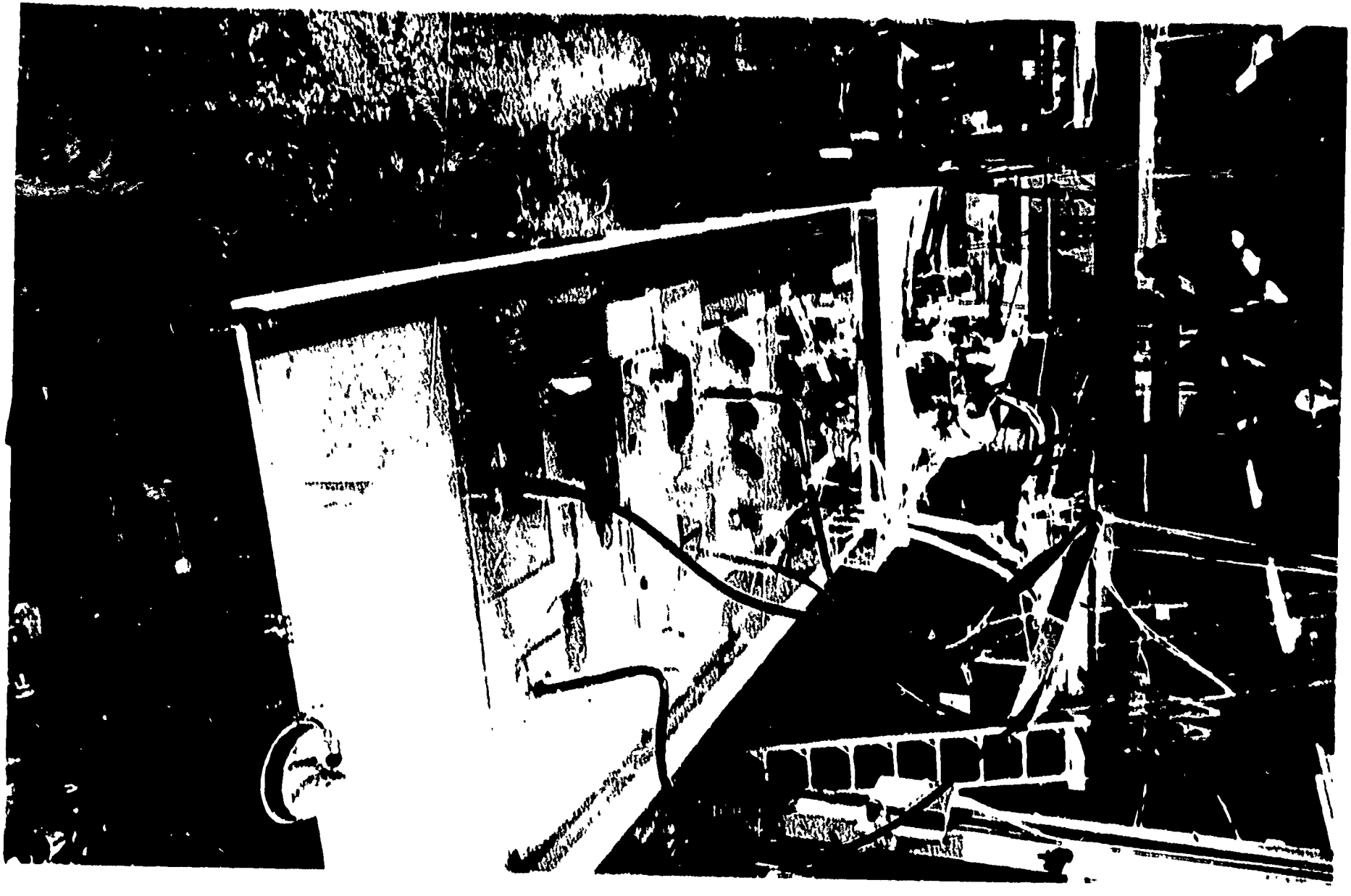

Figure 1.1 SNARK facility (1-MV, 50-nsec pulsed electron accelerator).

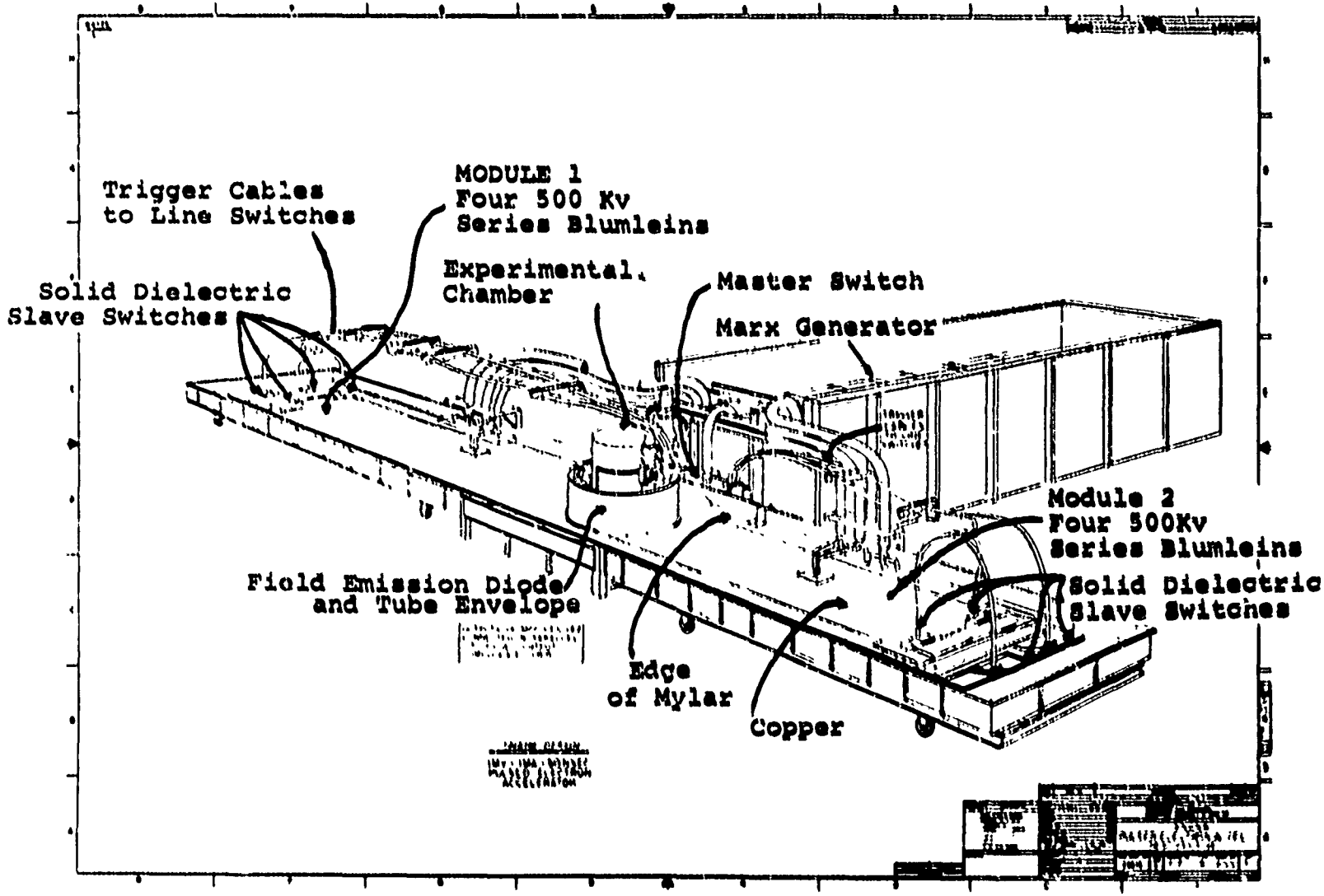

Figure 1.2 SNARK design, 1 MV, 50-nsec pulsed electron accelerator.

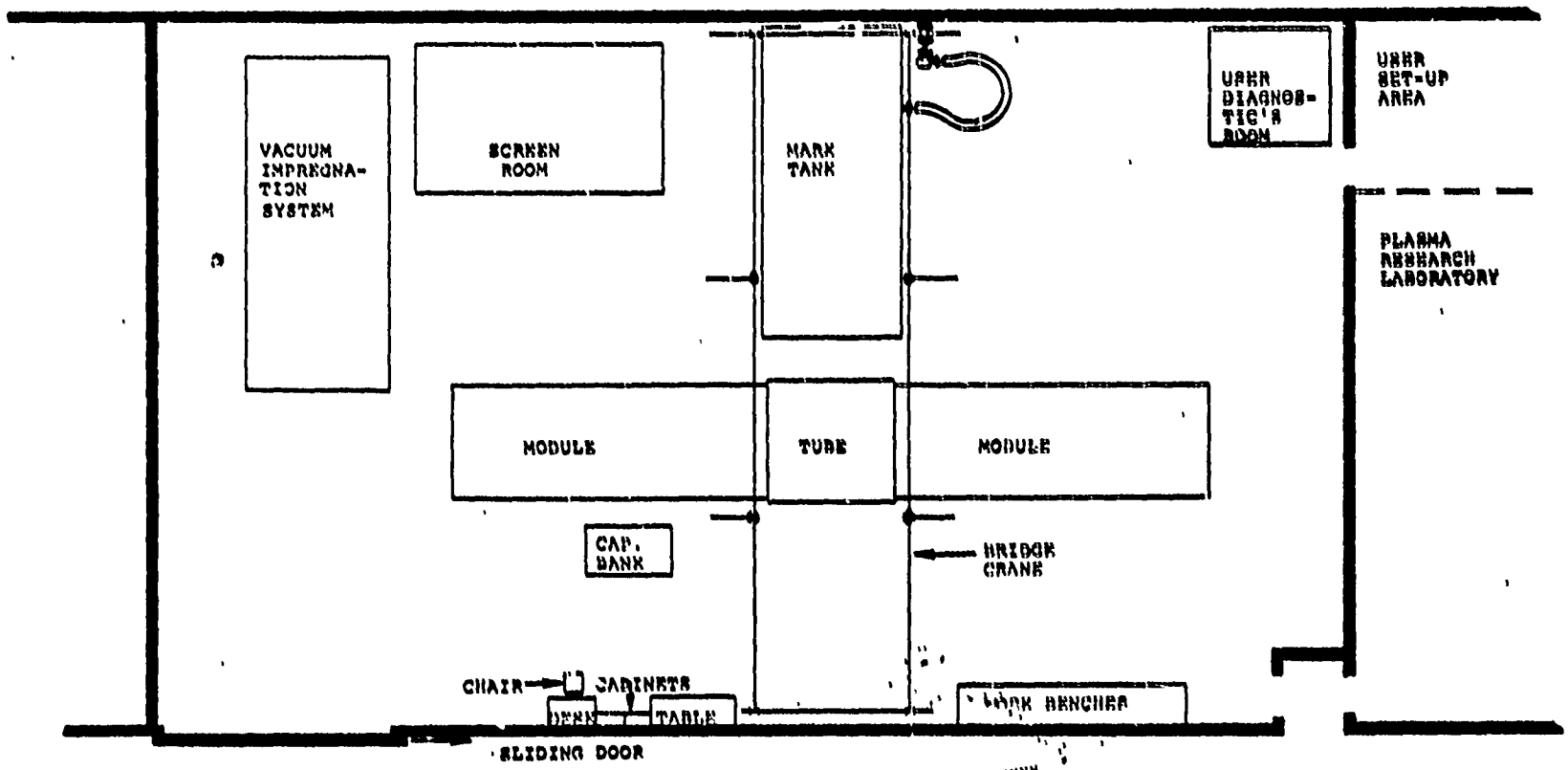

xxxxxxxxxxxxxxxxxxxxxxxxx
See the following pages
for greater details.
xxxxxxxxxxxxxxxxxxxxxxxxx

Figure 1.3 Facility layout

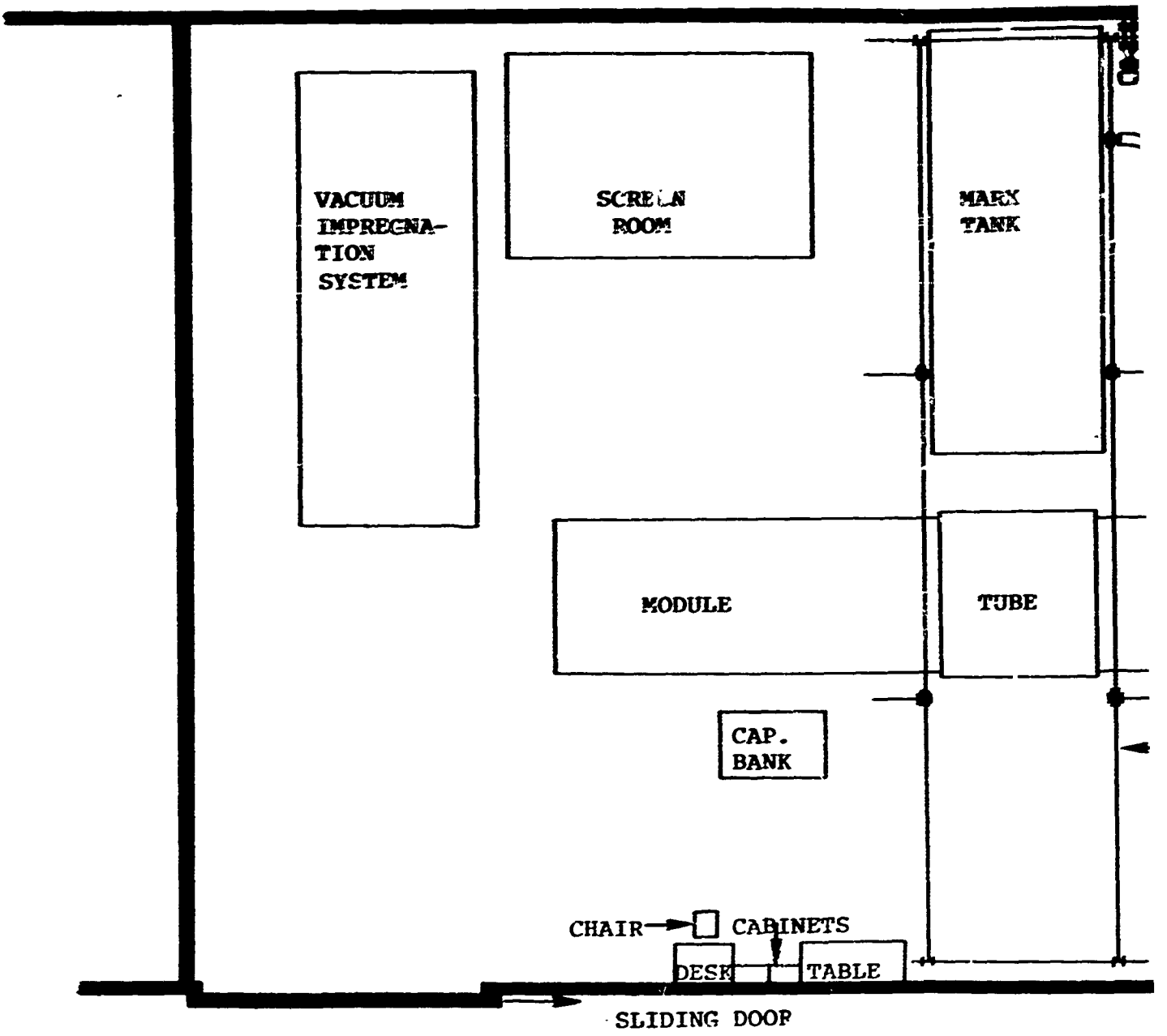
VACUUM IMPREGNA-TION SYSTEM
SCREEN ROOM
MARX TANK
MODULE
TUBE
CAP. BANK
CHAIR
CABINETS
DESK
TABLE
SLIDING DOOR

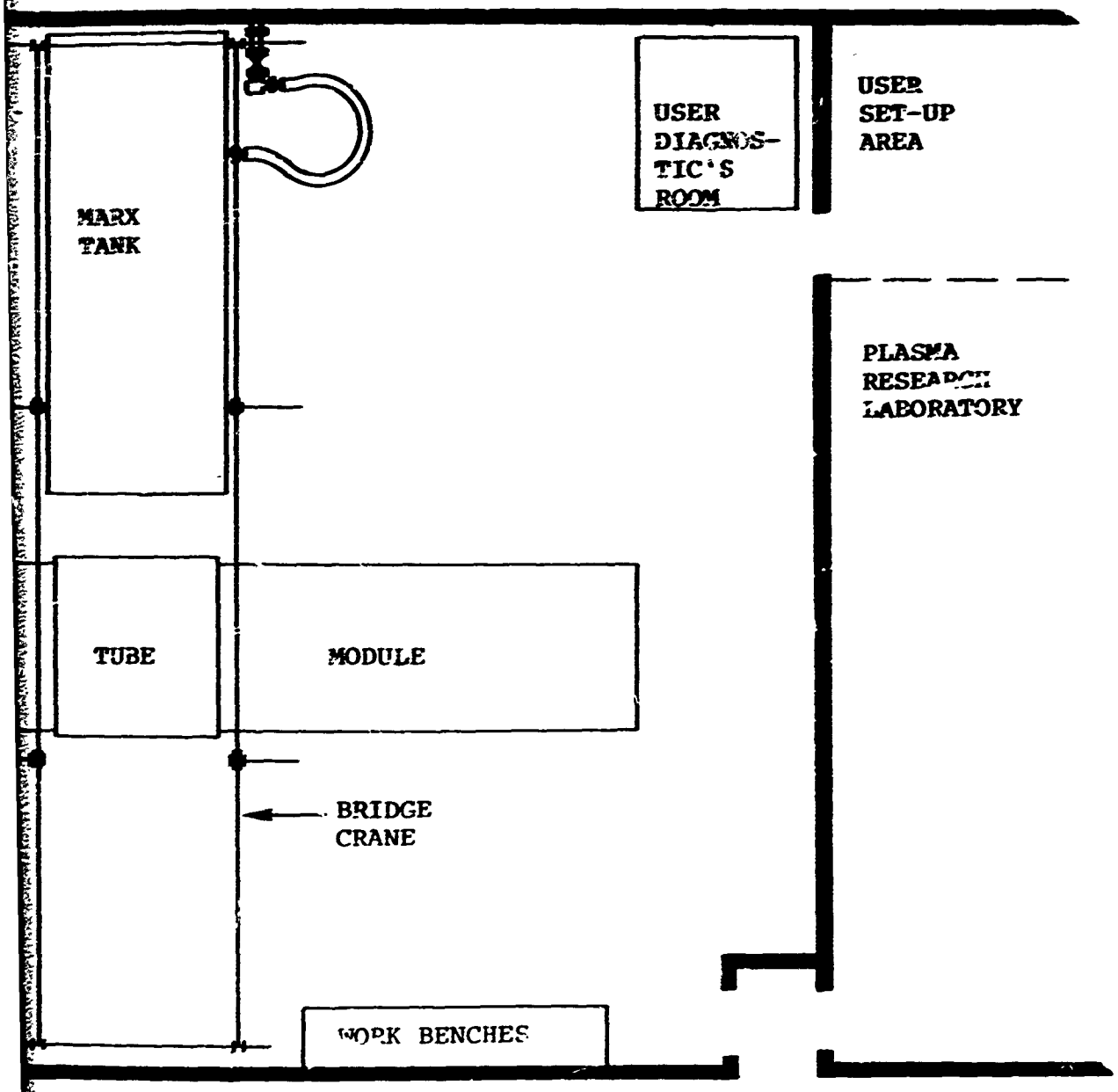

Figure 1.3 Facilitv layout

The tube assembly consists of a single annular, angled epoxy insulator and a short (~ 3 foot diameter) vacuum transmission section feeding a centrally located diode. A ~ 2 centimeter gap spacing is used in the vacuum transmission section to give an overall tube inductance (not including the diode region) of ~ 30 nanohenries. The anode plate is removed after each shot by means of an overhead electric hoist to facilitate cleaning and re-oiling of the tube interior. The pulsing rate averages 8 to 10 shots per eight hour shift, but can be higher or lower depending upon the complexity of the experimental setup in the target chamber.

Nominal generator output specifications for a 1.5 ohm load are listed below:

Peak Voltage	800 kV
Peak Current	530 kA
Pulse Duration	70 nsec (FWHM)
Total Beam Energy	30 kJ

Although the generator has operated at voltage and current levels of $\gtrsim$ 900 kV and $\gtrsim$ 750 kA respectively with $\gtrsim$ 35 kJ total beam energy, the generator is normally operated at the nominal levels quoted above to achieve relatively maintenance-free operation.

Electron beam environments in the target chamber depend on the desired area coverage. For the 100 to 130 cm^2 irradiation area conditions (using longitudinal magnetic guide fields for beam control) typically 75 to 80 percent of the energy in the diode can be delivered to the target. The smaller irradiation area conditions require use of small area cathodes which are

typically higher impedance and more inductive than the 100 cm^2 cathodes used for the larger areas. Hence the beam energy in the diode is somewhat reduced from the nominal 30 kJ quoted above.

Table 1.1 summarizes the available electron beam environments. We have listed both peak and mean electron voltage levels, total beam energy both in the diode and at the target location, fluence levels for given irradiation areas, and peak dose levels, based on measured deposition versus depth profiles. The underlined values indicate measured data. Other numbers indicated are conservative extrapolations from measured data (in other words they correspond to environments which are accessible in our opinion with minimal or zero change to existing hardware).

Table 1.2 lists the electron beam diagnostics routinely used. Table 1.3 describes material and structural response diagnostics available for use in experiments. Support Services available to users are outlined in Table 1.4.

TABLE 1.1

SNARK ELECTRON BEAM OUTPUT CAPABILITIES

	Peak Voltage (kV)	Mean Voltage (kV)	Total Beam Energy (kJ)	Total Transported Energy (kJ)	Irradiation Areas		10 cm^2 Irradiation Area	
					Fluence (cal/cm^2)	Peak Dose (cal/gm)	Fluence (cal/cm^2)	Peak Dose (cal/gm)
100 cm^2 cathode. Longitudinal magnetic guide field.	850	600-650	30	23	40	250	x	x
	650	500	20	16	30	300	x	x
	500	350	15	12	20	320	x	x
Neutral gas focusing guide cones.	550-600	400	20	3-4	x	x	100-150[a] (6 cm^2 area)	1500[b]
25 cm^2 cathode. Converging magnetic guide field.	850	600-650	20	16	x	x	380	> 2000
	600	450	12	10	x	x	240[a]	> 2000[c]

[a] Measured using Faraday cup at target.

[b] Inferred from fluence and assumed deposition versus depth profile.

[c] Preliminary result--dose is definitely sufficient to produce front surface vaporization in carbon.

TABLE 1.2

ELECTRON BEAM DIAGNOSTICS

- **DIODE VOLTAGE MONITORS**

  Two separate monitors measure the voltage waveform applied to the tube envelope. These records are then corrected for the induced voltage component, L dI/dt, to give the diode accelerating voltage.

- **DIODE CURRENT MONITOR**

  This monitor is a self-integrating Rogowski coil that surrounds the cathode shank.

- **SCINTILLATOR PHOTODIODE**

  Used to monitor electron beam generated bremsstrahlung as a cross check on the pulse length inferred from the voltage and current monitors.

- **GRAPHITE CALORIMETRY**

  Available in the form of segmented arrays for fluence measurement over flat or curved surfaces, and also as 0.005 inch foil stacks for measurement of deposition versus depth profiles.

- **FARADAY CUPS**

  Varities are available which can be used in magnetic fields. The Faraday cups monitor transported current and are used when fluence levels above the damage threshold of graphite prevent the use of standard calorimetry.

TABLE 1.3

MATERIAL AND STRUCTURAL RESPONSE DIAGNOSTICS

- **STRESS VERSUS TIME MEASUREMENT**

  Quartz gages
  Strain gages
  Laser interferometer

- **IMPULSE MEASUREMENT**

  Momentum traps photographed with a high speed (HYCAM) movie camera.

  Ballistic pendulum (not presently available, however, modification of a standard pendulum for use in the SHARK vertical beam geometry would be straightforward).

- **PHOTOGRAPHIC DIAGNOSTICS**

  High speed (HYCAM) movie camera
  Optical framing camera

TABLE 1.4

SUPPORT SERVICES

- RECORDING ELECTRONICS
- SCREEN ROOM
- MODEL SHOP--PREPARATION ROOMS
- COMPUTER SERVICE--CODE LIBRARY
- CONSULTING SERVICES
- MACHINE SHOP
- METALLOGRAPHIC LABORATORY
- PHOTOGRAPHIC LABORATORY

SECTION 2
BEAM DEVELOPMENT TASKS

2.1 LARGE AREA (~ 100 cm^2) ELECTRON BEAMS

At the onset of the program the goal was the production of relatively uniform fluence electron beams with ~ 100 cm^2 cross-sectional area over arbitrary shaped target areas. For the reasons advanced in the Introduction (Section 1.1) the longitudinal magnetic guide field approach was chosen as most desirable from the view points of target access and promising transport efficiency. Experiments addressed to beam transport in longitudinal fields had been carried out at Cornell, NRL and PI (References 5, 6, 7), however the total beam energies had been considerably lower than those available on SNAKE and fluence uniformity control had received only minimal study. Due to the marked success of the B_z field technique for transporting and shaping the SNAKE beams the originally envisioned backup approaches (linear pinch-B_θ-transport and beam mixing in neutral using numerous magnetically isolated cathodes) were quickly dropped. The following paragraphs describe the beam transport hardware and results.

2.1.1 Transport System Design Considerations. Major design considerations for the 100 cm^2 electron beam system were as follows:

- Rectangular beam geometry
- Magnetic field strength sufficient for efficient transport and control
- Slow magnetic field period to avoid field perturbations from possible conducting targets.

The requirement to irradiate ring structures and cantilevered beams suggested a rectangular cathode. A 2½ inch by 7 inch size was chosen as the best compromise. The diode hardware design was made capable of accepting cathodes up to 4 inches wide and 9 inches long. To successfully transport the electron beam a longitudinal magnetic field of 7.5 kG was estimated to be required (Reference 8). In order to minimize the magnetic field volume it was decided to use a solenoid of rectangular cross-section. A model solenoid was fabricated to study field uniformity. The winding density on both ends of the solenoid was varied until a uniform field was obtained the entire length of the coil. Final field uniformity was 11 percent and 13 percent in the longitudinal and transverse directions.

Once the winding density was established the only other criteria to satisfy were the magnitude of the required field (about 8 kG) and the period of the applied field. Under the assumption of 2 inch by 7 inch by 1/8 inch thick aluminum samples, a solenoid with a period of 20 milliseconds was estimated to be required to keep the magnetic field uniform within ± 10 percent throughout the sample. With a period requirement of 20 milliseconds, the physical dimensions of the vacuum system and the capacitance of the pulsed solenoid capacitor bank fixed (252 μfd at 20 kV), the number of turns on the solenoid was calculated from $\omega = 1/\sqrt{LC}$ to be 1000 turns. The B_z field

component of a rectangular solenoid having N turns and dimensions $x = \pm a$, $y = \pm b$ and carrying a current I is:

$$B_z = \frac{I}{4}\pi^{-1}\mu I \left\{ x_1 \left| r_1 (r_1 - y_1) \right|^{-1} - x_1 \left| r_4 (r_4 + y_3) \right|^{-1} \right.$$

$$+ x_3 \left| r_2 (r_2 - y_1) \right|^{-1} - x_3 \left| r_3 (r_3 + y_3) \right|^{-1}$$

$$+ y_1 \left| r_1 (r_1 - x_1) \right|^{-1} - y_1 \left| r_2 + x_3 \right|^{-1}$$

$$\left. + y_3 \left| r_4 (r_4 - x_1) \right|^{-1} - y_3 \left| r_3 (r_3 + x_3) \right|^{-1} \right\} \cdot N$$

where (x, y, z) is the field point in the positive quadrant and r_1, r_2, r_3 and r_4 are the distances from successive corners to the field points. The components of r_m are x_m, y_m, and z_m. This calculation showed that the maximum magnetic field would be 15 kG when driven by the bank at 20 kV charge. Measured field strength was 12 kG. The final solenoid was 38 centimeters in length and 25 x 35 centimeters for the rectangular dimensions. The coil form and the vacuum chamber were constructed from PVC to allow effective field penetration.

2.1.2 Diode and Beam Transport Hardware. The hardware required for generation and transport of the large area beam is shown schematically in Figure 2.1. A uniform longitudinal magnetic field is applied from the cathode emission surface to the target location to produce a beam which retains the general cross-sectional shape of the emission surface. The cathode consists of a solid aluminum transition piece, a thin (magnetically transparent) stainless steel rectangular stalk, and a

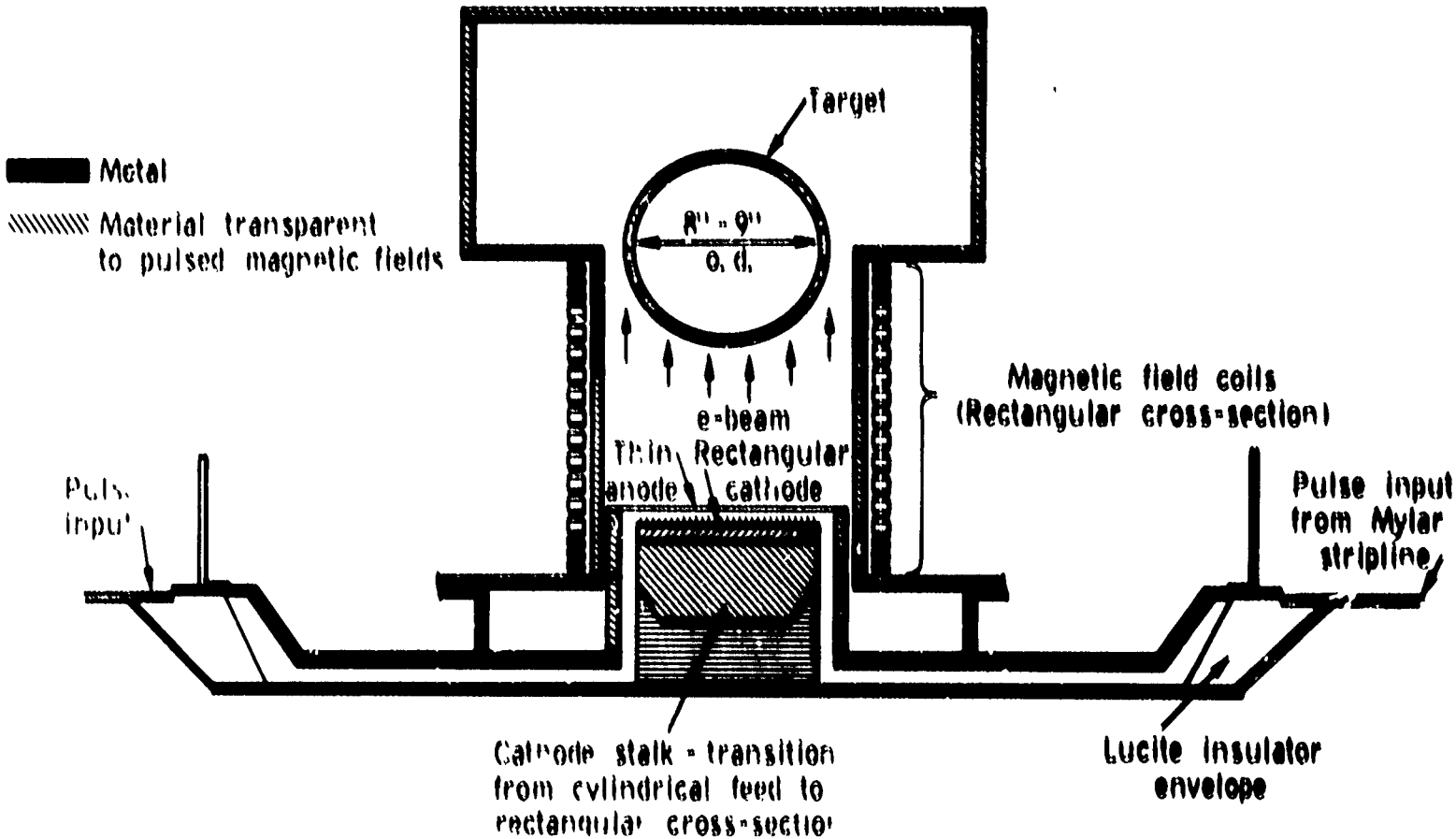

Figure 2.1 Longitudinal magnetic field system for SNARK.

replaceable emission surface (in this case, steel roll-pin emitters) (Figure 2.2). The cathode is surrounded by a magnetically transparent anode extension, shown in Figure 2.3, which provides a ground plane above the cathode and separates the diode vacuum region from the beam transport (drift) region. The beam transport chamber, surrounded by the magnetic field coil, is shown in Figure 2.4. This assembly slides over the anode extension and the transport region vacuum can be controlled through ports in the top. The field coil itself is driven by a 252 mfd, 20 kV, capacitor bank which can be fired synchronously with the electron beam machine.

2.1.3 Measurements of Beam Characteristics. The approach for the initial experiments was to generate a large area, uniform beam and transport this beam a short distance (10 to 25 cm) using an externally applied longitudinal magnetic field. Previous experiments on SNAF had shown that an applied field of 7.5 kG and 1000 nT were optimum transport parameters (Reference 8). Using these parameters, transport efficiencies of 75 to 80 percent were measured at the target location.

Diode Behavior. Two types of cathodes were used during the experiments; one was a field enhanced cathode that used roll pins for the emitter surfaces (as shown in Figure 2.2). The other type employed a solid emission surface fabricated from a high resistivity material such as graphite or conducting epoxy. Beams from the solid surface cathodes appeared to have less transverse electron energy as will be discussed later.

Impedance values for both cathode types were found to be in excellent agreement with the Langmuir-Child's law predictions

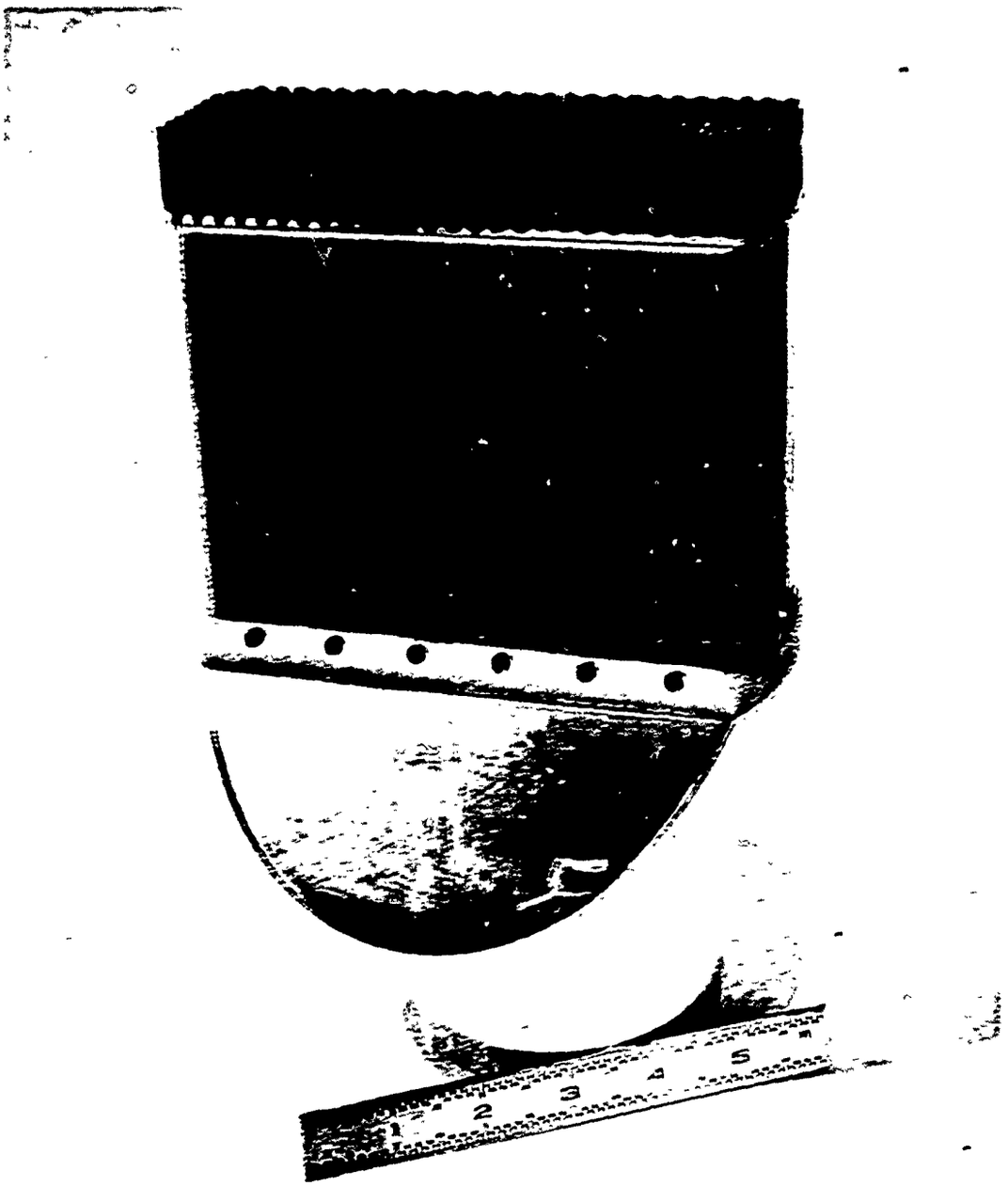

Figure 2.2 100 cm^2 rectangular cathode (2-1/4 in. x 7 in.)

A1430

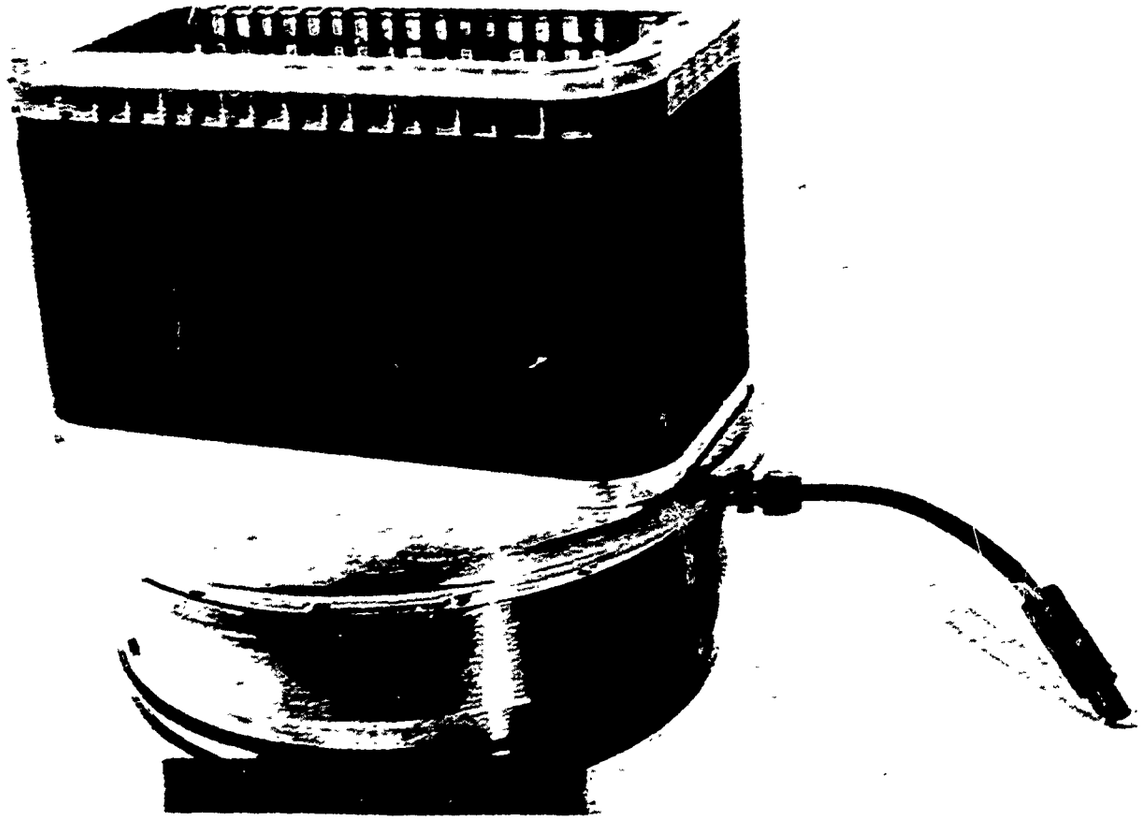

Figure 2.3 Magnetically transparent anode extension.

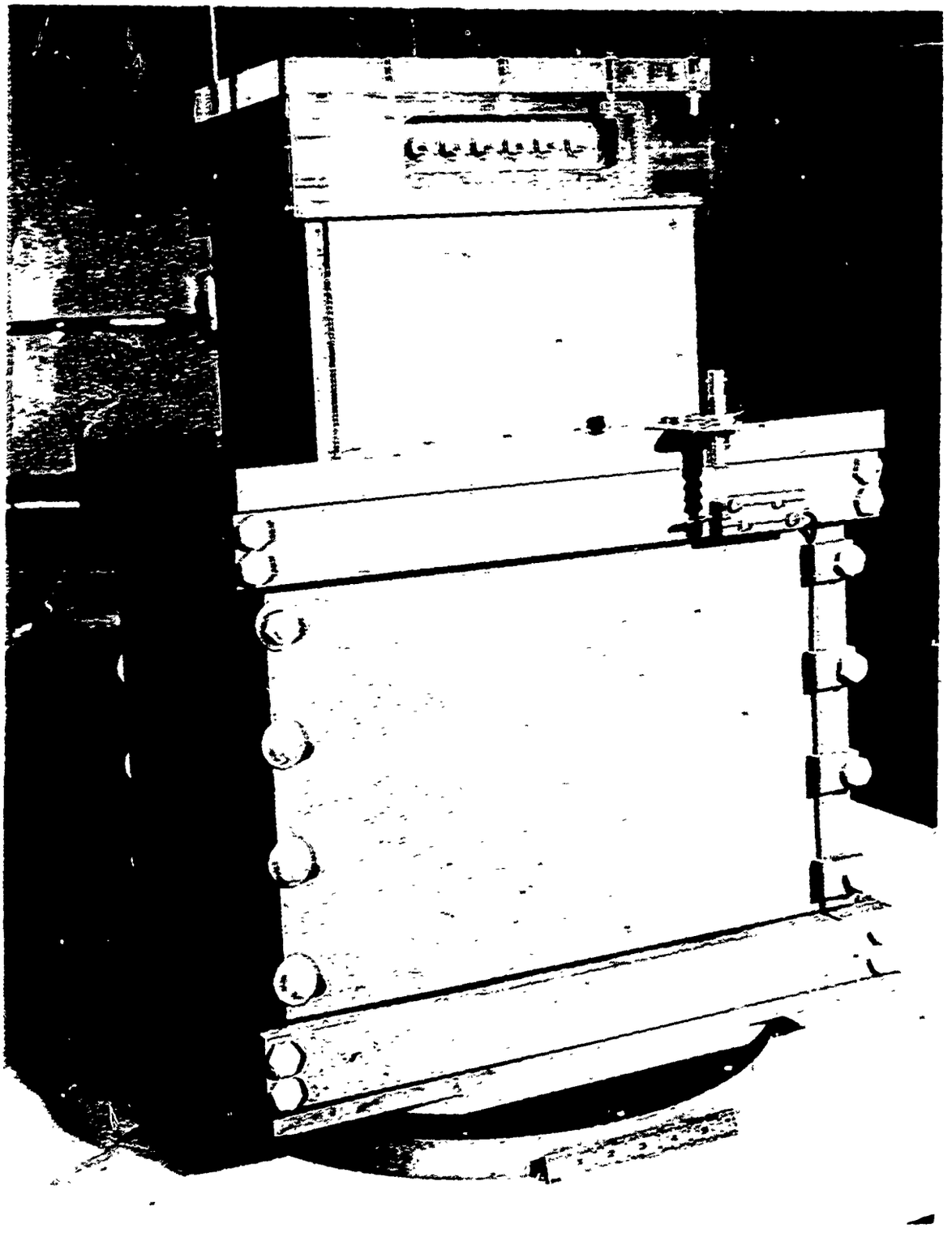

Figure 2.4 Magnetic field coil and vacuum chamber assembly.

A1425

for space charge limited flow, $Z = 136 d^2/V^{\frac{1}{2}}(MV)A$ (where d = anode-cathode gap and A = cathode area). Impedance data is shown in Table 2.1 for a wide range of anode-cathode gap spacings. Agreement with Child's law is typically within 10 percent.

Diode impedance lifetimes were more than sufficient for the SNARK pulses. Impedance lifetimes of 110 to 120 nanoseconds were observed at gap spacings of 3 millimeters and the impedance lifetimes exceeded 150 nanoseconds for the 6 to 7 millimeter gap spacings normally used.

TABLE 2.1

DIODE IMPEDANCE AT PEAK CURRENT

Shot No.	Anode-Cathode Gap (mm)	Peak Voltage (kV)	Peak Current (kA)	Impedance (ohms)	Langmuir-Child's Law Predicted Impedance* (ohms)
800	4.5	600	555	1.08	1.12
801	4.5	600	575	1.04	1.12
1051	5.0	642	495	1.30	1.33
1055	5.0	690	476	1.45	1.29
1183	6.0	770	405	1.90	1.75
1186	6.0	800	478	1.67	1.72
1189	6.75	830	387	2.14	2.14
1209	7.75	820	350	2.34	2.83

$$^{*}Z_{LC} = \frac{136}{V^{\frac{1}{2}}(MV)} \frac{\pi d^2}{A}, \text{ where } A = 100 \text{ cm}^2$$

A rotation of the beam was observed during transit between the cathode and anode. A collimator with a 3 cm x 15 cm hole in it was placed behind the anode. Damage to the front face of the collimator indicated the beam rotated in the anode-cathode region while damage to a target 25 cm away indicated the collimated beam did not rotate (Figure 2.5). The angle of rotation was measured for several different values of B_z and is listed in Table 2.2. The rotation angle was also inversely proportional to B_z. Sample holders were fabricated to hold diagnostics at the proper angle to correct for the rotation.

TABLE 2.2

BEAM ROTATION VERSUS APPLIED FIELD

Angle of Rotation (degrees)	B_z (kG)
9	6.0
5	7.0
2	8.0

The diode impedance and impedance lifetime data quoted above refer to the 2¼ inch x 7 inch cathodes (100 cm^2) in a 7.5 kG magnetic field. Despite the gross effect of the field in preventing severe beam pinch in the anode-cathode gap, we found that the beam intensity at the anode plane was non-uniform for planar surface cathodes. Radiographic and calorimetric diagnosis of the beam from the flat cathodes indicated an intensity peak along the major axis of the cathode (Figure 2.6a). The cathode was subsequently shaped (dished) in the center until a uniform beam was achieved at the target (Figure 2.6b). The final shape of the cathode was dished along both axes with the center 2 mm

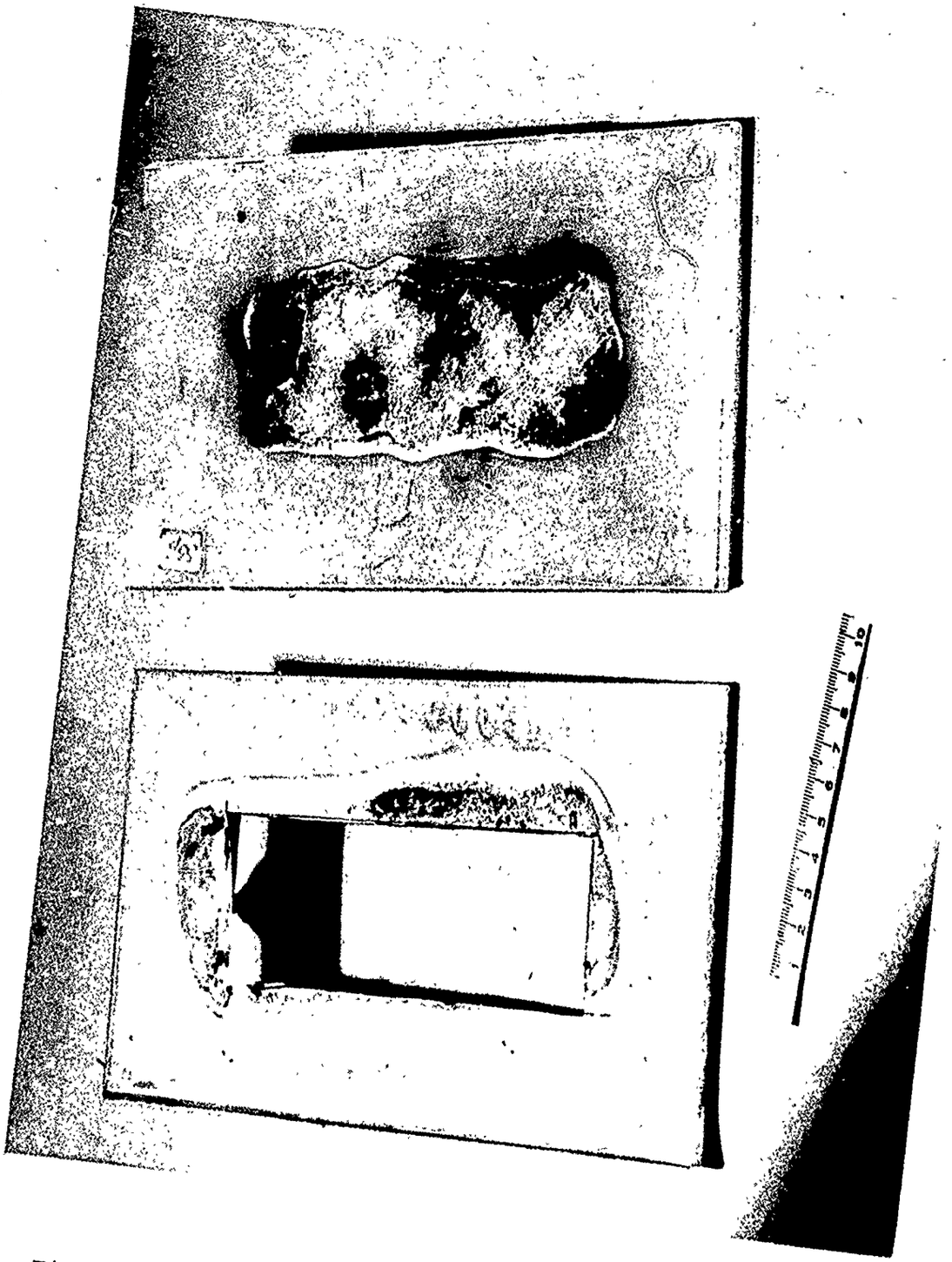

Figure 2.5 Rotation of the beam. Top sample was on the anode, bottom sample was 10 inches from the anode on the same spot.

A346

(a)

(b)

Figure 2.6 Radiographs of cathodes.
(a) Flat cathode showing nonuniform emission
(b) Transported beam after shaping

lower than the outer edges. Figure 2.7 shows the calorimetric results of the shaped cathode with a dotted outline of the total beam size. This calorimeter measurement shows fluence variation of less than 20 percent standard deviation, with an extreme variation of ± 30 percent.

Transported Beam Characteristics. Transported beam characteristics were dependent on both the field strength and cathode type. With the roll-pin cathodes there was some expansion of the beam during transport and some fluting at the edges. The amount of expansion and the peak to peak size of the flutes is inversely proportional to the applied magnetic field and is of the order of the Larmor radius (~ 0.5 cm). Beam areas were typically 120 to 130 cm^2 and 75 to 80 percent transport efficiencies were observed.

The beams from solid surface cathodes showed different transport behavior. The most striking feature of the beams produced with a graphite cathode was the absence of beam divergence. The transported beam was the same size as the emitter surface. Shaping the graphite cathode in the same manner as the roll pin cathode produced a reasonably uniform beam. One disadvantage of the graphite cathode was the adhesion of anode and target debris to the surface. It was necessary to scrape the cathode after each shot resulting in surface scratches that produced hot spots in the transported beam. In an effort to eliminate this problem a search was made for a hard, high resistivity material. A copper conducting epoxy was tried that produced the same results as the graphite cathode except molten material did not adhere to its surface. It also had another advantage, once the desired cathode shape was attained, a mold could be fabricated, and subsequent cathodes could be poured to the correct shape.

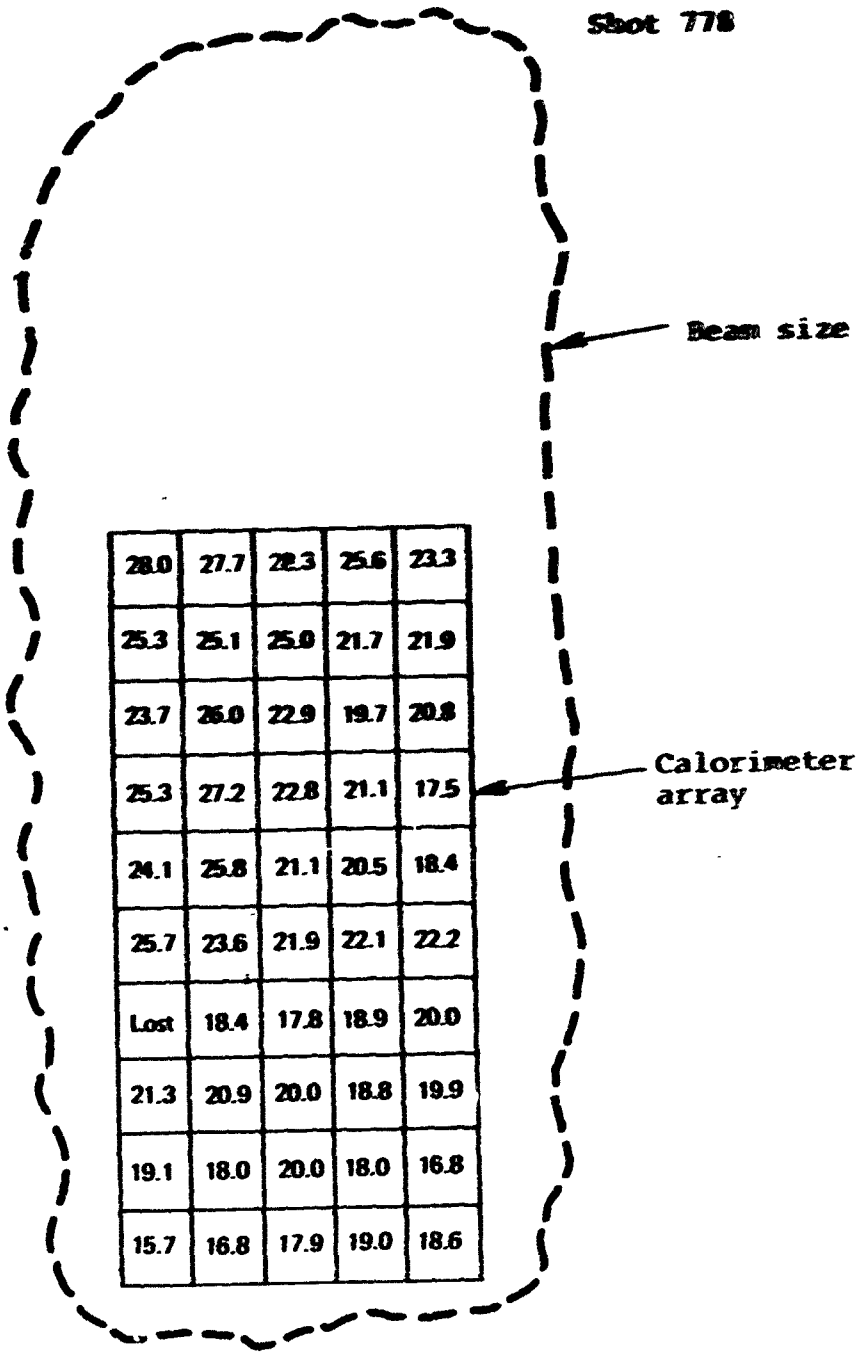

Figure 2.7 Calorimeter output of beam after 10 cm transport. Average cal/cm^2 = 21.6+3.3; Area = 120 cm^2; Total energy at target = 2600 cal = 11 kJ; Energy in injected beam = 15 kJ.

The absence of beam divergence with the solid surface cathodes immediately suggested that the beam was colder, meaning less transverse electron energy and therefore a smaller gyro-radius. Since the high resistivity cathodes had smooth emission surfaces the electric fields produced are nearly normal to the cathode surface, while the field lines from a roll pin are not everywhere normal to the plane of the emission surface. This results in significant radial electric fields. This radial electric field will produce an electron beam with more transverse electron energy. For a given cathode size and a constant anode cathode spacing the conducting epoxy cathodes were slightly lower impedance than the roll pin cathode where the impedance of a cathode is inversely proportional to the area of the emission surface. A solid cathode has more emission area than a roll pin cathode thus agreeing with the inverse area dependence.

The transport efficiency for the high resistivity cathodes appeared to be lower (60 to 65 percent) than those produced from the roll pin cathode. It is possible that loss due to shank emission was enhanced by the use of a high resistivity emission surface. The loss mechanism was not investigated in this program but it is believed that a more careful design of the cathode shank and reducing the thickness of the high resistivity cathode will minimize electron loss. Even though the transport efficiency was less for the conducting epoxy cathodes, the fluence at the target remained comparable to that for the roll-pin cathodes since they produced smaller area beams.

Damage craters in flat targets were used as a gross measure of beam size and uniformity. Figures 2.8 and 2.9 show typical damage craters in sparesyl and epoxy samples. The epoxy sample also shows a uniform rear surface spall crater over ~ 130 cm^2 in addition to a front surface vaporization crater. Damage craters from the 100 cm^2 beams were similar.

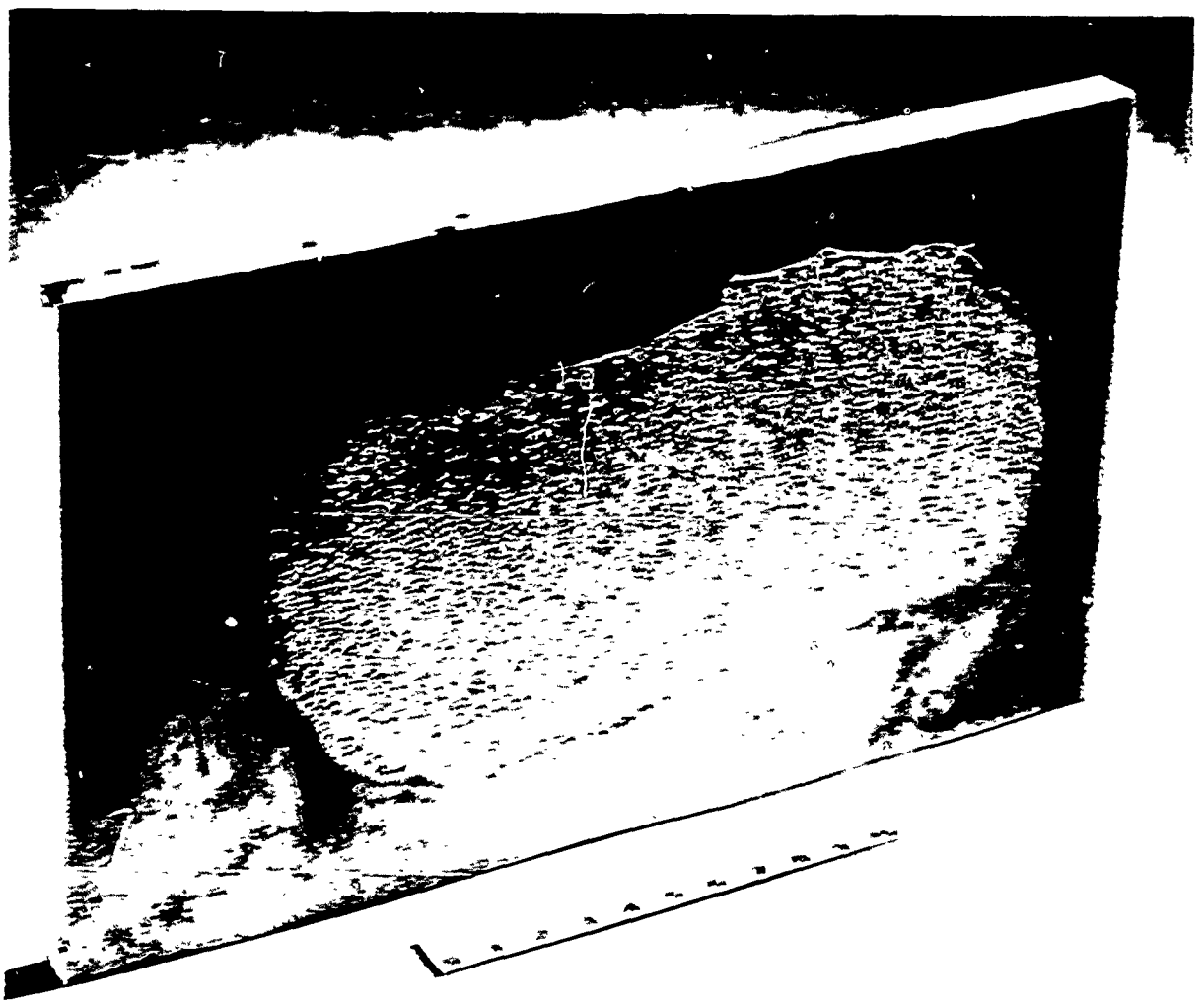

Figure 2.9 Front surface crater produced in spacesuit sample. Approximately 130 cm^2 irradiation area.

(a) Front surface crater

(b) Rear surface spall area

Figure 2.9 Damage to 1/2-inch-thick epoxy.

A684

More detailed characterization of the beams was accomplished with calorimetry. Calorimetry included "standard" 1 cm x 1 cm graphite blocks mounted in 25 cm^2 square arrays, as well as several other calorimeters developed during the program. These included a graphite block curved calorimeter, graphite foil (0.005 inch) depth-dose stacks, "button" type graphite fluence calorimeters (1 cm^2 discs), and a high resolution relative uniformity diagnostic consisting of a tantalum foil and a shielding block with small holes backed by TLD's (in this case the bremsstrahlung radiation produced in the tantalum was monitored at selected points with thermoluminescent dosimeters). Descriptions of these diagnostics are given in the Appendix.

Results of the fluence measurements over planar areas after beam transport to the target have been summarized in Section 1.2. Fluence levels of 40 cal/cm^2 over 130 cm^2 at peak voltages of 850 kV (mean voltages up to 650 kV) have been measured.

Energy deposition in surfaces curved with respect to the beam direction was investigated by use of the curved calorimeter. This calorimeter was comprised of an array of pairs of flat blocks (one normal to the beam direction and the other angled to the beam direction) which approximated a 6-inch-diameter ring. The results from the curved calorimeter shots show approximately equal total energy deposited in the angled blocks and in the normal blocks (within the accuracy of the data). The average ratio of the energy deposited in the angled blocks divided by the energy in the normal blocks for 6 shots is plotted as a function of position in Figure 2.10. The ratio is approximately unity for all of the positions. This result is surprising in view of the fact that increased electron reflection has been observed when targets are angled with respect to the incident

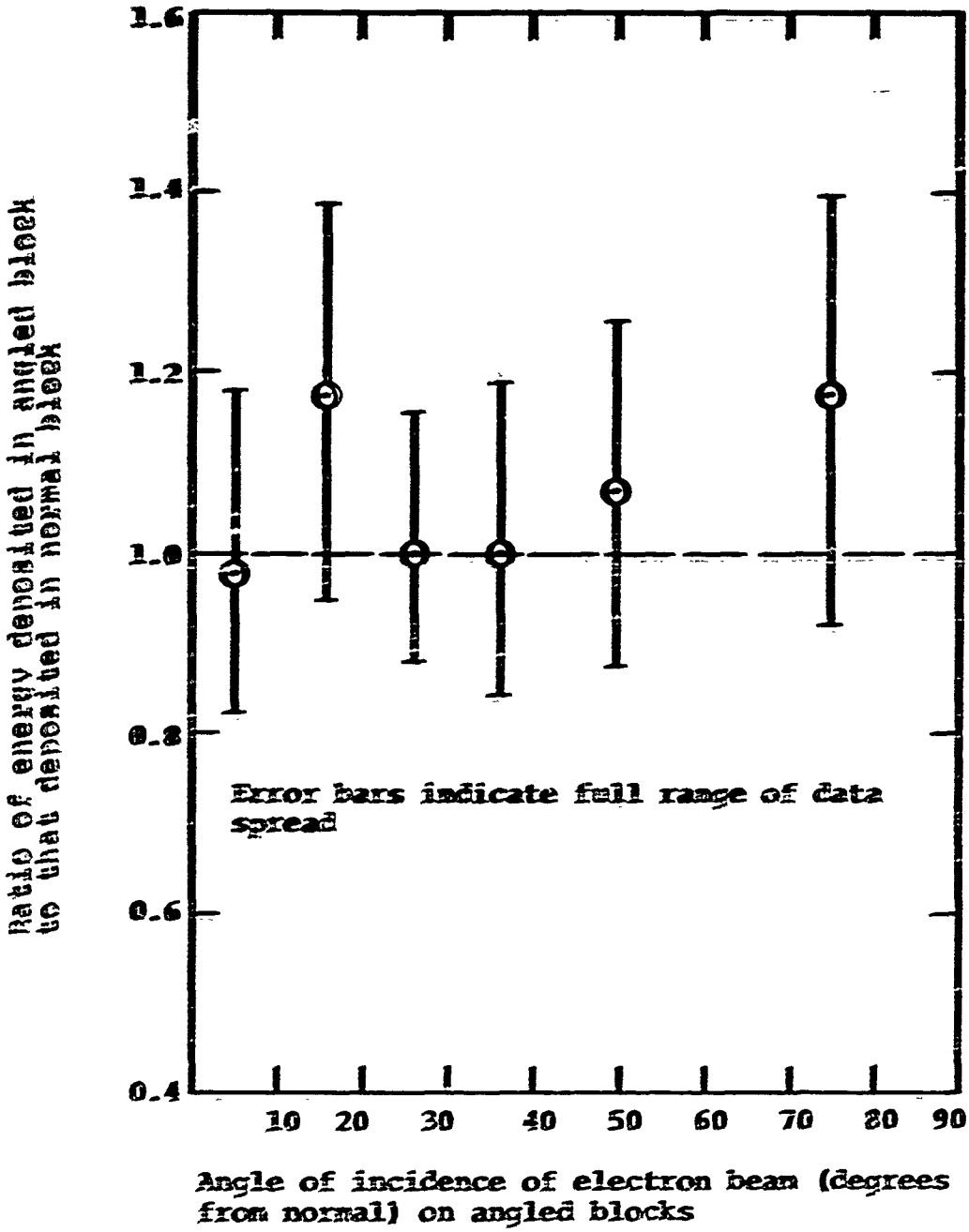

Figure 2.10 Variation of energy deposited in angled and normal blocks.

electron direction (for the case of no guide fields). Apparently the longitudinal magnetic field acts to prevent massive electron reflection from angled surfaces to produce a cosine-like fluence loading around the surface of a ring.

Although some difficulty was experienced with loss of calorimeter blocks, useful data could be obtained from most shots since there were two pairs of blocks at each incidence angle. Figure 2.11 shows a typical calorimetric output. If one assumes values for the missing blocks and corrects for the fact that the calorimeter has an area of 58 cm^2 and the beam an area of 120 cm^2, the energy in the transported beam is 11 kJ. There was 15 kJ in the injected beam giving a transport efficiency of 75 percent.

When a cylindrical ring is placed in the beam of electrons the fluence should vary approximately as cos θ, where θ locates a given point on the ring. All of the data from the angled blocks was normalized to the same fluence level and averaged. Figure 2.12 shows a plot of these points with cos and cos^2 curves shown for reference. The points fit the cos^2 curve better than they do the cos curve. The reason for this is unclear since the fluence is measured to be relatively uniform over a flat plane. It is possible that the boundary condition affected by the curved beam termination causes slight beam expansion as the beam center is progressively removed by the convex target.

Deposition prifiles were measured for several different mean electron energies. One depth dose calorimeter was placed normal to the beam at the center of the beam while another one was placed normal to the beam but at the edge of the beam. The two deposition profiles were similar indicating that there was

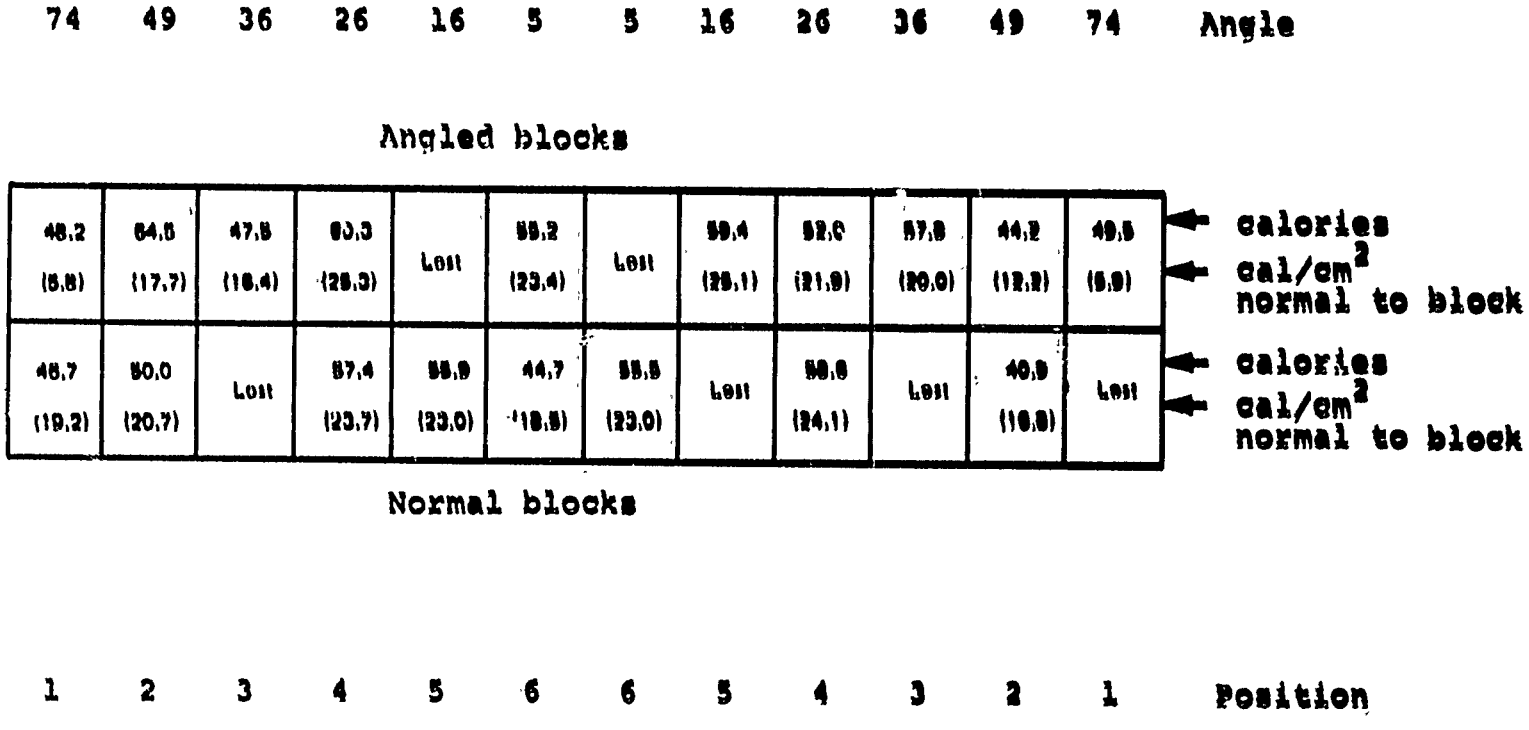

Figure 2.11 Output of curved fluence calorimeter.

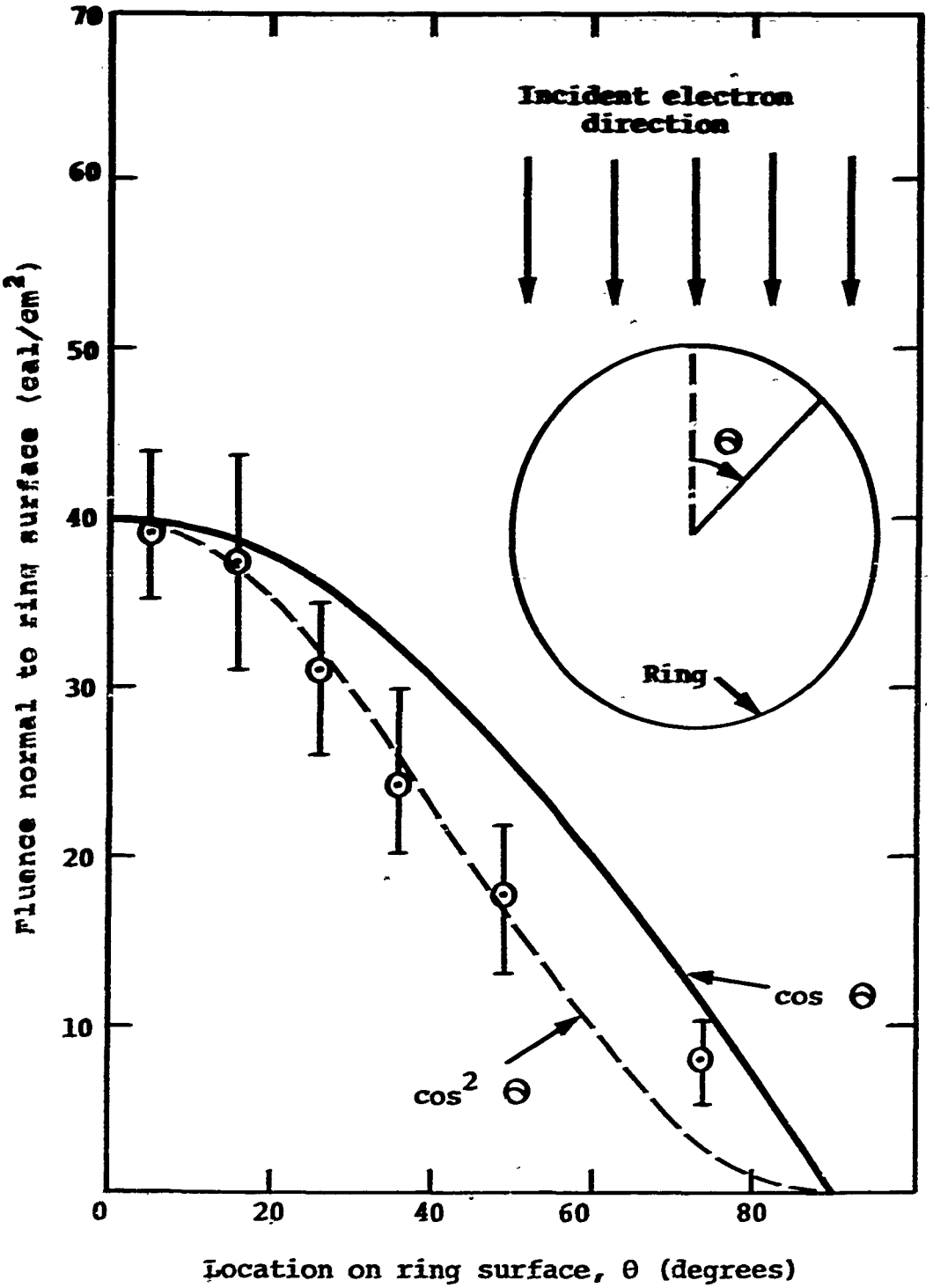

Figure 2.12 Measured loading of a ring surface.

little change in beam characteristics from the center to the edge. The electron energy spectrum given from the voltage and current monitors was used to calculate electron deposition profiles for different mean angles of electron incidence (transverse velocity components). These calculations were performed with a Monte Carlo electron transport code. Figures 2.13, 2.14, and 2.15 show comparisons between the measured and calculated deposition profiles. The measured deposition profiles using a roll pin cathode are best fit by calculations assuming approximately a 50 degree average angle of electron incidence $\langle\theta\rangle$. This indicates that $\gtrsim 1/2$ the electron energy is in motion transverse to the propagation direction (presumably in helical motion around the longitudinal magnetic field lines).

The normal (90 degree) depth dose calorimeter at the edge was then replaced by a 45 degree depth dose calorimeter and the shots repeated to determine if the deposition profile was altered when the energy was deposited in an angled target. Typically the 45 degree depth dosimeter did show a change in the deposition profile (Figure 2.16), in that the front surface dose appeared to increase slightly. Use of thinner calorimeter foils would give more resolution of this apparent effect. The deposition profiles and the fluence for both the conducting epoxy and the roll pin cathodes were similar.

Figure 2.17 shows selected energy deposition profiles measured from 300 keV to 600 keV mean electron energy beams. These measurements were also taken with the graphite depth dose calorimeter (graphite foil density 1.80 gm/cm^3).

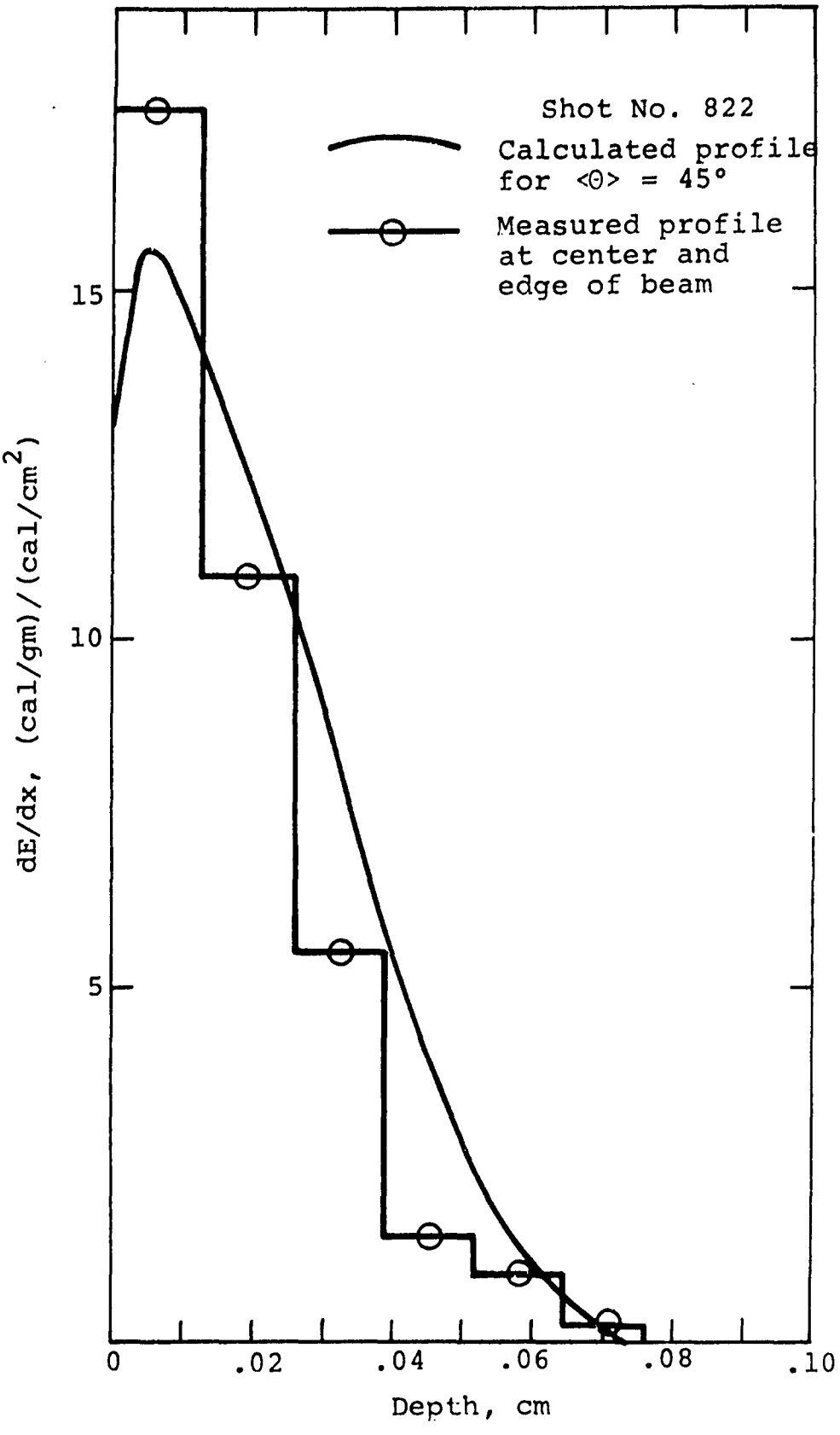

Figure 2.13 Electron deposition profile for <E> = 300 keV.

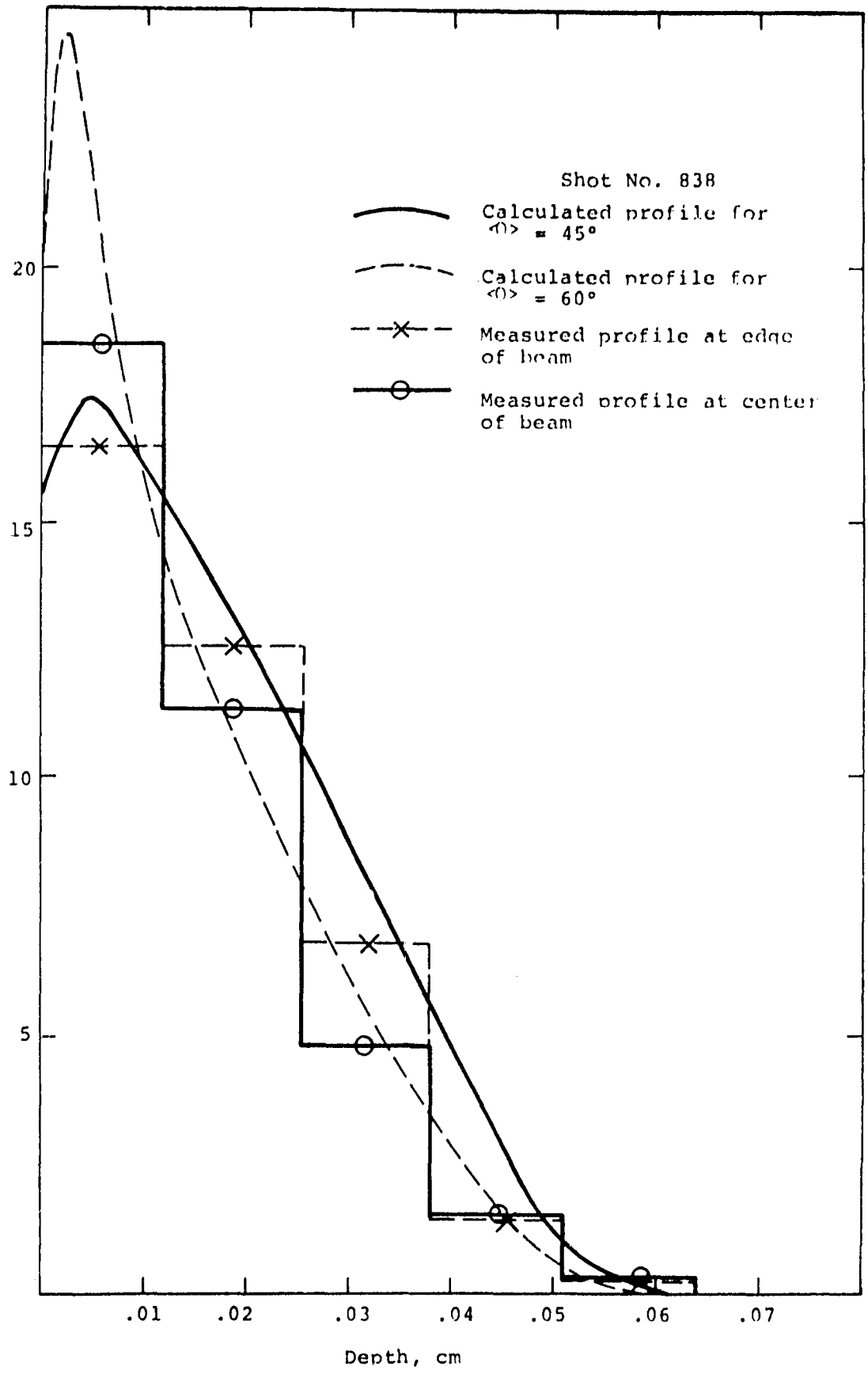

Figure 2.14 Electron deposition profile for <E> = 332 keV

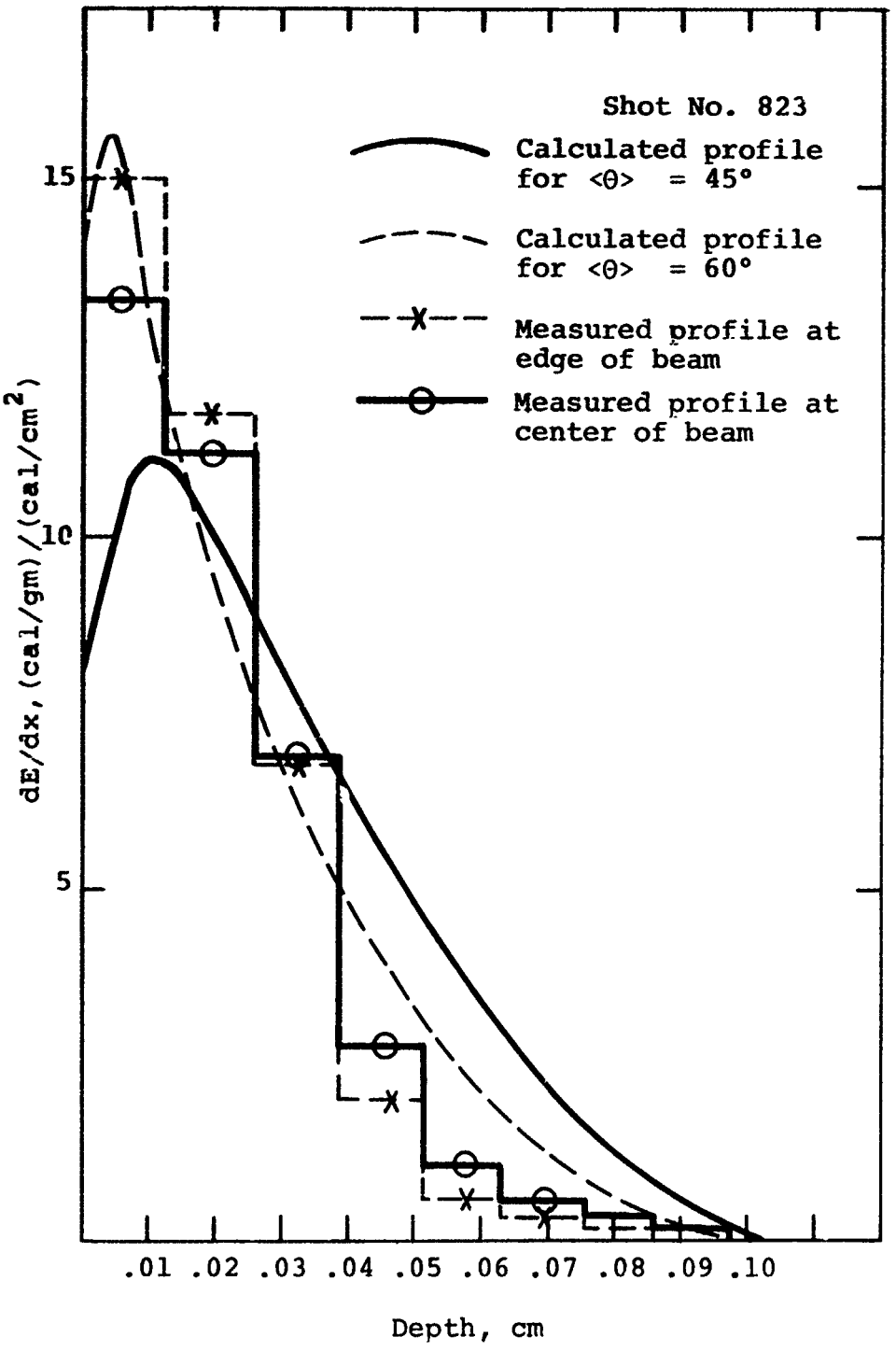

Figure 2.15 Electron deposition profile for <E> = 420 keV.

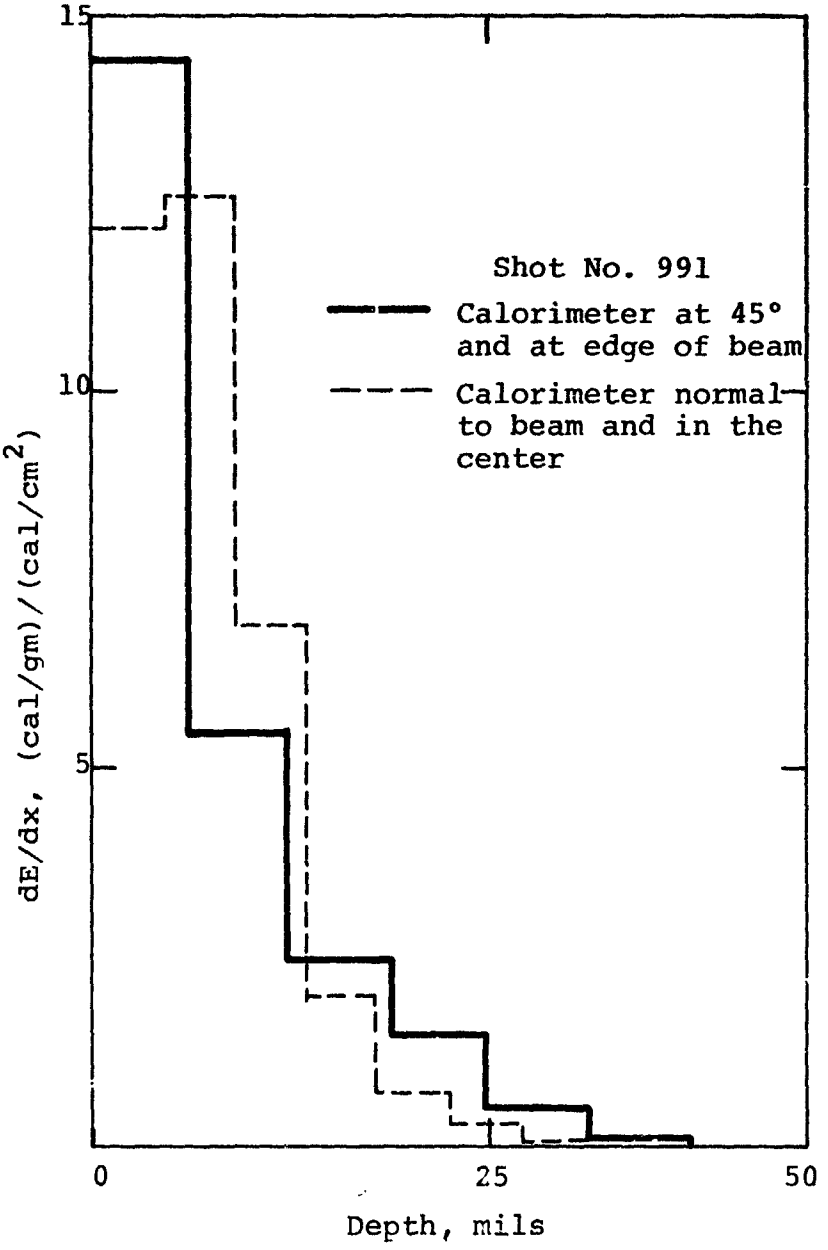

Figure 2.16 Electron deposition profile for <E> = 420 keV

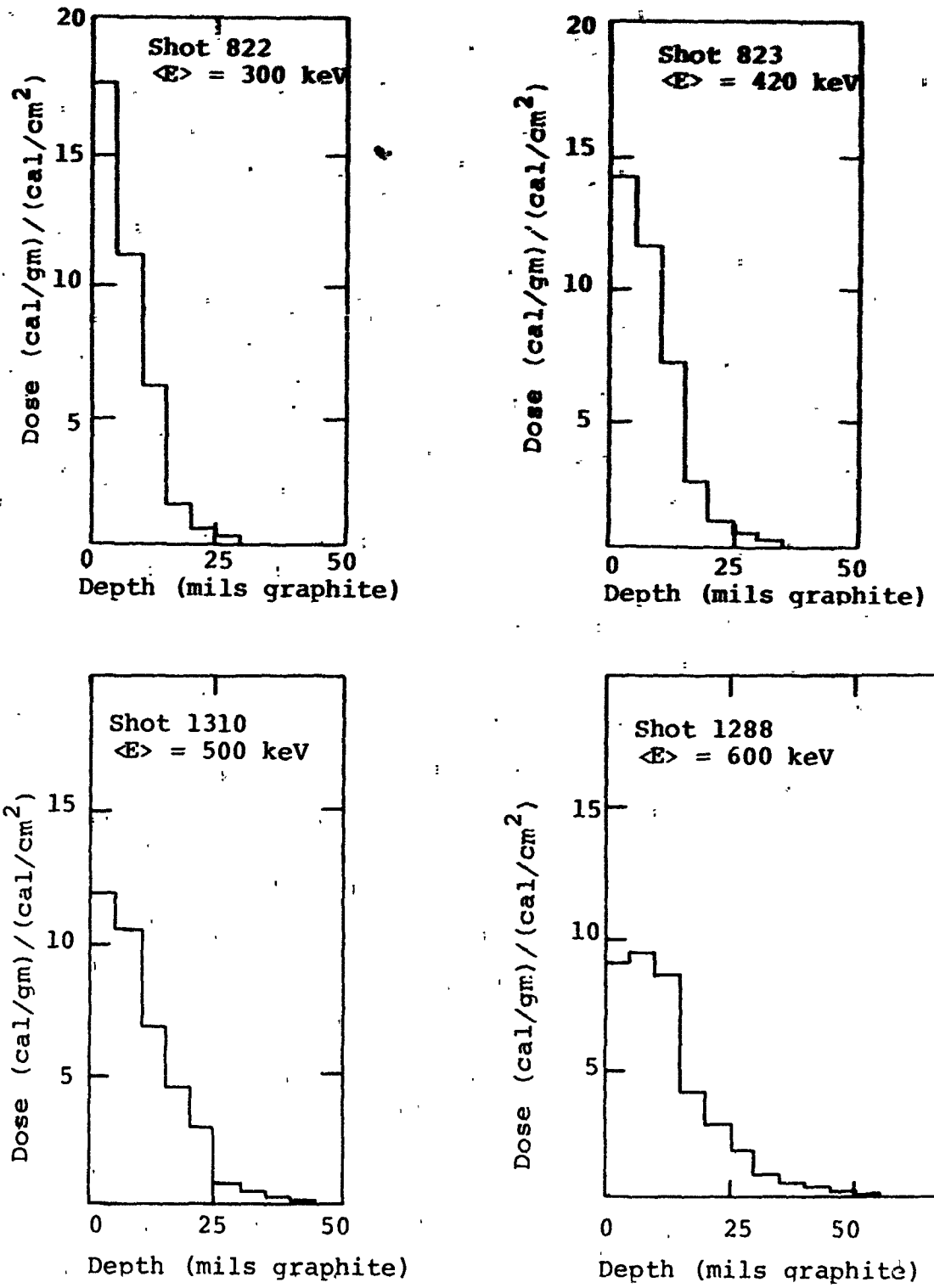

Figure 2.17 Energy deposition profiles from 300 to 600 keV

As discussed in preceding paragraphs, cathode shaping was performed to generate beams uniform to ± 20 percent within the resolution of the 1 cm^2 fluence calorimeter blocks. More finely resolved diagnosis with the TLD array dosimeter and X-radiography revealed small scale $\lesssim$ 1/4 cm^2 non-uniformities in the beams. These characteristics were interpreted to arise from localized high spots on the cathode surface which emitted higher than average current density. A somewhat more uniform beam was produced with the conducting epoxy cathode than with the roll pin cathode. When the electron beam impinged on an aluminum target, there was some nonuniform back spall produced. In an effort to produce a more uniform beam scattering foils were placed between the anode and the target plane.

Scattering foils make the electron beam more uniform by "smearing out" local irregularities in fluence. When an electron passes through a foil that is thin compared to the electron range, there is a probability that it will be scattered through an angle θ. If, for example, all electrons at a point X enter the foil normal to the surface, then they will emerge with a range of angles and therefore cover a larger area because the transverse energy that has been introduced makes the particles gyrate around the applied field lines and cover an area of πr^2 (where r is the radius of gyration). By passing through several foils the inhomogeneity can be spread over several gyroradii.

The maximum uniformity is obtained when the scattering is maximized but this also maximizes energy deposited in the foils. Since it is desired to deliver as much energy as possible to the sample and not the scattering foils, a compromise must be reached that balances fluence against uniformity.

The calorimeters are only sensitive to macroscopic non-uniformities. The microscopic nonuniformities were diagnosed by the rear surface spall of an aluminum target. Samples shot without scattering foils showed nonuniform back spall suggesting "hot-spots" in the beam. Samples shot with scattering foils did not show this. Figure 2.18 shows a comparison of targets shot at the same energy levels with and without scattering foils. To show that scattering foils did allow electrons to cross magnetic field lines, a one-inch-wide piece of polyethylene was placed immediately behind the anode producing two beams, each 2½ inches by 3 inches. When these two beams were transported through scattering foils, they combined to form a rectangular beam, Figure 2.19.

2.1.4 Summary and Conclusions. The technique of large area beam generation and control using external longitudinal magnetic fields has been successfully applied to the SNARK generator. Hardware and diagnostics have been constructed and are now part of the existing SNARK facility. Present hardware can produce 100 to 130 cm^2 area beams and the technology has been developed to allow easy access to both larger and smaller irradiation areas. The magnetic field system is a relatively slow period pulsed solenoid which allows placement of conducting samples at the target plane with minimal perturbation to the sample and/or the applied field.

Fluence levels and deposition profiles have been measured throughout the operating range of SNARK (300 keV to 650-keV mean electron energies). Fluence levels of 40 cal/cm^2 over 130 cm^2 are available at 650 keV mean corresponding to peak dose levels of 250 cal/gm and heating to 55 to 60 mils of graphite.

Figure 2.18 a Beam uniformity. Front surface damage, no scattering foils.

A1421

Figure 2.18 b Beam uniformity. Pear surface damage, no scattering foils.

A1427

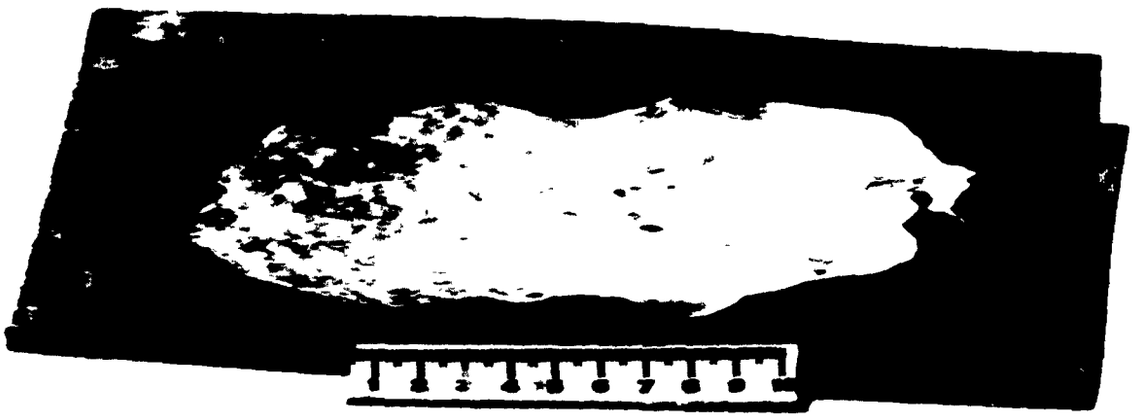

Figure 2.18 c Beam uniformity. Front surface damage, with scattering foils.

A1424

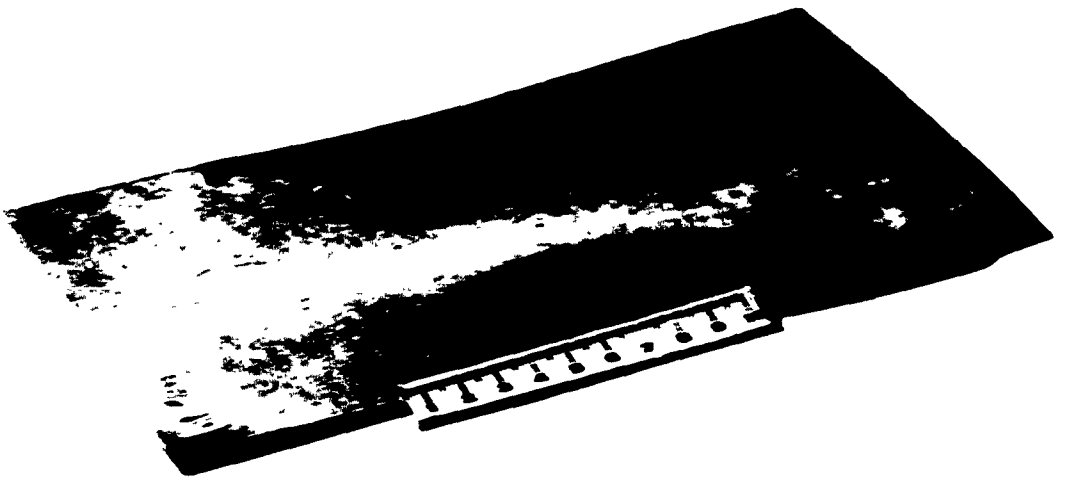

Figure 2.18 d Beam uniformity. Rear surface damage, with scattering foils.

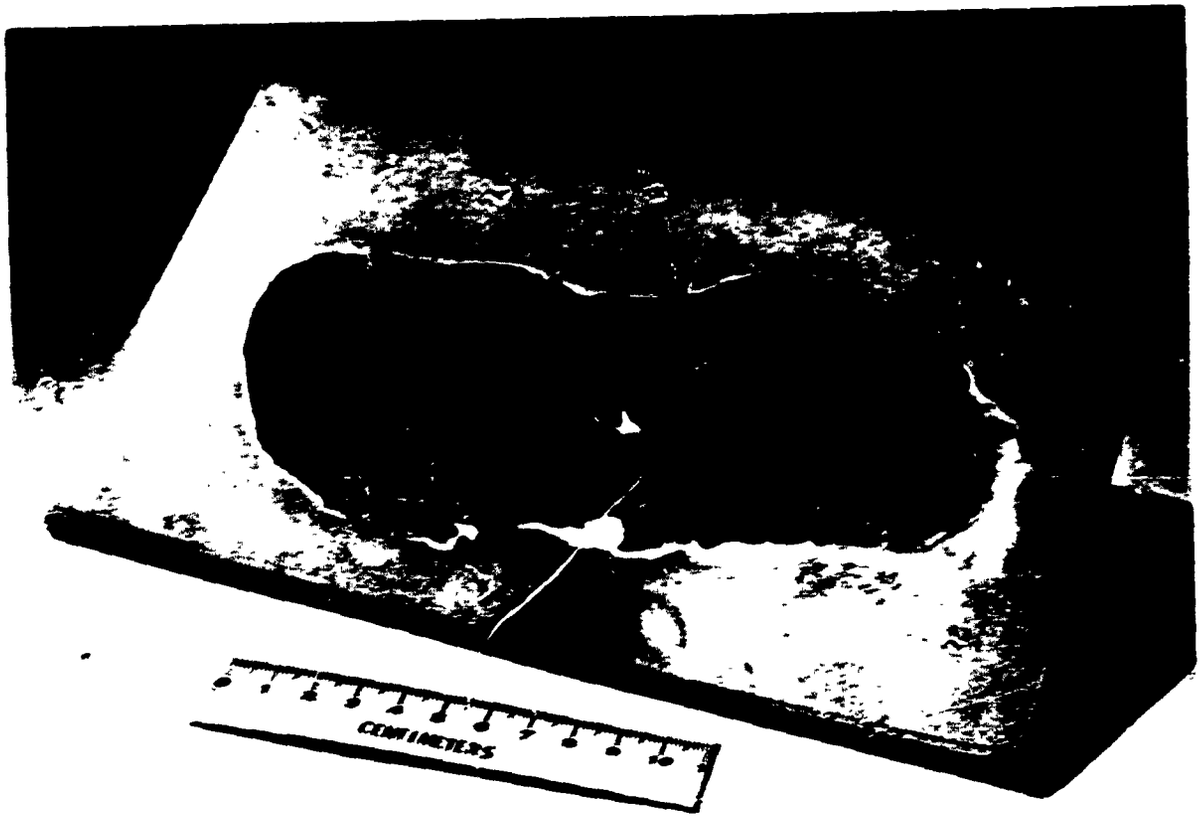

Two 5.6-cm x 8.4-cm beams were propagated 1 cm apart. These two beams passed through five foils of ¼-mil Mylar and merged except for a single spot in the center.

Figure 2.19 Merging of two beams.

A1103

Gross fluence uniformity of ±20 percent (1 cm^2 resolution area) has been obtained by means of cathode shaping. Smaller area nonuniformities have been effectively eliminated by means of solid surface cathodes and scattering foils placed between the diode and the target.

Transport efficiencies of 75 percent are notably lower than those typically found in the linear transport experiment described in Reference 8. During the recent advanced X-ray converter work (DNA contract 01-71-C-0052) several experiments had the cathode shanks at angles to the applied B_z fields. This arrangement typically gave lower transport efficiencies than those in which the shank was parallel to the direction of the applied B_z field. The combination of the angled surfaces and the fact that the applied field is diverging in that region could enhance electron loss to the anode extension pieces. Reference to Figure 2.1 of this report shows that the present experiment has an angled surface in the diverging field region. In this region electrons are probably being lost resulting in a somewhat lower transport efficiency. This phenomenon was not realized until late in the program and it was decided not to correct the situation since it would involve an extensive modification to the hardware. Future hardware will be designed in such a way to eliminate this problem.

2.2 SMALL AREA ($\lesssim$ 10 cm^2) ELECTRON BEAMS

Small area electron beam development was attempted in three separate experiments, the first two of which were supported under this program. The most successful technique to date utilizes beam compression in a converging magnetic field from an initial 25 cm^2 circular beam area to deliver 80 to 90 percent of the diode energy to a 9 to 10 cm^2 circular area. Fluence levels obtained by this technique have been summarized in Section 1.2. The first attempt at small area beam generation utilized a small area cathode ($\sim$ 5 cm^2) placed in a uniform magnetic field. Section 2.2.1 discusses this work and the limitations of the approach. Although average fluence levels of 100 to 200 cal/cm^2 were obtained, the beam uniformity was generally poor and total beam energy was low.

The second approach (detailed in Section 2.2.2) was a return to the neutral gas-guide cone beam control technique. The tests were technically successful in that the loss of energy due to

lack of containment of high transverse energy electrons agreed with past work (only 25 to 30 percent of the diode energy reached the target location). Beam uniformity was greatly improved over that observed in the first approach. Fluence levels of 100 to 125 cal/cm^2 over 5 cm^2 were achieved.

The third and most successful approach (beam compression in a converging magnetic field) is outlined in Section 2.2.3. Results to date indicate acceptable uniformity and high transport efficiency. This technique is felt to have the greatest potential for generation of high fluence environments over ~ 10 cm^2 on SNARK.

2.2.1 Small Area Cathode in a Uniform Magnetic Field. The first approach to generation of small area ($\leq$ 10 cm^2) electron beams was a straightforward extension of the successful technique found for control of large area beams; i.e., use of a small area cathode in a uniform external longitudinal magnetic field extending from the cathode to the target. The diode region was configured as shown in Figure 2.20. Experiments indicated this technique to be of marginal usefulness for the following reasons:

1. Impedance of the 5 cm^2 cathode was found to be too high for efficient transfer of energy from the pulse lines to the load (attempts at lowering the diode impedance by decreasing the anode to cathode gap spacing resulted in very short impedance lifetime and minimal transfer of energy from the pulse lines to the load).

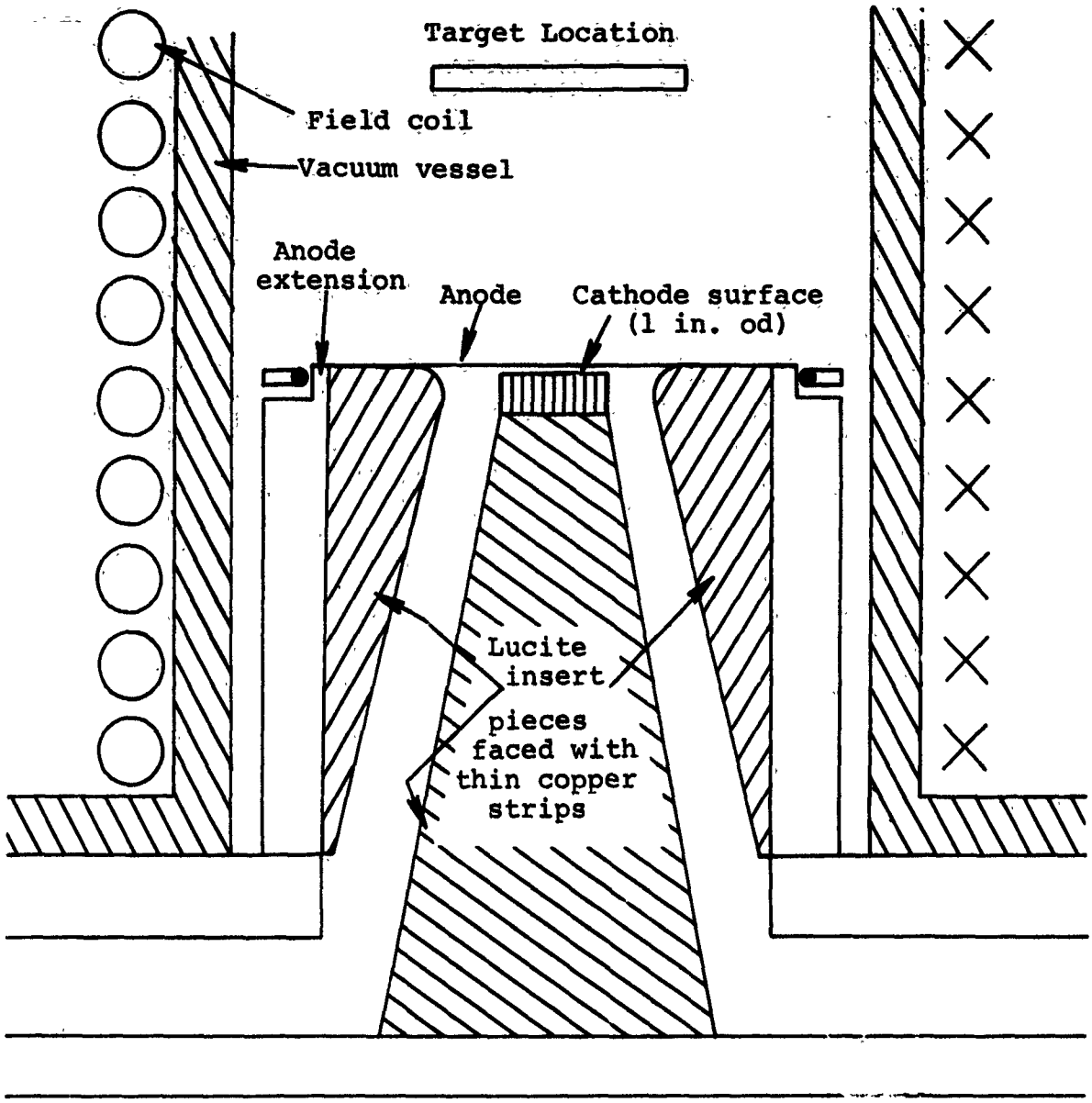

Figure 2.20 Diode configuration used in first small area beam control experiment.

2. Significant shank emission (electron emission from the cathode stalk surface to the anode extension) produced cumulative damage to the copper strips which formed the cathode stalk and anode extension surfaces. This energy was not available in the form of an extractable electron beam. Our conclusion is that shank emission is enhanced by the B_z field lines which connect the cathode stalk and anode.

3. Fluence uniformity at the target location was poor. Although average fluence levels of 100 to 200 cal/cm^2 were obtained the damage pattern produced in graphite samples showed the existence of local hot spots in the beam.

2.2.2 Neutral Gas Focusing in Conducting Guide Cones. In view of the relatively low total energy which was contained in the small area beams, using the longitudinal guide field technique, we decided to apply the technique of neutral gas beam focusing (without external fields) that has been useful on lower current machines. We expected and observed significant total beam energy loss with this technique (25 to 30 percent of the injected energy reached the target location), however the fluence uniformity was greatly enhanced. Fluence levels of ~ 125 cal/cm^2 were produced over 5 cm^2 at mean electron voltages of 400 kV.

Beam uniformity and transport away from the exploding anode were obtained by gas-focusing in a graphite guide pipe, shown in Figure 2.21.

Fast diagnostics were used to obtain accurate representation of the voltage, diode current, net current and primary current. These diagnostics are required in order to accurately determine the deposition profile for a particular sample irradiation.

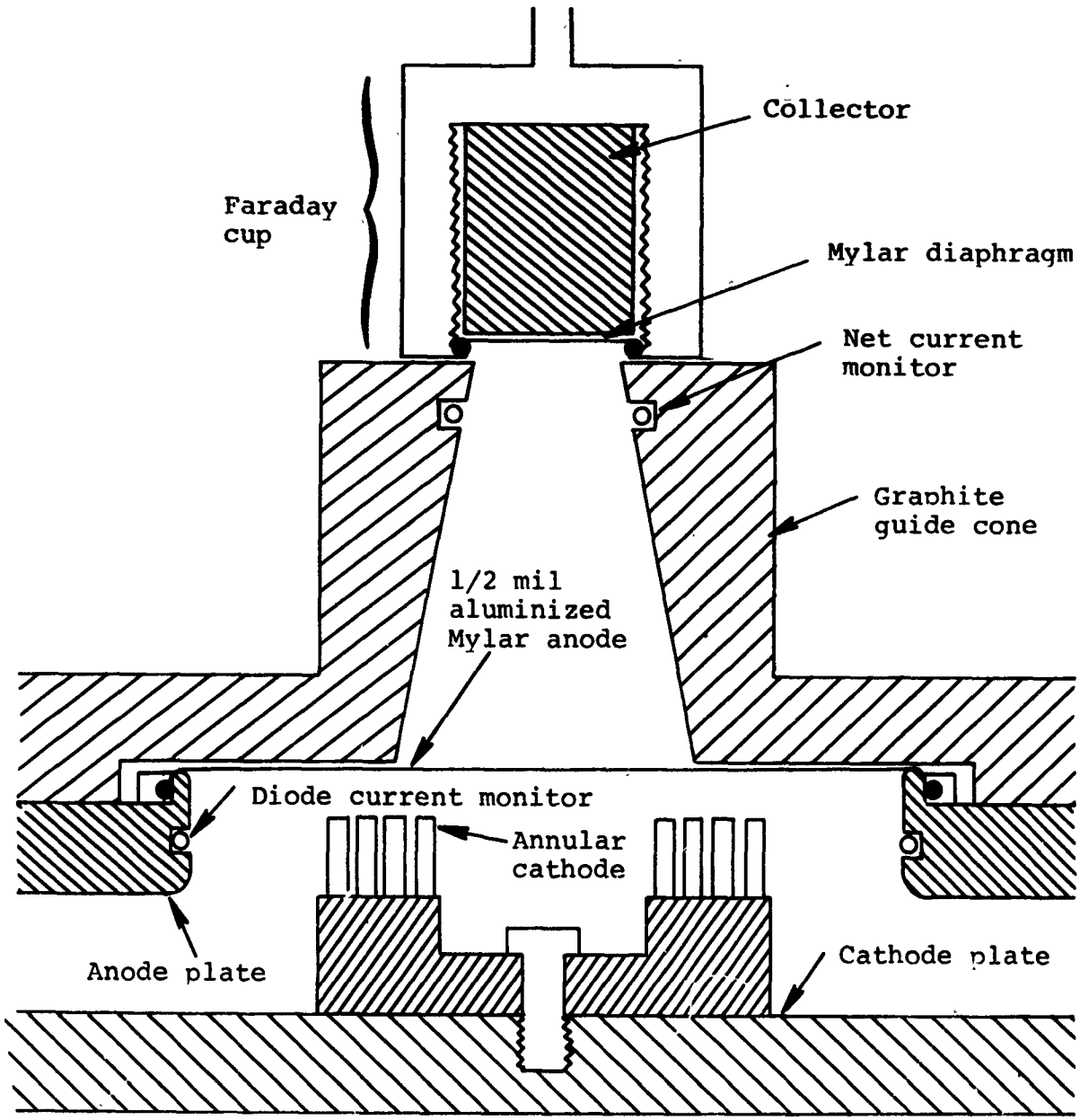

Figure 2.21 Graphite guide cone geometry and beam diagnostics.

The capacitive line voltage monitor, in addition to measuring the diode voltage, will also measure the inductive voltage drop across the tube insulator structure. A subtraction of the inductive component (determined by shots in which the diode voltage is zero, i.e., shorted) must be made on the recorded waveform. Primary current measurements cannot be made during an actual sample irradiation. Hence, correlations must be obtained between measured primary current, net current, and diode current. By careful control over drift chamber pressure, diode impedance, and line output voltage, it was possible to make a very accurate ($\leq \pm 10$ percent) scale of primary currents for sample shots from diagnostic shots in which a Faraday cup was used. The correlation between Faraday cup current and diode current is shown in Figure 2.22. The product of primary current waveform and accelerating voltage will yield the total calories in the beam as shown in Figure 2.23.

In addition to the voltage waveform and power spectrum, it is necessary to have an estimate of the mean angle of incidence for the primary electrons to obtain an accurate deposition profile. The fact that the electrons strike the target with a non-normal angle is caused by the transverse energy of the beam. By knowing the accelerating voltage, net current, and primary current, the average angle $\langle\theta\rangle$ at any instant in time can be estimated from (Reference 3):

$$\tan \langle\theta\rangle = \sqrt{\frac{\langle\beta_\perp{}^2\rangle}{\langle\beta_\parallel\rangle^2}}$$

$$\frac{\langle\beta_\perp{}^2\rangle}{\langle\beta_\parallel\rangle^2} = \frac{2}{\sqrt{\left(\frac{34 \times 10^3 \beta\gamma}{I_{pr}(1-f_m)^{\frac{2}{2}}}\right)^2 + 1} - 1}$$

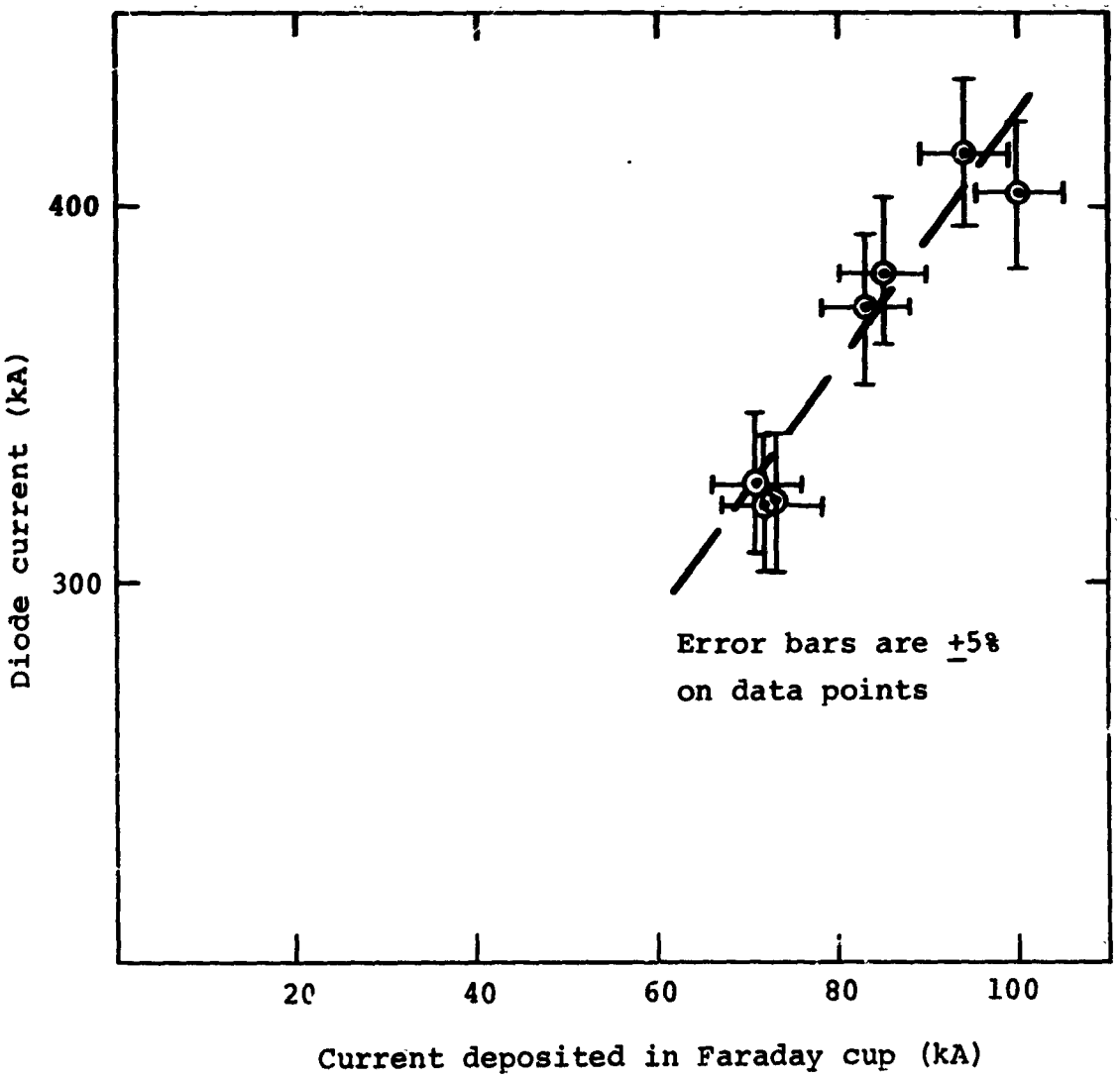

Figure 2.22 Diode current--Faraday cup current correlation

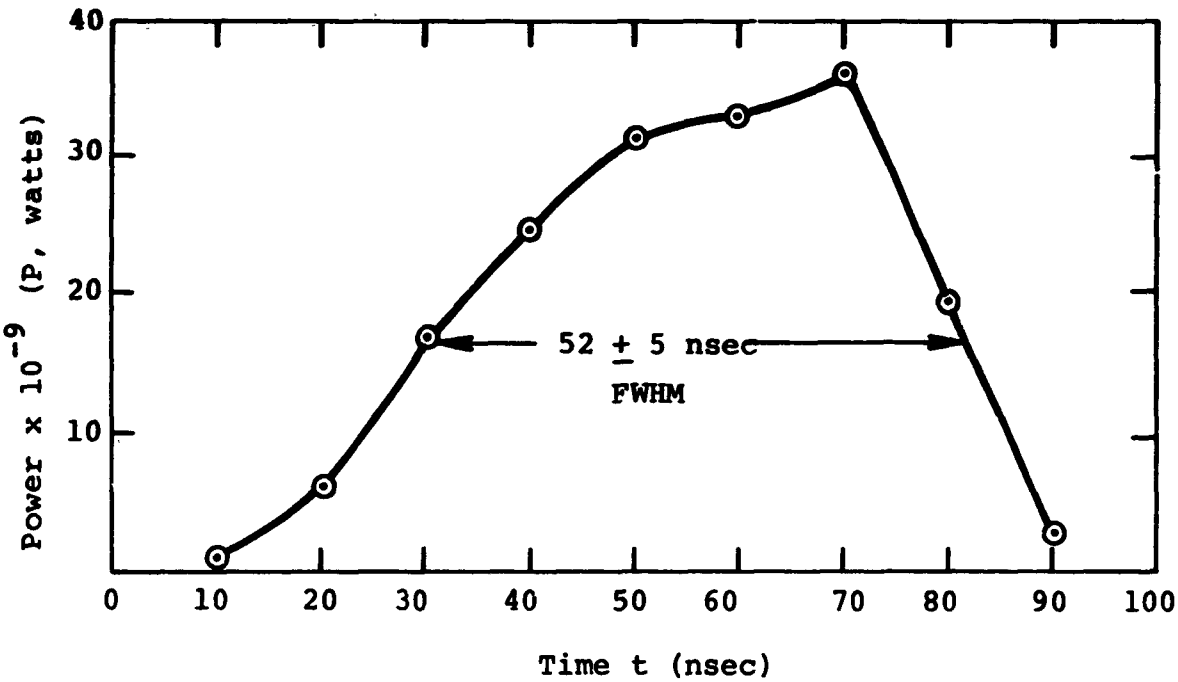

Figure 2.23 Electron beam power versus time

where I_{pr} = primary current (amps)

$\beta_\perp$ = transverse electron velocity/velocity of light

$\beta_\parallel$ = longitudinal electron velocity/velocity of light

$$\beta^2 = \beta_\parallel{}^2 + \beta_\perp{}^2$$

$(1-f_m) = I_{pr}/I_{net}$, $I_{net} = I_{pr}$ minus backstreaming plasma current

This angle has been determined as a function of time during the electron pulse and is shown in Figure 2.24. The mean angle is averaged over the power pulse by

$$\langle\bar{\theta}\rangle = \frac{\int_0^\infty (V\cdot I)\langle\theta\rangle\, dt}{\int_0^\infty (V\cdot I)\, dt}$$

to obtain an average incidence of ~ 60 degrees.

The above diagnostic and analytic techniques were used to determine beam characteristics for a set of impulse experiments performed on SNARK. This work is further described in Section 3. In summary, fluence levels of 100 to 125 cal/cm^2 were produced by the guide cone technique. The beams were uniform over 5 cm^2 but uniformity was not consistent in that the beam was not centered on about one-third of the shots.

2.2.3 Beam Compression in Converging Magnetic Fields. Recent work supported by Contract DNA 001-72-C-0176 has shown

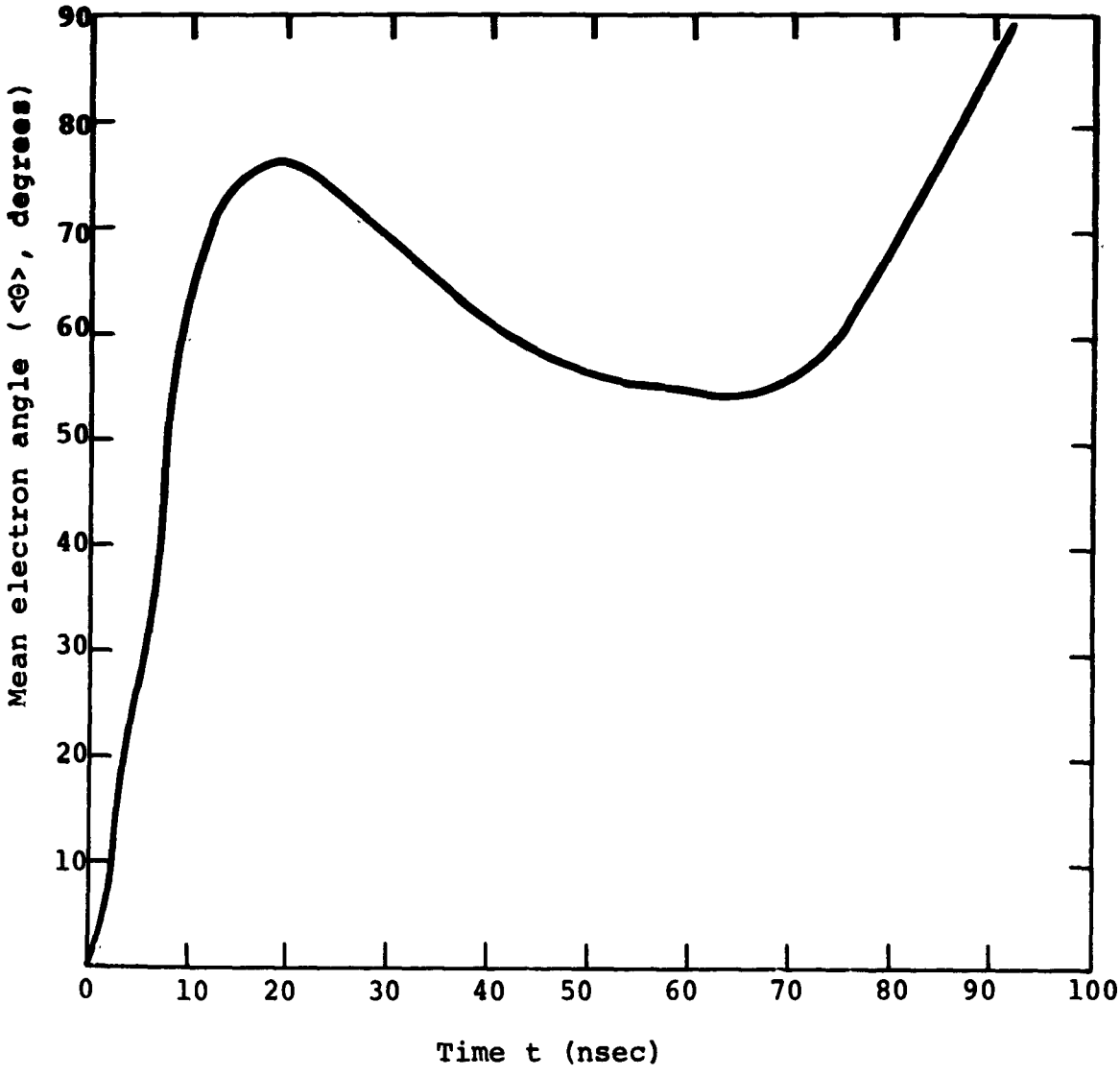

Figure 2.24 Electron mean angle of electron incidence as a function of time.

that an electron beam can be compressed by factors of three using a magnetic mirror. The mirror field is formed by using "pancake" magnets of varying winding densities. The mirror ratio is changed by replacing part of the magnet array. The solenoid is shown in Figure 2.25. The magnetic mirror is adjacent to the diode. This position minimizes the transport distance and any electrons reflected by the mirror might possibly be reflected by the cathode and eventually pass through the mirror. The experiment is shown schematically in Figure 2.26.

A 25 cm^2 area solid surface cathode was used in these tests. As observed with the 100 cm^2 rectangular cathodes, the diode impedance at peak current was found to be in excellent agreement with Langmuir-Child's law predictions,

$$Z = \frac{136}{V^{1/2}(MV)} \frac{\pi d^2}{A} .$$

Impedance data for several shots is listed in Table 2.3. The levels are within 15% of the 2.58Ω predicted from Child's law.

TABLE 2.3

IMPEDANCE CHARACTERISTICS OF 25 cm^2 SOLID SURFACE CATHODE IN B_z

Shot No.	Peak Voltage (kV)	Peak Current (kA)	Impedance Lifetime (nsec)	Impedance (ohms)
1418	650	245	100	2.65
1419	650	262	100	2.48
1421	650	294	110	2.21
1436	650	294	120	2.21
1441	650	255	125	2.55

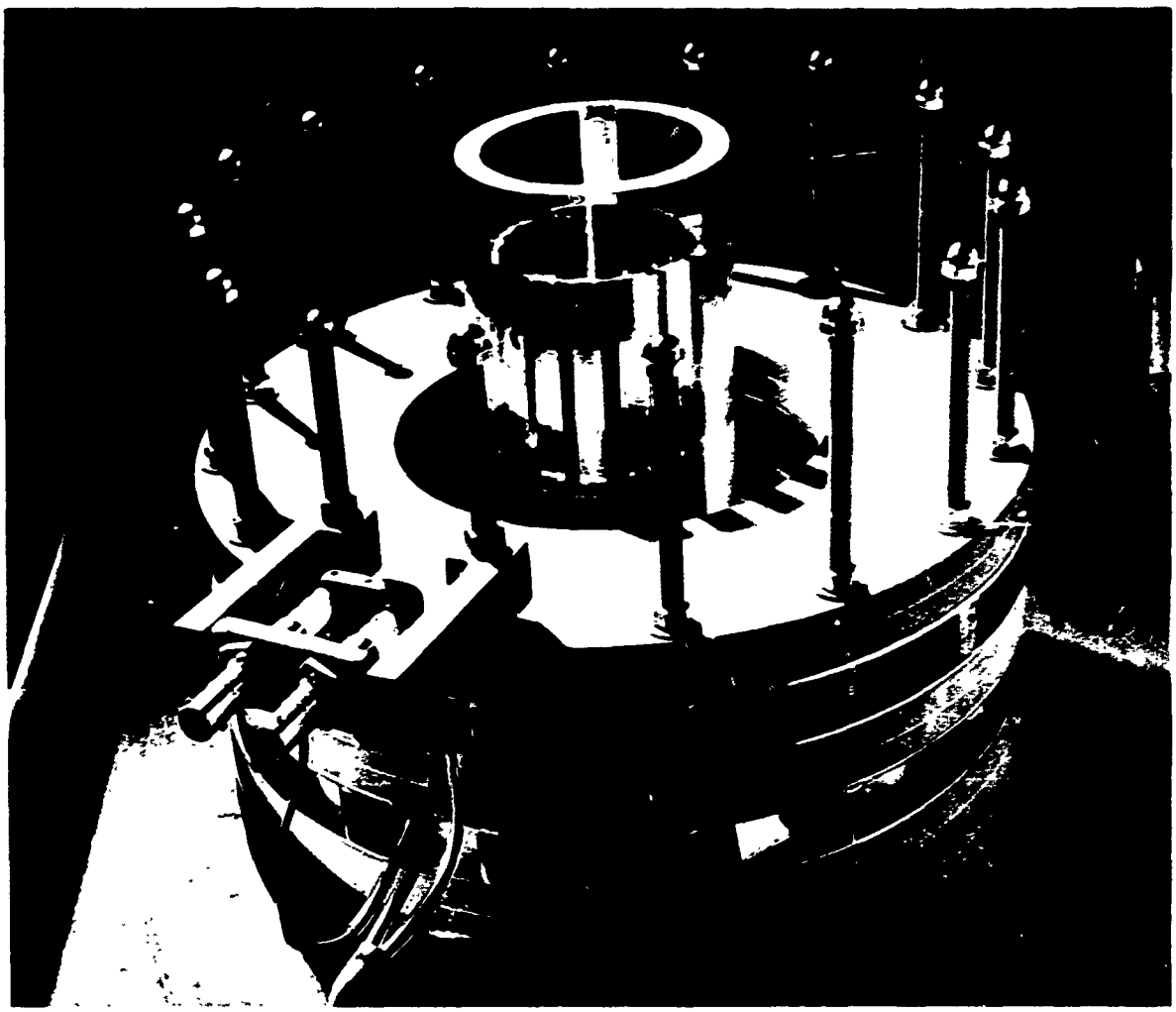

Figure 2.25 PIML coil and vacuum envelope.

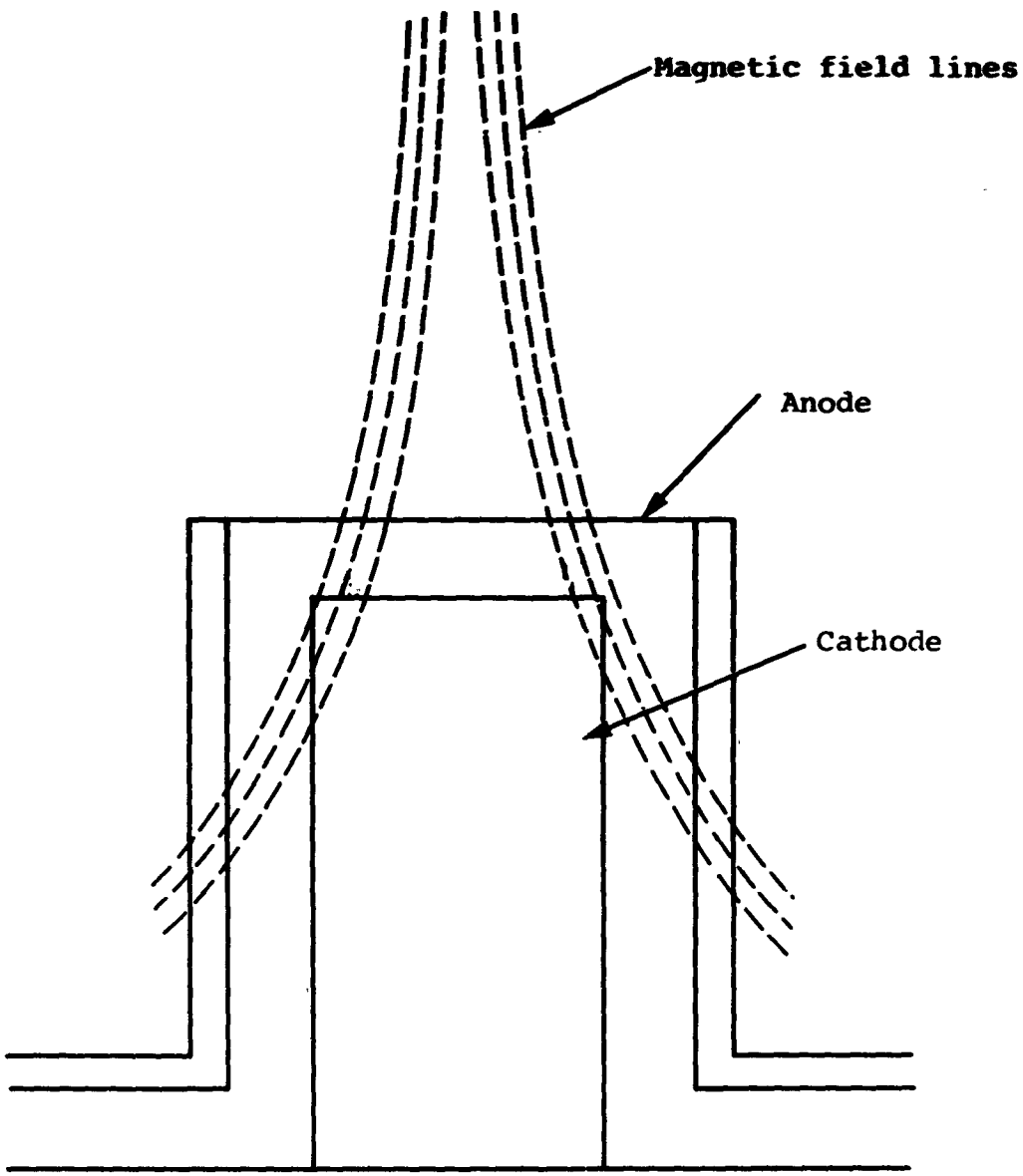

Figure 2.26 Diode compression experiment.

At mirror ratios of 1.5 to 3.0, transport efficiencies are ≈ 90 percent while the transport efficiencies at higher mirror ratios of 4.0 to 4.5 are about 65 percent. The targets show that the beam has a hot core. In this set of experiments this was no cause for concern since flat cathodes were being used. Shaping the cathodes as discussed previously and scattering foils would produce a uniform beam.

Front surface damage produced with these high fluence beams is discussed in Section 3.1.

2.2.4 Summary and Conclusions. Of the three approaches to generation of ≤ 10 cm^2 irradiation area electron beams at SNARK output levels, the most promising to date is beam compression in a converging longitudinal magnetic field.

At present the diode is considered to be the limiting factor in production of uniform small area high dose environments. In order to avoid impedance collapse during the pulse, anode-cathode gaps of at least 3.5 mm were found to be required at 650 kV peak voltage (100 to 125 nsec impedance lifetimes were observed at 3.5 mm A-K gaps). Diode impedance levels (in ~ 8 kG longitudinal fields) were in excellent agreement with Langmuir-Child's law predictions and gave emission current densities of 13 to 14 kA/cm^2 at 3.5 mm gap spacings. This present limit on current densities at the cathode surface implies that a relatively large area cathode must be used to give diode impedance levels enough for efficient energy extraction from the pulse lines. (It should be noted that these comments refer strictly to diodes in B_z fields. Much higher current densities can be achieved at the anode plane without B_z fields, for example typical self-pinched

beams have $J \leq 100\text{-}200$ kA/cm^2. However these current densities have only been achieved over small areas ($\lesssim 1$ cm^2) and the current density is grossly non-uniform.)

Generation of high dose environments using longitudinal fields then depends critically on the limits of beam compression from the initial 13 to 14 kA/cm^2 (at 650 kV peak). This work has shown the importance of cathode surface characteristics in controlling the "compressibility" of SNARK beams. Notably, solid surface cathodes appear to generate beams with less initial transverse energy and these beams have been compressed through a 3/1 mirror field with high (~ 90 percent) efficiency.

In comparison to the large area beam environments, the small area beams are still in the developmental stage. However the initial results of beam compression work are encouraging, at least one high dose environment ($\approx$ 10 kJ over 10 cm^2 at 650 kV peak) is available from SNARK, and present work under DNA contract DNA001-72-C-0138 (at 300 kV electron voltage levels) should lead the way to effective utilization of this technique for routine materials irradiation experiments.

SECTION 3

PILOT MATERIAL AND STRUCTURAL RESPONSE EXPERIMENTS

In addition to the beam development work described in Section 2, several sets of experiments were addressed to irradiation of materials and structural sections using the beams that have been developed. Section 3.1 describes general observations of material damage in samples used in the course of the beam characterization tests. Section 3.2 presents a summary of experiments in which rings and cantilevered beams were irradiated with the large area beams. Response diagnostics included strain gages and high speed (Hycam) motion picture records. Section 3.3 gives a shot summary for the McDonnell-Douglas Teflon irradiation experiments.

3.1 GENERAL OBSERVATIONS OF MATERIAL DAMAGE

Several examples of material damage produced under electron beam irradiation have been presented in Section 2 in support of uniformity and dose level diagnostics. Damage typical of the large area beam irradiation is shown in Figure 2.9. Peak dose levels of $\sim$ 300 cal/gm at mean voltage ranges 350 kV to 650 kV are more than sufficient to produce incipient front surface melt in aluminum and front surface vaporization in phenolic or epoxy. In addition to the front surface loading of materials, an example of the effects of in-depth loading is shown in Figure 3.1. In this case the aluminum plate (1/16-inch thick) was heated in depth over a 2-1/2-inch x 7-inch area. Yielding of the aluminum

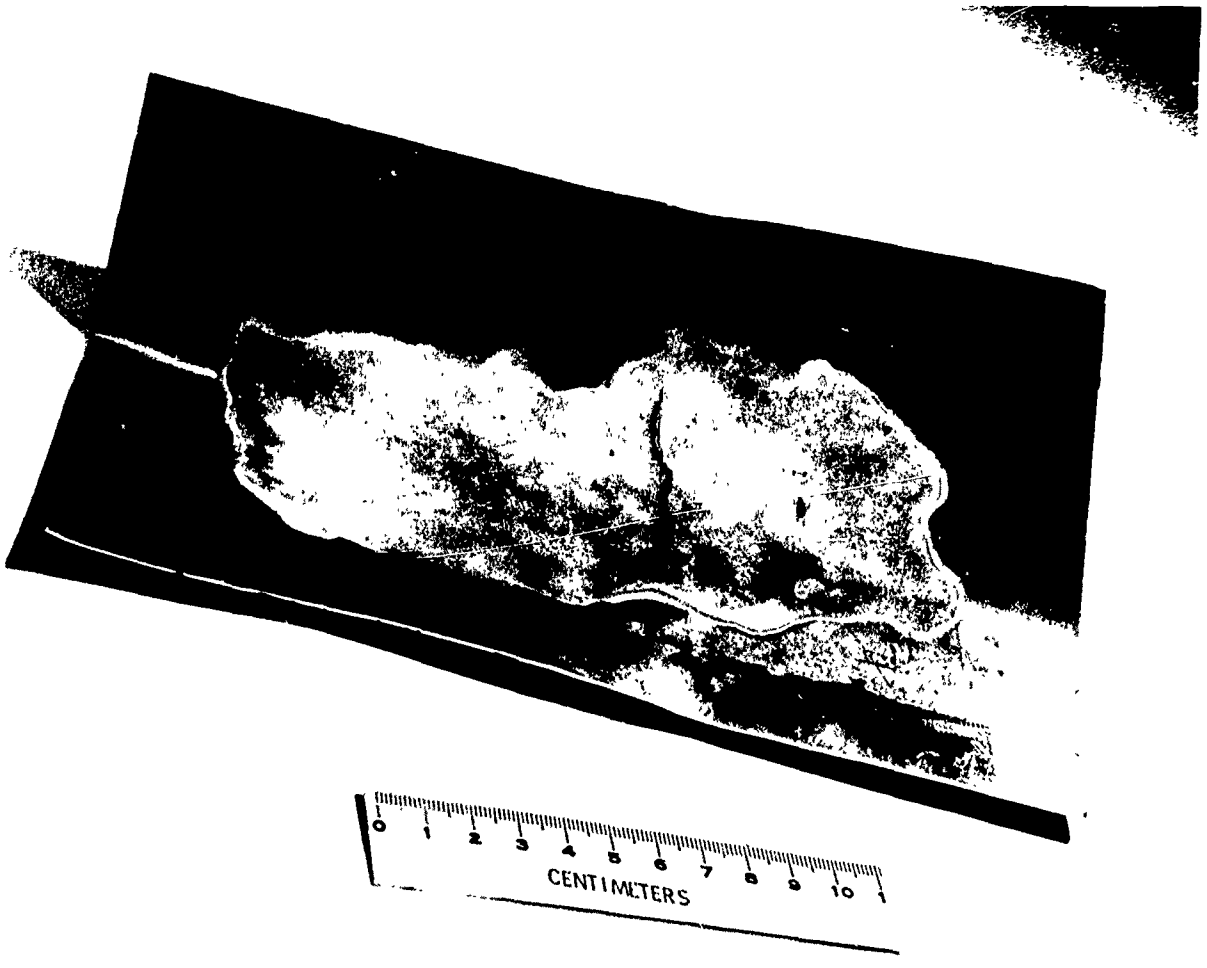

Figure 3.1 Fracture induced by thermostructural response of irradiated aluminum sample.

A1432

near the front surface followed by thermal relaxation caused the sample to curl, first along the short dimension of the plate, and then along the long dimension. The stiffening of the plate produced by the first curl set up a condition where the sample cracked due to the stresses induced by the second curl.

An example of material damage at high dose level is shown in Figure 3.2 . In this case, at an estimated dose level > 2000 cal/gm, the front surface of the graphite sample showed vaporization and spallation. Rear surface spall in 1/8- to 1/4-inch-thick graphite is also typically observed under these irradiation conditions.

3.2 TEST IRRADIATIONS OF STRUCTURAL SECTIONS

Several shifts of pulsing were devoted to test irradiations of aluminum rings (6-inch o.d., 1-1/4-inch wide, 40 mils thick) and cantilevered aluminum beams (8 inches long, 1-inch wide, 40 mils thick). In addition to the observation of permanent deformation and material removal we tested the applicability of active diagnostics for measurement of structural response (strain gages and high speed motion pictures).

A bridge circuit (Figures 3.3 and 3.4) was designed for the strain gage system in an attempt to provide cancellation of common mode noise signals. The gage current was pulsed to allow operation at higher current levels to improve the signal-to-noise ratio. In addition to the test gage on the sample, a dummy gage was mounted near the active gage on a separated block of aluminum. This gage formed the other leg of the bridge circuit. In this manner, an independent noise measurement could also be made. Figures 3.5 and 3.6 illustrate the first experiment performed on

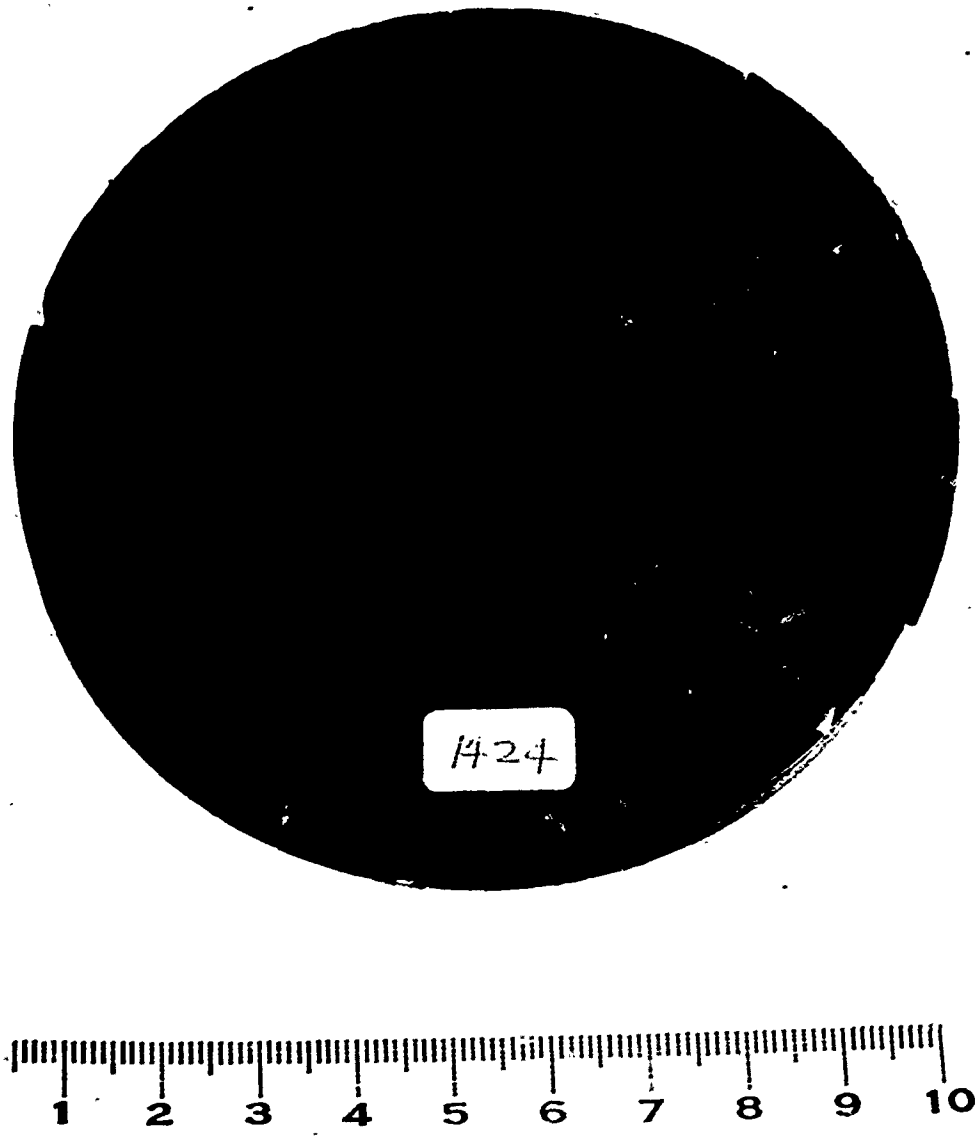

Figure 3.2 Graphite sample at 450 keV mean energy.

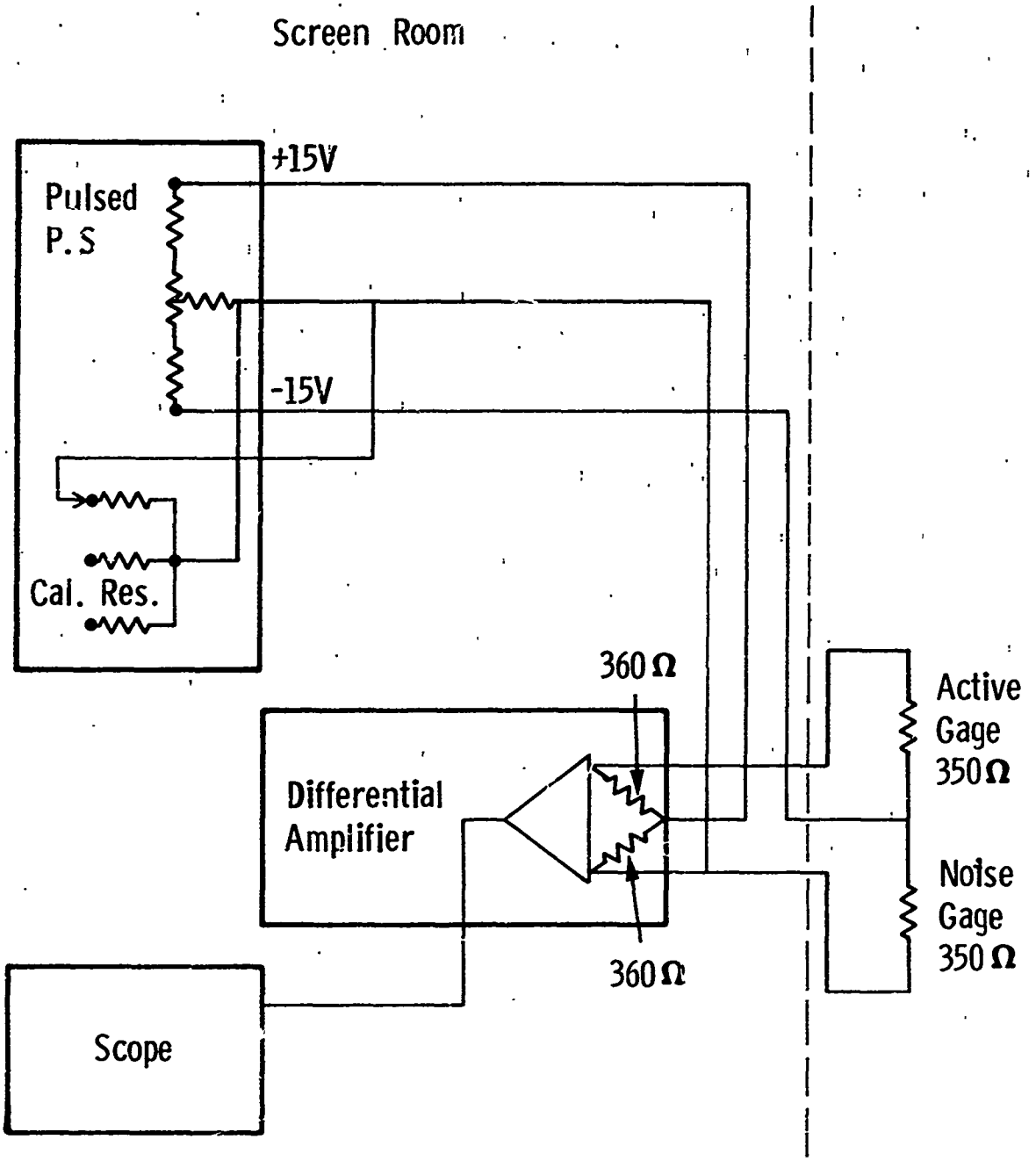

Note:
Strain Gage Type - BLH FAE-065-3550 (SR4 Foil gage)
Gage Factor - 1.94%
Gage Resistance - 350.0 ± 0.5Ω

Figure 3.3 Schematic of strain gage power supply and differential amplifier system.

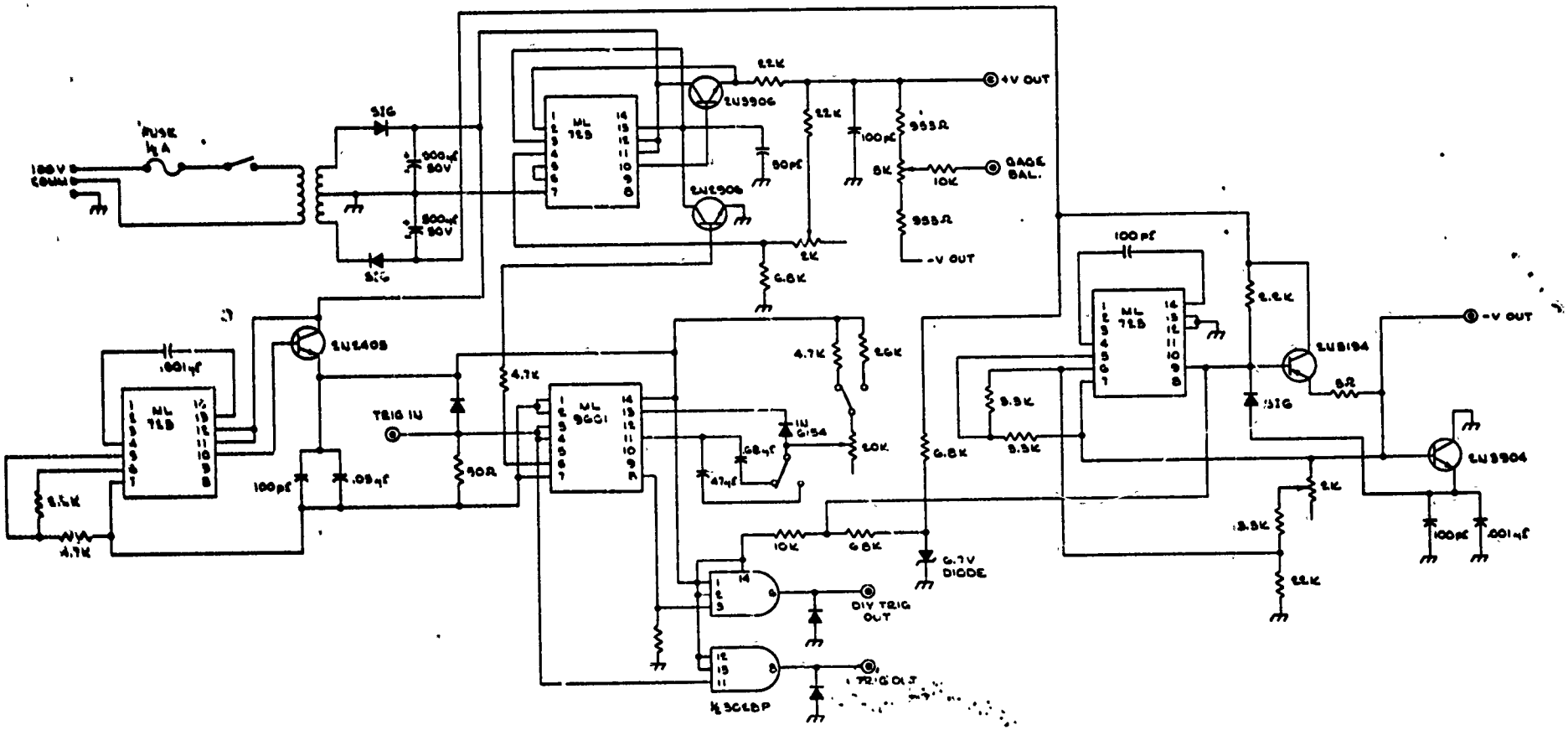

Figure 3.4 Pulsed power supply for strain gauge experiments

See the following pages for greater detail.

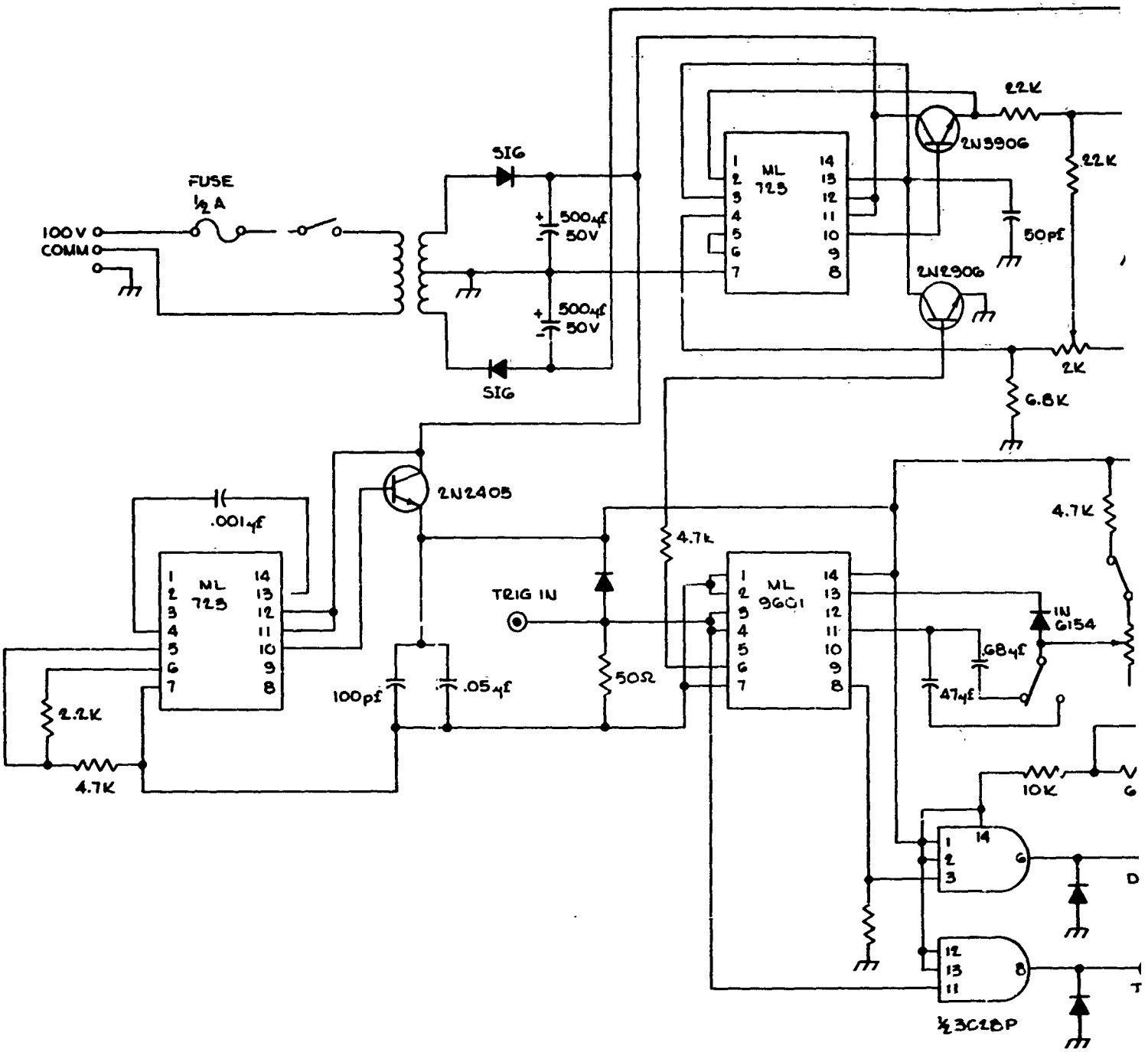
100 V
COMM
FUSE
½ A
SIG
500μf
50V
500μf
50V
SIG
ML
725
2N3906
22K
22K
50pf
2N2906
2K
6.8K
2N2405
.001μf
4.7K
4.7K
TRIG IN
ML
9601
IN
G154
.68μf
.47μf
100pf
.05μf
50Ω
2.2K
4.7K
10K
½3C12DP

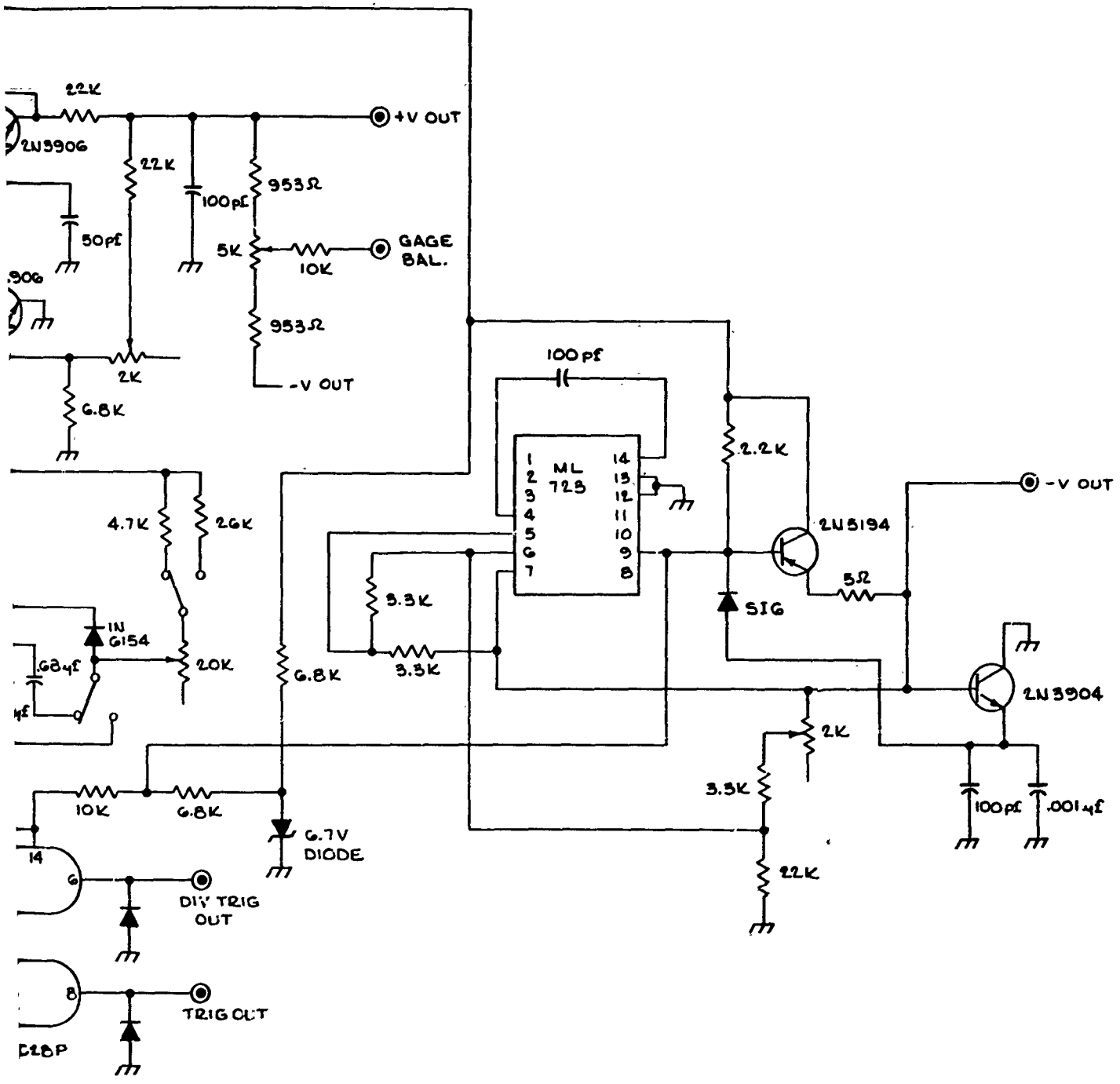

Figure 3.4 Pulsed power supply for strain gauge experiments

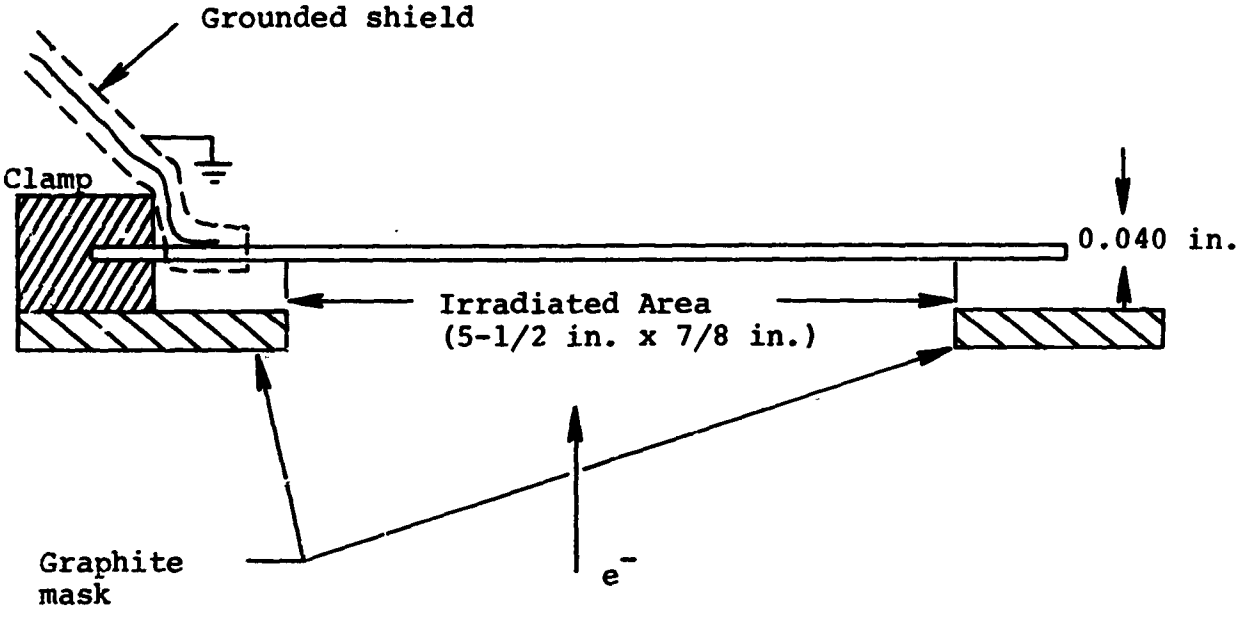

Figure 3.5 Side view of cantilever beam experiment.

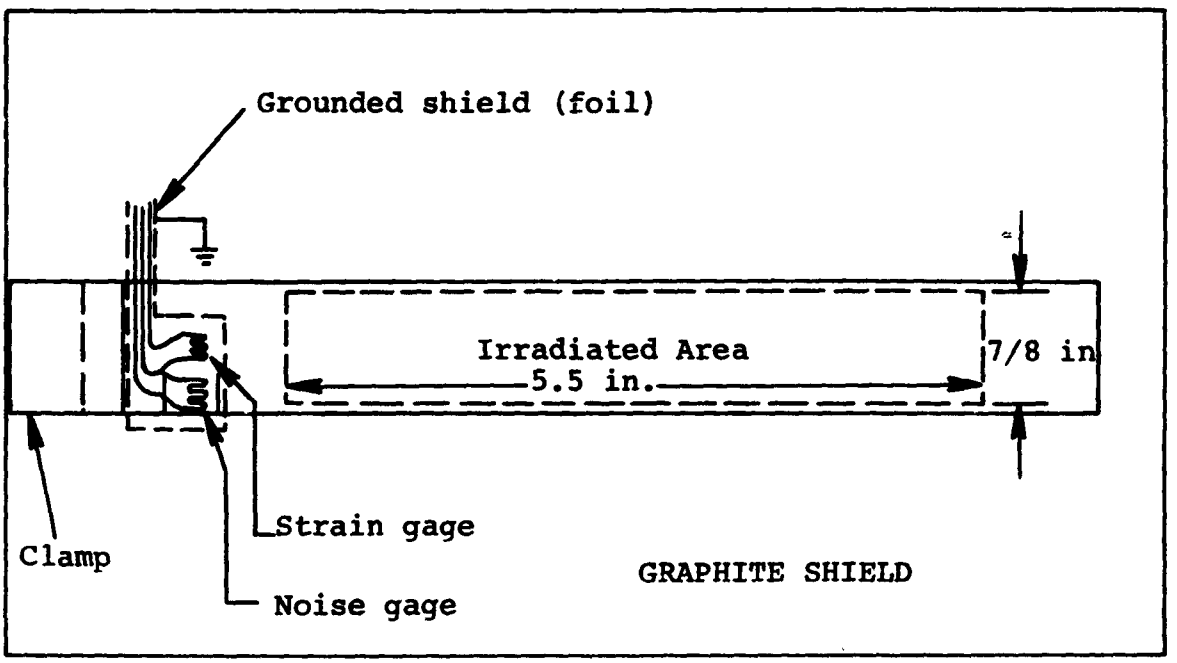

Figure 3.6 Top view of cantilevered beam experiment.

a cantilevered beam. An unbroken ground plane surrounds the strain gages and electron deposition in the cables is prevented by a graphite mask. Strain gage measurements on the response of the cantilevered beam to electron deposition were successful and a typical trace is shown in Figure 3.7. The nominal electron spectrum and fluence for this shot were <E> = 525 keV and 35 to 40 cal/cm^2. The photograph in Figure 3.8 shows front surface damage and gross deformation experienced by the cantilevered beam.

As anticipated the initial strains seen by the gage are compressive caused by the upward impulsion loading. The residual compressive strain was confirmed by an observed permanent flexural deformation of the beam at the gage location. The scale factor for this shot was 5.56×10^{-3} strain/volt.

Strain gage measurements on rings pose a more difficult shielding problem due to geometrical constraints. A modified shield was made up as shown in Figure 3.9 and 3.10. Initial measurements indicated a higher noise level as well as an erratic strain signal. The noise was due mainly to shielding difficulties which resulted in electron deposition in the cables. It was subsequently found that the poor strain signals were caused by defective bonding. The bonding problem has been solved and at this time it is felt that a high degree of confidence could be placed in future ring measurements.

The optical system used to measure rigid body translation in the ring experiments is shown in Figure 3.11. To protect the camera from the noise environment, a filter was installed in the camera body and a line choke was also used. Due to the present dimensions of the electron beam chamber, it was not possible to

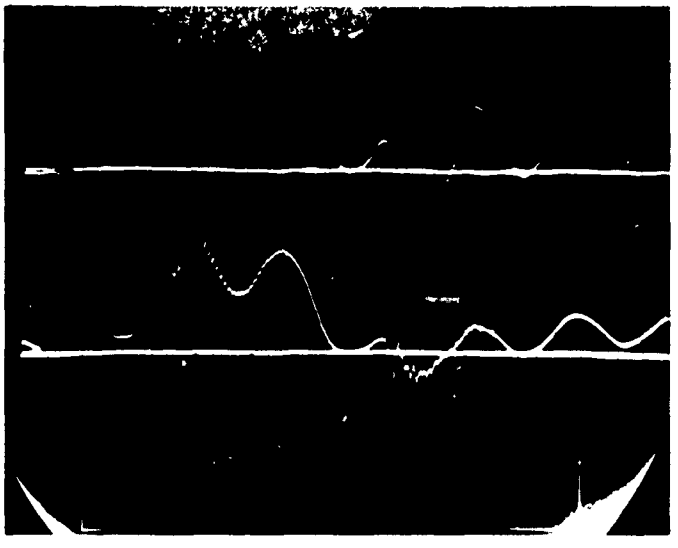

0.2 V/cm

0.5 V/cm
5 msec/cm
4 msec pretrigger

Positive voltage indicates compressive strain

Figure 3.7 Strain gage trace from cantilever beam experiment.

A1419

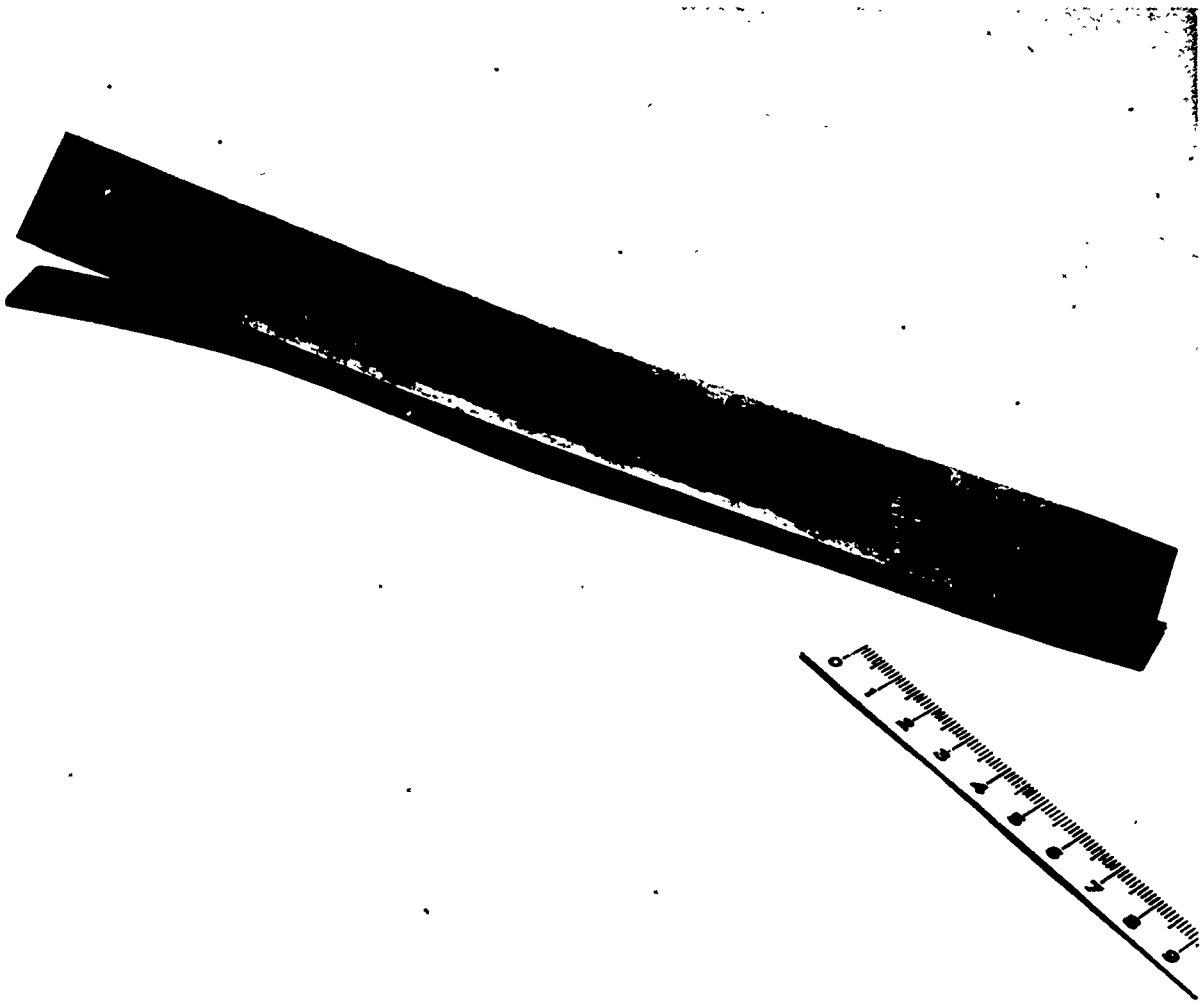

Figure 3.8 Irradiated cantilevered beam, front surface view.

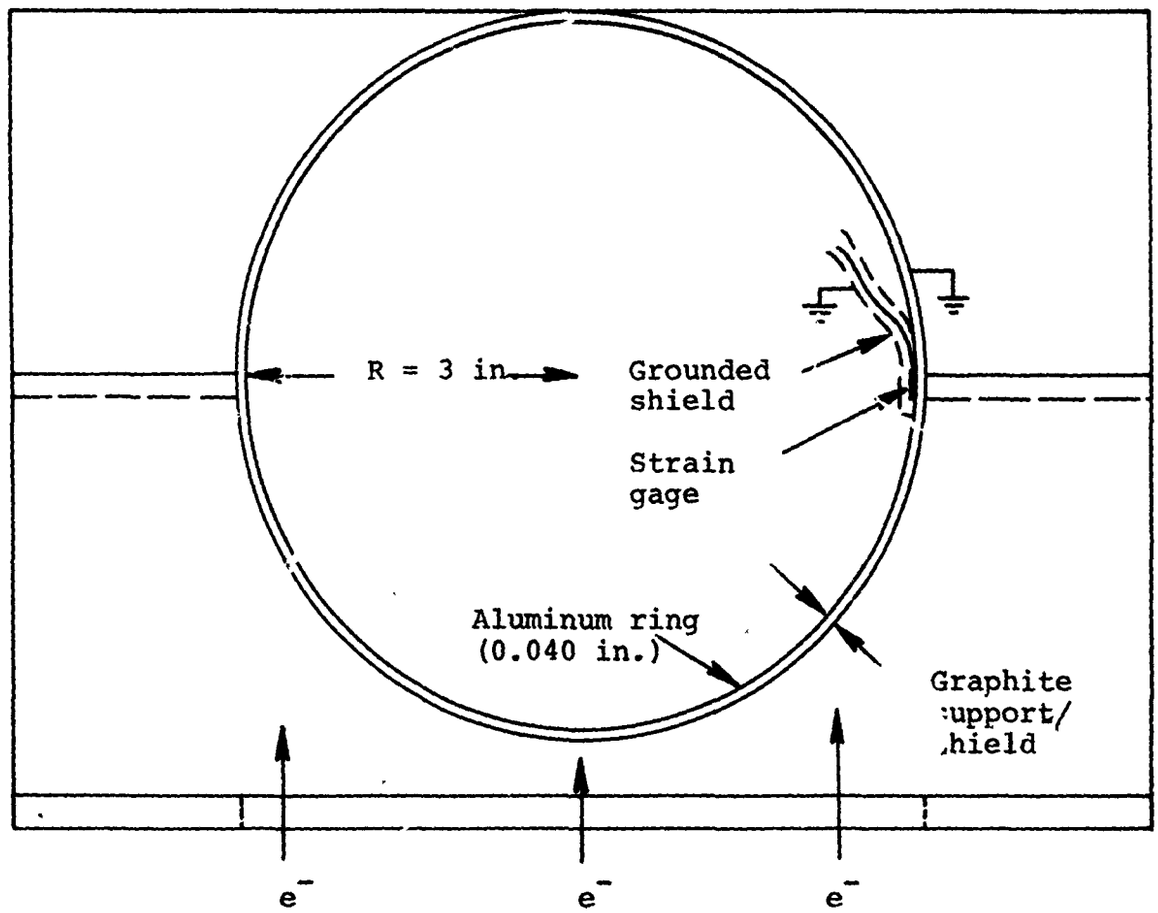

Figure 3.9 Side view of aluminum ring and shield configuration.

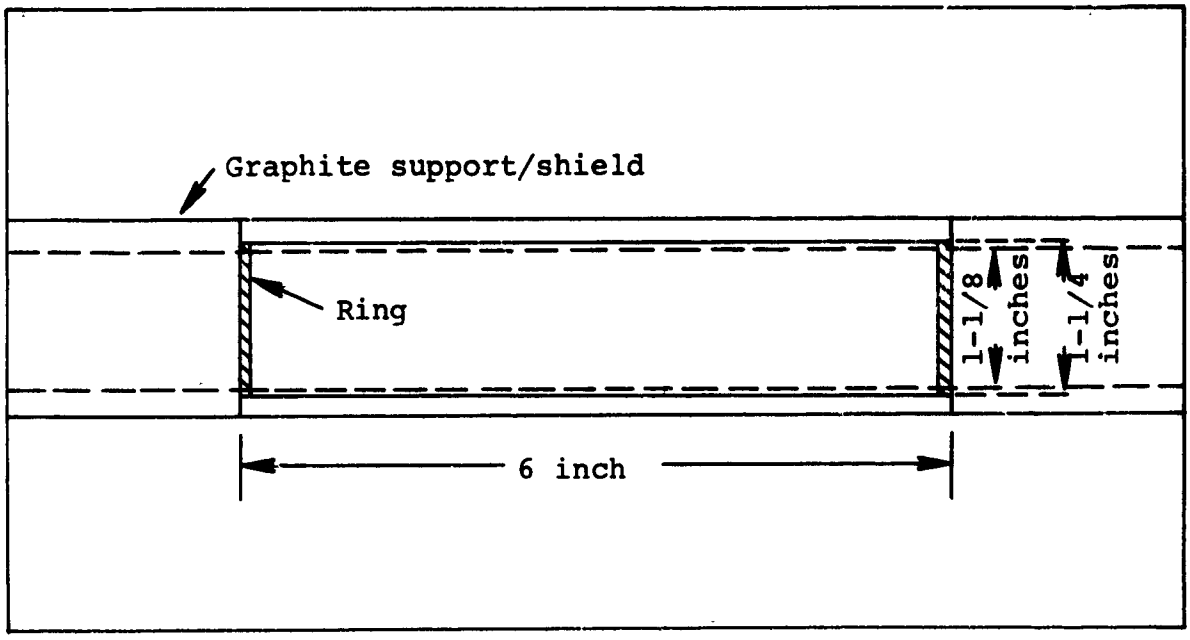

Figure 3.10 Top view of modified shield.

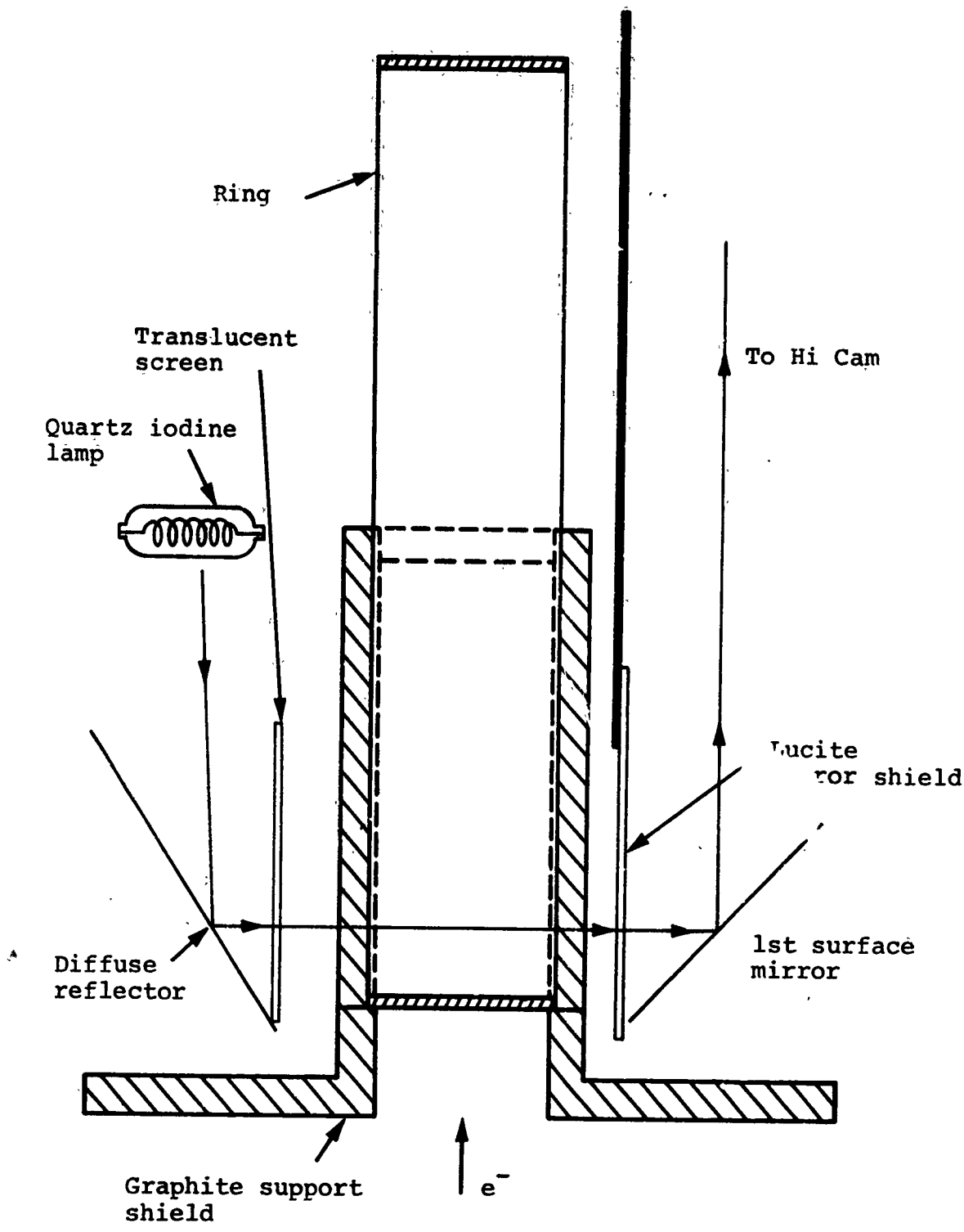

Figure 3.11 Optical system

view more than a 120 degree arc of the ring. Back lighting was employed using a quartz diode lamp to illuminate a white translucent screen. The optical image path had to be shielded from the anode debris and this was done by means of a rectangular pipe. Photographs of irradiated rings are given in Figure 3.12a and 3.12b. High speed movie frames are reproduced in Figure 3.13.

In the initial experiments, high-speed color film was used in an effort to store a greater amount of information. This film, however, has a slower speed and coarser grain structure than the standard black and white film. As a result, the lens had to be opened as wide as possible, severely reducing the depth of field. This, in addition to the coarser grain structure, caused a reduced image quality. However, the momentum delivered to the ring can be estimated from the film to be $\approx$ 15 to 18 kilodyne-sec.

3.3 SMALL IRRADIATION AREA EXPERIMENTS

This section presents a summary of the experiments performed under DNA direction for McDonnell-Douglas in November 1971. The purpose of the testing was to measure dose and fluence levels via interpretation of impulse measurements in Teflon (using various thickness graphite filters placed in front of the sample). Impulse measurements were taken using momentum traps (flyers) photographed with a high speed movie camera. The electron beams were produced by neutral gas focusing in graphite guide cones, the only technique sufficiently developed at that time for small area beam generation. Fluence levels of 100 to 125 cal/cm^2 were produced over $\sim$ 5 cm^2 for these tests. Problems of off-center beam impingement on the sample occurred on about one third of the shots, however these problems have been eliminated by the recent magnetic mirror approach to high fluence beam generation.

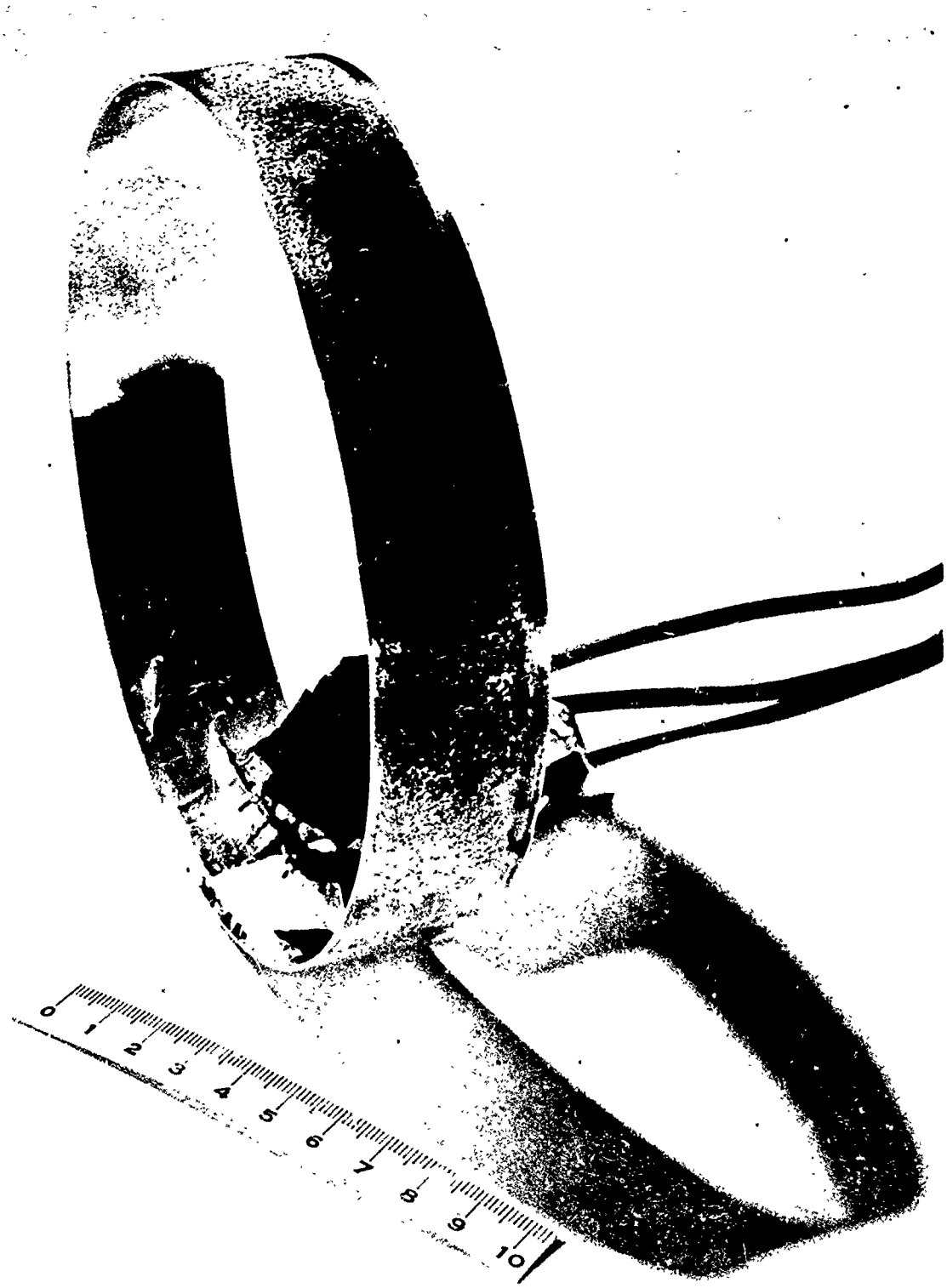

Figure 3.12 a Irradiated ring

A1429

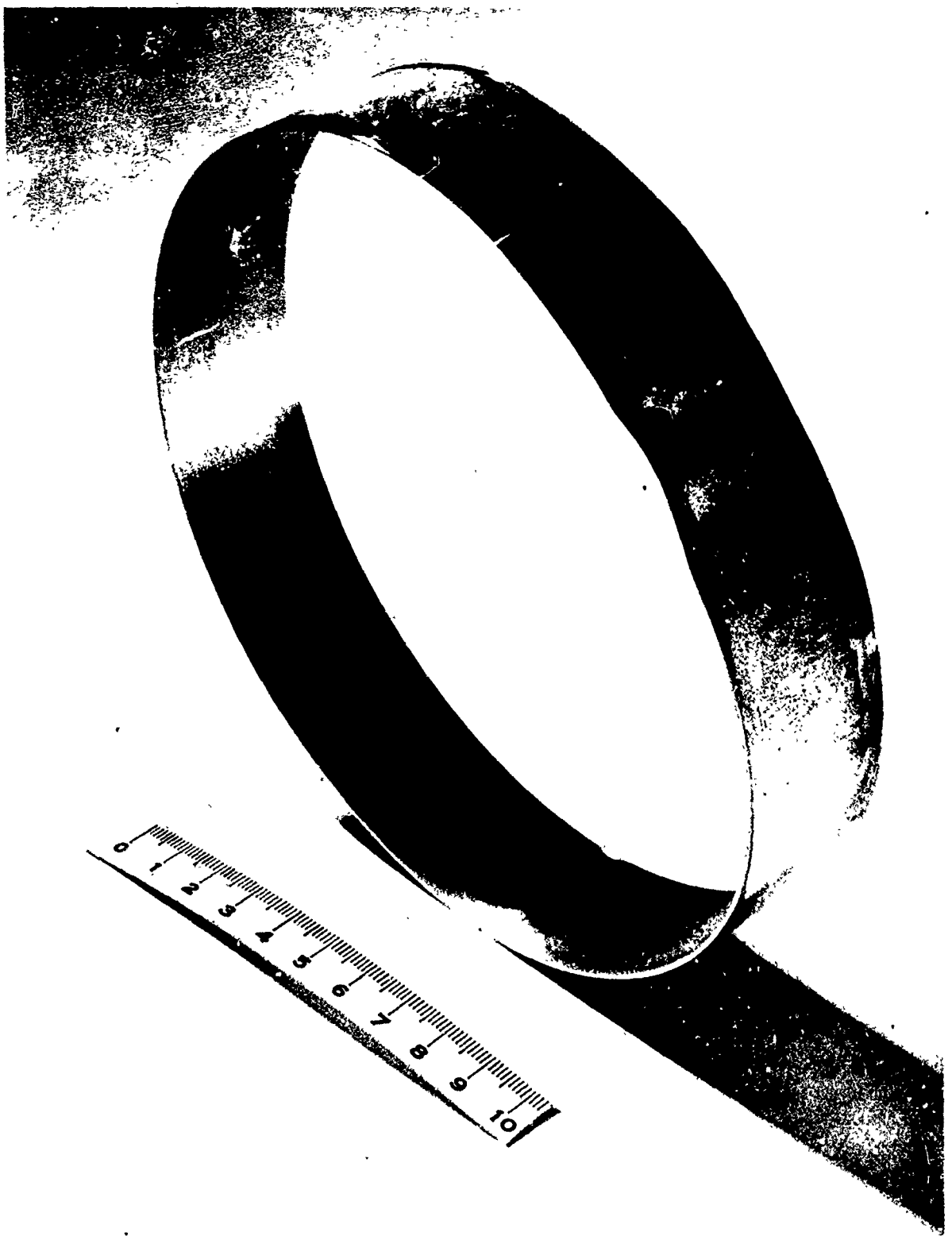

Figure 3.12 b Irradiated ring

A1416

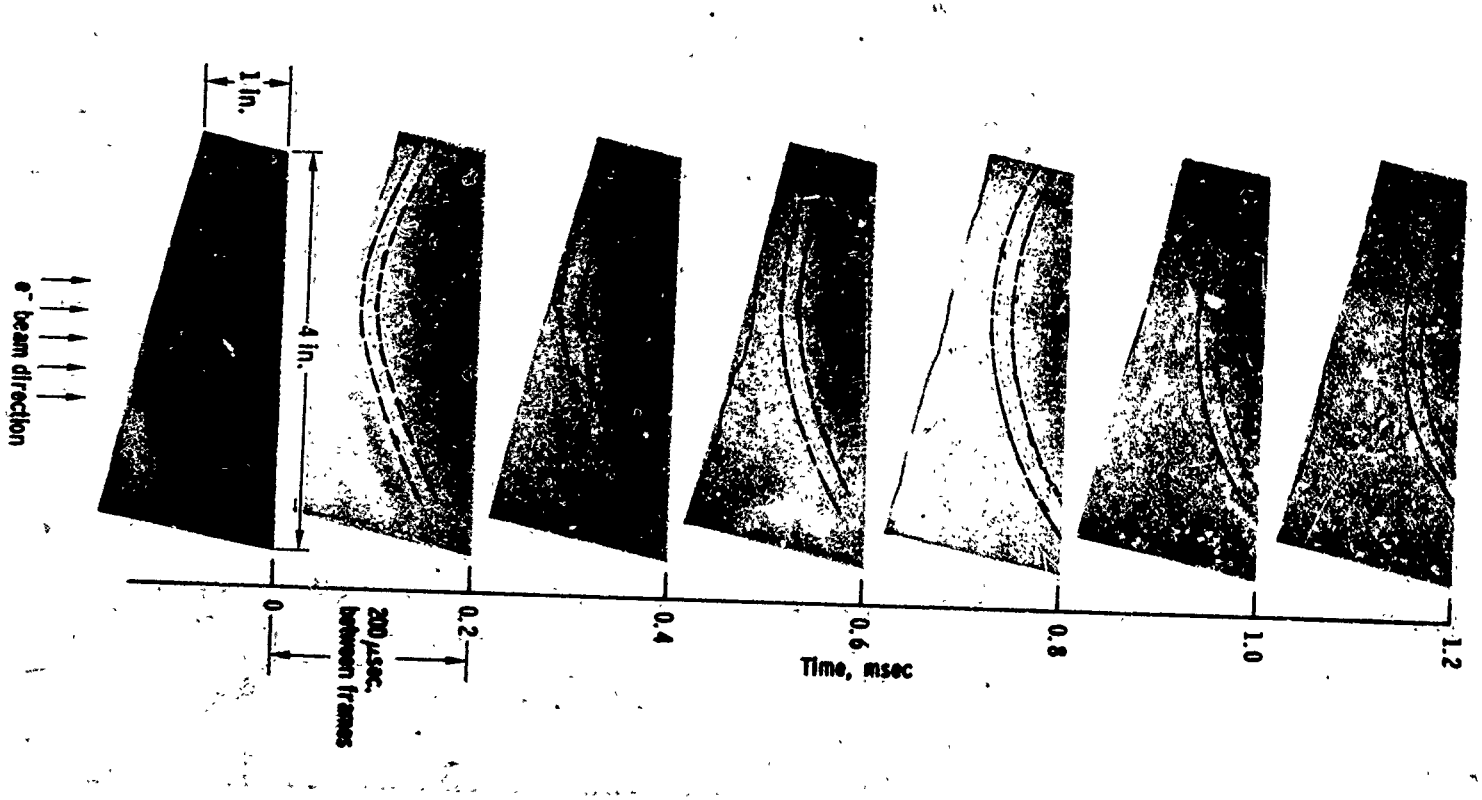

Figure 3.13 High speed movie frames of 120 degree arc from 6 inch ring.

Table 3.1 represents a summary of the 21 shots taken over the two day testing period. What is readily apparent is SNARK's high level of reproducibility. At the 225 kV switch setting, the pulse charge (the voltage to which the Blumleins are charged by the Marx generator) varied by no more than ± 5 percent.

The line voltage and diode current show correspondingly a small shot-to-shot variation. Of the total shots fired, only shots 965 and 966 could be considered bad shots. In both of these, the diode shorted during the first few nanoseconds of the pulse due to a poorly installed cathode. When this condition was rectified the machine returned to its previous operating level. Mean voltage level for all except shots 965 and 966 was 390 keV ± 10 percent.

Fluence levels were estimated from the diode current--Faraday cup current correlation established as described in Section 2.2.2. A 5 cm^2 beam area was assumed. Impulse data and beam areas for individual shots should be obtainable from McDonnell-Douglas. With the exception of the short pulse duration shot (975) the average total energy incident at the target was 112 calories with $\lesssim$ 10 percent extreme deviation on any given shot.

TABLE 3.1
SHOT SUMMARY FOR MDAC TESTING

Shot No.	Pulse Charge Voltage (kV)	Peak Line Voltage (kV)	Peak Diode Current (kA)	Primary Faraday Cup Current (kA)	Mean Electron Energy $\langle E \rangle$ (keV)	Net Current (kA)	Angle of Mean Electron Incidence (degrees)	Total Calories at Target (cal)	Fluence at Target[a] (cal/cm^2)
957	199[b]	531	343		286	46.3	58.6	--	--
958	227	645	412	93	351	71	68.5	560	112
959	236	721	374	82	390	119	--	585	117
960	233	721	384	85	390	N.A.	--	590	118
961	--	--	--	--	--	--	--	--	--
962	227	695	403	100	377	64	62.3	580	116
963	218	721	326	71	390	54	61.7	530	106
964	217	632	370	(82)	340	74	73.1	510	102
965	233	544	811[c]	0	0	--	--	0	0
966	227	556	764[c]	0	0	--	--	0	0
967	231	771	322	(73)	417	58	63.1	550	110
968	233	784	360	(81)	425	73	69.1	610	122
969	220	720	331	(72)	390	--	--	520	104
970	227	733	309	(66)	396	56	64.8	540	108
971	229	733	361	(81)	396	53	58.1	570	114
972	235	784	335	(73)	425	53	59.3	552	110
973	237	796	326	(70)	430	--	--	565	113
974	230	733	330	(72)	396	63	67.0	540	108
975	224	657	365	(83)	355	66	67.8	350	70[d]
976	237	771	326	(70)	417	70	70.8	540	108
977	230	745	361	(81)	405	52	57.8	540	108

[a]Calculated on the basis of 5 cm^2 beam area.

[b]Machine set to fire at 200 kV on this shot. All others used 225 kV switch.

[c]Short circuit in diode.

[d]Short pulse duration.

SECTION 4
CONCLUSIONS

As a direct result of work carried out under this contract, a range of large area (~ 100 cm^2) electron beam environments have been established using the SNARK generator. The environments are well characterized and are now available for use in material and structural response experiments. A summary of fluence levels, mean electron voltages, and irradiation areas is given in Section 1.2.

Small area (≈ 10 cm^2) irradiation environments have not received the attention given to the 100 cm^2 beams, however, recent beam compression experiments have yielded promising results. Notably fluence levels high enough to produce front surface vaporization and spall in graphite have been achieved over 10 cm^2 areas.

Apart from resulting in new simulation capabilities on SNARK, the real impact of this work has been the successful development of longitudinal guide field techniques for high-current electron beam generation and control. The guide field approach has shown to be effective in delivering a large fraction of the available diode energy to a target of arbitrary shape. Overall efficiencies for high ν/γ SNARK beams are ≥ 75 percent compared to neutral gas transport techniques giving 20 to 30 percent of the diode energy. Neutral gas transport techniques have been shown to give even lower efficiencies for higher ν/γ (higher current) electron beams, however no ν/γ limit has yet appeared for efficient transport in longitudinal magnetic fields.

REFERENCES

1. W. T. Link, Electron Beams from 10^{11}-10^{12} Watt Pulsed Accelerators, IEEE Trans. Nuc. Sci., 777 (1967).

2. G. Yonas and P. Spence, Dynamic Effects of High v/γ Beam Plasma Interactions, Record of Tenth Symposium on Electron, Ion, and Laser Beam Technology, L. Marton, Ed., San Francisco Press Incorporated, May 1969.

3. P. Spence, Observation of Transverse Energy Components in High Current Electron Streams, Bull. Am. Phys. Soc., Series II, 14, 11, November 1969.

4. G. Loda, High v/γ Electron beam Generation Using a 100 kV Mylar Stripline, Bull. Am. Phys. Soc., Series II, 15, 11, November 1970.

5. J. Bzura and S. Linke, Electron Beam Energy Transport in Magnetic Fields, Bull. Am. Phys. Soc., Series II, 15, 11, November 1970.

6. J. Block, et al., NRL Relativistic Electron Beam Program, Record of Eleventh Symposium on Electron, Ion, and Laser Beam Technology, R. F. M. Thornley, Ed., San Francisco Press Incorporated, May 1971.

7. C. Stallings, High v/γ Electron Beam Propagation in a Preionized Gas with a Longitudinal Magnetic Field, Bull. Am. Phys. Soc., Series II, 15, 11, November 1970.

8. S. Putnam, et al., Production of Advanced X-ray Sources Using Intense Relativistic Beams, Volume I: Intense Beam Generation, Transport, and Diagnosis, PIFR-227/294, Physics International Company, San Leandro, California, September 1971.

APPENDIX

ELECTRON BEAM DIAGNOSTICS

A.1 CALORIMETRY

Graphite calorimetry was used extensively to measure fluence levels and deposition versus depth profiles for the large area beams. The types of calorimeters developed and/or used on this program are discussed in this Appendix. All active calorimetry signals (thermocouple outputs) were monitored on a Vidar unit. The Vidar is a continuously scanning microvolt meter with a printed readout. In order to maximize signal-to-noise ratio, the Vidar unit was installed in a separate RF-shielded room and shielded cable was installed between the electron beam generator and the screen room.

Fluence and fluence uniformity were quantitatively measured in a plane normal to the beam propagation direction using arrays of 1 cm by 1 cm by 0.8 cm and 1/2 cm by 1/2 cm by 0.8 cm graphite calorimeter blocks of the type commonly used at Physics International Company. The blocks are attached to a low thermal conductivity epoxy resin board with aluminum screws. The thermocouple (which measures the temperature rise of the block following electron deposition) is also attached with the screw and is compressed between the graphite and the epoxy board. The blocks are spaced 5 to 10 mils apart to minimize heat transfer between adjacent blocks. The calorimeter was positioned in the beam to intercept one half of the 100 cm^2 beam. A polyethylene mask was used around the outside of the calorimeter and provided a means of correcting for the total beam area.

This calorimeter was later replaced by a 50 channel, 1 cm^2 graphite disc element calorimeter that sampled the entire beam area. The area of each calorimeter was 1 cm^2 and had a thermocouple attached to the back with an aluminum screw. Each graphite block was mounted in a nylon rod. The calorimeter holder was a large graphite block that held the nylon rods and let the graphite calorimeter head come flush with the surface. The holes in the block were drilled oversize so the graphite calorimeter blocks would not touch the holder thus minimizing heat transfer.

A new type of calorimeter was designed to measure fluence distribution on a curved surface. Twelve graphite blocks, 1/2 in. by 3/4 in. by 1/8 in., were placed on a semicircular mount having a 6-inch diameter (see Figure A.1). The blocks were normal to the incident beam direction. Adjacent to the normal blocks were twelve additional blocks, also 3/4 inch wide, placed at varying angles from 15 degrees to 87 degrees and intercepting the same beam area as the normal flocks. The angled blocks approximate the surface of a ring. Each block had a small hole drilled in its back side and a thermocouple was press-fitted into the hole. The block was attached to a ceramic standoff with a resiliant epoxy.

Deposition profiles were measured using a graphite depth dose calorimeter. The depth dose is similar to other depth dose calorimeters commonly used at Physics International Company except thin graphite foils were used. The graphite was 0.005 inch thick and had a thermocouple attached with a small piece of copper tape. Each graphite foil was separated by 0.03 inch thick resin board. A drawing of the calorimeter is shown in Figure A.2.

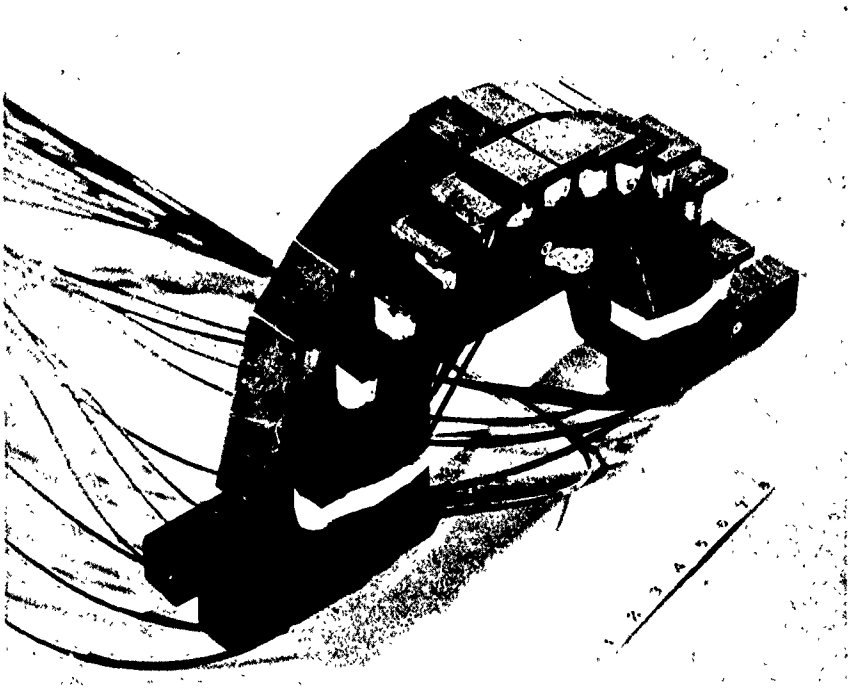

Figure A.1 Curved fluence calorimeter.

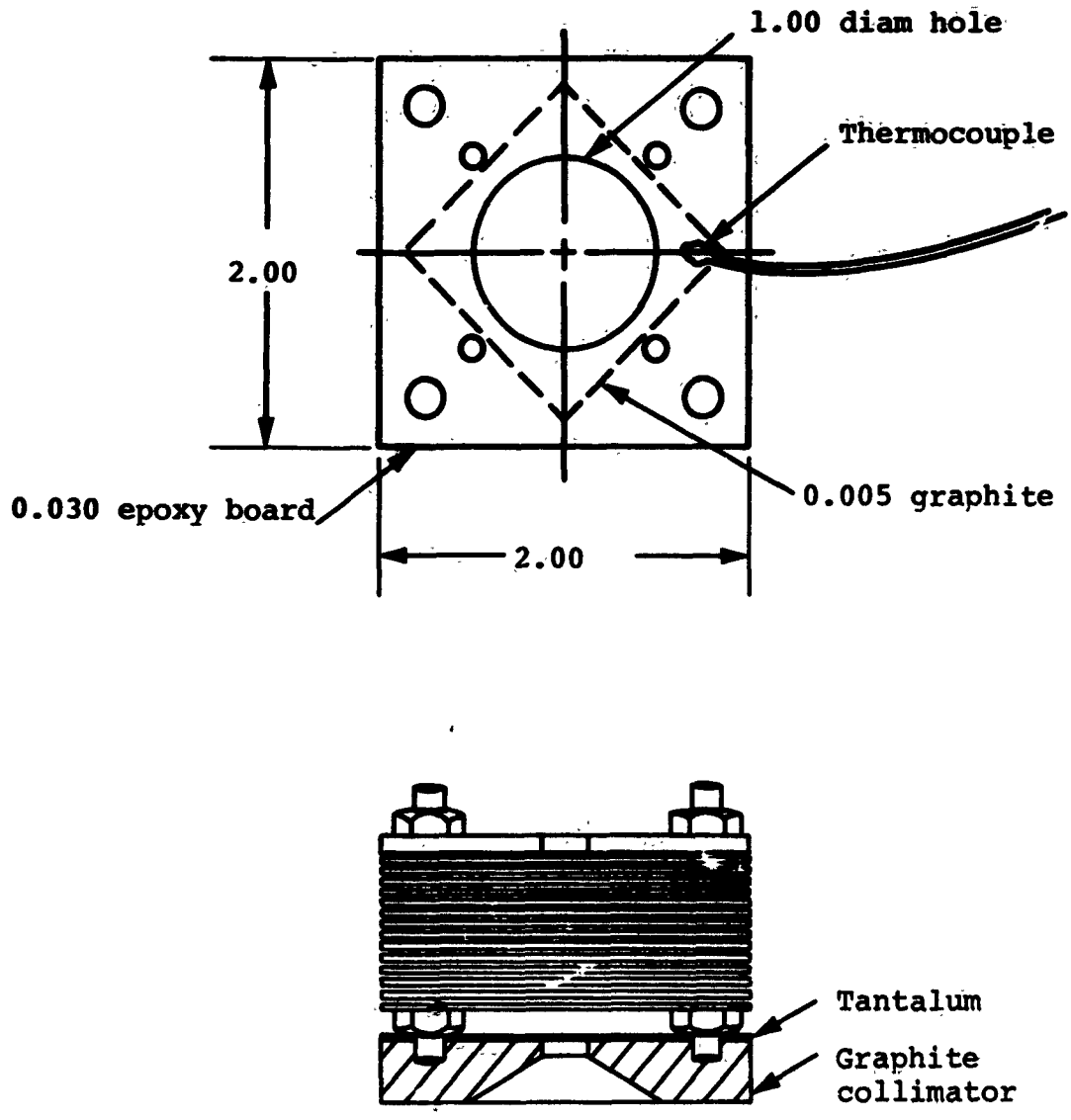

Scale: 1/1

Figure A.2 Graphite depth dose.

Heating and cooling curves were run on the calorimeter to see if the method of attaching the thermocouple was satisfactory and to check on heat conduction between the foils. A graphite collimator backed by a 5 mil piece of tantalum with a 1/4 inch diameter hole was used to define the incoming beam of electrons. Two types of depth calorimeters were used, one was normal to the incident electron beam, while the other was at 45 degrees.

A.2 VOLTAGE AND CURRENT MEASUREMENTS

Electrical measurement of the electron beam spectrum was accomplished by use of voltage and current monitors on the generator. The injected current was measured with a self-integrating Rogowski coil placed around the cathode. The voltage was measured with capacitive voltage monitors, one in each of SNARK's two modules. The line monitors are external to the tube and must be corrected for the inductive voltage drop across the tube before the true accelerating potential is known. The inductance was measured by firing short circuit shots and was found to be 40 nH. The voltage, V_i, lost due to inductance is given by

$$V_i = L \frac{dI}{dt}$$

The dI/dt term is measured at intervals on the current trace and V_i at each point is calculated and subtracted from the line voltage to give the true accelerating waveform, V. The I and V waveforms were then used to find the total beam energy E (for comparison with the calorimeter data) and the mean electron energy <E> by numerically plotting the following integrals:

$$E = \int_0^t VI \, dt$$

$$\langle E \rangle = \frac{\int_0^t VI \, dt}{\int_0^t I \, dt}$$

where E is the pulse length determined by a photodiode. A complete set of waveforms is shown in Figure A.3.

V_1 622 kV/cm
50 nsec/cm

V_2 632 kV/cm
50 nsec/cm

750 kV peak

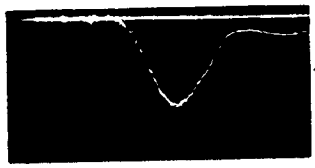

I_o 183 kA/cm
50 nsec/cm

450 kA peak

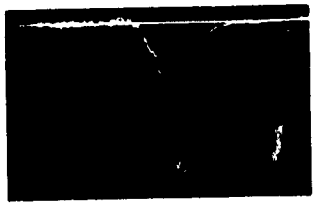

Photodiode 5 V/cm
50 nsec/cm

Figure A.3 Output waveforms.

A1433